University of Zurich[UZH]

Department of Informatics

Exploiting Embodiment in the Design of Bipedal Robots

A dissertation submitted to the Faculty of Economics, Business Administration and Information Technology of the University of Zurich

for the degree of
Doctor of Science (Ph.D.)

by

Harold Roberto Martínez Salazar

from Colombia

Accepted on the recommendation of

Prof. Dr. Rolf Pfeifer
Prof. Dr. Auke Ijspeert

2013

The Faculty of Economics, Business Administration and Information Technology of the University of Zurich herewith permits the publication of the aforementioned dissertation without expressing any opinion on the views contained therein.

Zurich, July 17, 2013

Head of the Ph.D. program in informatics: Prof. Dr. Abraham Bernstein

Acknowledgements

I would like to take this opportunity to thank Prof. Dr. Rolf Pfeifer for giving me the opportunity to join his excellent research team. I am thankful for his inspiring advice, and suggestions through my stay in the lab. I have enjoyed very much the time in this environment of creativity and scientific discussion. I also would like to thank Prof. Dr. Auke Ijspeert for being co-reviewer of this thesis, and to Prof. Dr. Elaine Huang for joining the PhD. committee. A very special thanks to Prof. Dr. Art Kuo who let me visit his lab and run an experiment in his facilities. I would like to show my appreciation to Prof. Dr. Harmut Geyer for his valuable advice and critical opinion which has inspired several research questions developed in this thesis. I cannot thank enough my friend and colleague Dr. Juan Pablo Carbajal who supported me in any respect, with scientific questions, technical problems and fruitful scientific discussions. My gratitude further goes to Dr. Hugo Gravato Marques for his effort of proofreading. Credit should be given to Dr. Hidenobu Sumioka, Dr. Max Lungarella for their support with information theory analysis. I want to express my most sincere appreciation to all the lab members for their valuable help and support in all the projects that I have been working on as part as my doctoral studies. They all have been all extremely collaborative and made the lab the most wonderful working environment. I owe a debt of gratitude to my wife Juanita for her loving support and unconditional help through all these years.

Abstract

State of the art bipedal robots are capable of basic locomotion skills. In general, these robots have stiff limbs and their control system selects a set of actions based on a fixed set of scenarios. However, their performance is still poor compared to humans. Recent findings have shown that compliant limbs are a key factor in human locomotion. This is related with the embodiment theory which suggests that the behavior of an embodied agent is a result of the interaction process between the agent and the environment. This interaction is defined by the interplay of its body dynamics, the controller and the sensory system. In this context, we can take advantage of the body morphology to define the appropriate behavior of a robot. In this study, we use the Spring Loaded Inverted Pendulum (SLIP) model as the conceptual model to study bipedal locomotion. We consider the precision of the action to define the regions in the phase space where human locomotion is possible. This model reproduces qualitatively bio- mechanical observables such as ground reaction forces for running, walking and gait transitions, duty factor, and hip excursion. This model also explains the hopping gait as a combination of running and walking. Based on these results, we can define a control strategy to produce robust locomotion and gait transitions. This strategy exploits the passive dynamics of the system, which reduces the amount of energy needed to control the system. However, the controller largely depends on the parameters of the model. For this reason, we performed an experimental study to assess the effect of changes of mass on the locomotion strategy. We developed the experiments on a treadmill, and collected data for three loads during walking and running. We analyzed the experimental data using dimensionless parameters from the SLIP model. We found that the changes in mass are compensated by changes in other parameters of the model. As a consequence, the dimensionless stiffness remains almost constant. In addition, we showed in a simulation study that a system with mass on the leg under appropriate conditions can reproduce the symmetric gait trajectories from the SLIP model. Based on these results, we proposed the SLIP model as a template to design bipedal machines.

Contents

1 Introduction **1**

2 Conceptual models and control strategies **5**
2.1 Conceptual models of walking 5
2.2 Conceptual models of running 7
2.3 Control strategies for walking 9
2.4 Control strategies for running 10
2.5 Conceptual models and control strategy from the perspective of theories of embodiment 12

3 Thesis contributions **15**
3.1 Mathematical framework 15
3.2 Constraints for human like locomotion 15
3.3 Compensation of disturbances with variation of morphological properties 16
3.4 Leg selection based on the SLIP model 17
3.5 Implications for design and control 17

4 Mathematical framework **19**
4.1 Return Map 19
4.2 Viability 21
4.3 Gaits and gait transitions 22
4.4 Conclusion 22

5 Constraints for human like locomotion **23**
5.1 Robustness 23
5.2 Gaits and gait transitions with robustness 25
5.3 Conclusion 26

6 Compensation through morphology **27**
6.1 Experiment and data analysis 27
6.2 Results 28
6.3 Conclusion 29

7 Leg selection based on the SLIP model **31**
7.1 SLIP model extensions 31
7.2 Leg features based on the SLIP model 32
7.3 Conclusion 33

8 Implications for control **35**
8.1 Morphological properties for locomotion 35
8.2 Conclusions 37

9 Discussion, future work and conclusions **39**
9.1 Summary of the results 39
9.2 Implications of the mathematical framework 41
9.3 Biomechanical predictions 42
9.4 Implication for robot design 43
9.5 Conclusion 43

A Exploiting the Passive Dynamics of a Compliant Leg for Gait Transitions **53**

B From walking to running a natural transition using the hopping gait **61**

C Robustness a criterion for gait transitions in bipedal locomotion **69**

D Covariation of Body Parameters for Compensation of Disturbances **99**

E SLIP Model Predicts an Anthropometric Leg **119**

F On the Influence of Sensor Morphology on Vergence **131**

G Curriculum Vitae **143**

List of Figures

2.1 Inverted pendulum model and its extensions. The simplest walking model is shown in a). In this system the mass at the foot (m_2) is infinitesimal and the mass at the hip (m_1) represents the body. The angle of the slope α is used to compensate with potential gravitational energy the energy losses at heel strike. McGeer [McGeer, 1990b] introduced the model shown in b) to study the effect of knees in locomotion. Chen et al. [Chen et al., 2007] developed the model in c) to find the conditions in which the model with knees can reproduce the results of the simplest walking model. The effect of rolling feet [Garcia et al., 2000] have also been explored with the model shown in d). Wisse et al. [Wisse et al., 2004] introduced the model shown in e) to explain the effect of the trunk in locomotion. 6

2.2 Spring-loaded inverted pendulum and its extensions. The SLIP model is shown in a). The model uses linear massless springs to represent the legs and a mass at the hip to represent the body. This model has been extended to consider the effects of the trunk as it is depicted in b). Rummel et al. [Rummel and Seyfarth, 2008] introduced the model in c) to consider the effect of nonlinear springs. This model uses a two-segmented leg with a linear torsional spring. In this system the segments of the leg are considered massless. McGeer [McGeer, 1990a] used the model shown in d). This model assumes mass in the legs, round feet, and a coil spring at the hip. Owaki et al. [Owaki et al., 2008] follow a similar model but with point feet as it is shown in e). To compensate the impact losses induced by the impacts of legs with mass the models depicted in d) and e) considered a slope with angle α for energy restitution. The effect of rolling foot in locomotion [Whittington and Thelen, 2009] has also been addressed with the model shown in f). 7

2.3 Characteristic ground reaction forces (GRF) observed in human locomotion. The dashed line represents the horizontal GRF, and the solid line represents the vertical GRF. The figure in the left shows the stance phase in walking and the figure in the right shows running. 8

4.1 Evolution of the SLIP model for walking, grounded running and running. The different phases are indicated as well as the section S where the system is observed. The possible initial conditions in the section S are given by the total energy of the system at midstance. The evolution of the gait depends on the selection of the angle of attack α. This is the angle between the leg and the ground at touch down. Walking and grounded running share the same phases. The difference between these gaits is the direction of the vertical velocity at touch down. Walking is produced by a negative velocity while grounded running by a positive. 20

4.2 Return maps in midstance. The system is observed in the section S and the energy defines the set of possible initial conditions. The evolution of the locomotion depends on the selection of the angle of attack α and the gait pattern. 21

4.3 Evolution of the SLIP model for hopping. The different phases are indicated as well as the section S where the system is observed. The evolution of the gait depends on the selection of the angle of attack β, and α. The angle β is used for the system to go from the single stance phase to the double stance phase. The angle α is selected to let the system switch from the flight phase to the single stance phase. 21

5.1 (Color online) Robust regions in the section $\mathcal{S}$. In all panels, the black star in the center of the sphere represents the maximum horizontal velocity. The solid line shows the set of initial conditions in which a gait can be periodic and symmetric. The (blue) light gray color represents the robust region of running. The (magenta) dark gray color represents the robust walking region. The shaded regions are one step robust transitions regions. The (blue) light gray shaded area is the region that using walking let the system to go to the robust running region. The (magenta) dark gray shaded area is the region that using running let the system to go to the robust walking region. The robust regions and robust transitions are calculated using intervals of at least $1^\circ$for the angle of attack. 24

8.1 (Color online) Controller. The panels show the angle of attack for each initial conditions in the section $\mathcal{S}$. For each energy there are two different controllers. Each control presents a policy to keep the system in robust running or walking as it is indicated in the title of column. For the controller in the column running control the system should use the running gait for all the initial conditions except the ones in the region enclosed with the shaded lines. In this region the system should use walking to bring the system to the robust running region. Similarly, for the controller in the column walking control the system should use always walking except in the region enclosed with the shaded lines in which the running gait will bring the system to the walking robust region 36

List of Tables

9.1 Models. The table shows the models used in this thesis and the research questions they addressed. 40

Chapter 1

Introduction

Despite the great technological advances in the field of robotics, state of the art robots like ASIMO [Sakagami et al., 2002], iCub [Tsagarakis et al., 2007] or HRP3 [Akachi et al., 2005] have relatively poor locomotion skills; they lack versatility, robustness and adaptability. Their behavior is limited to a set of motion patterns designed for a specific environment and they cannot cope with unexpected changes such as unforeseen uneven terrain. In contrast, in nature we can see many different creatures with rich, adaptive and diverse motor skills. An example of a rich motor skill is locomotion; humans can jump, run, crawl, walk and gallop with marvelous grace and dexterity. In many different terrains, humans by far outperform any bipedal walking machine. This is one of the reasons that has motivated the research to identify the relevant features in stable human locomotion. One main result from this effort is the identification of the limb compliance as a fundamental aspect for bipedal locomotion [Geyer et al., 2005]. These findings are aligned with theories of embodiment as they show that the morphological features play a central role in the development of behavior.

The embodiment theories propose that a creature engaged in an interaction with the environment induces a set of interrelations between the sensors, the control system, the body and the environment [Lungarella and Sporns, 2006]. For this reason, the behavior of a creature is the result of the dynamic coupling between the physical constraints imposed by the body, the information acquired by the sensor system, the environment in which the creatures are immersed and the actions selected by the control system [Pfeifer et al., 2007]. This strongly suggests that in the design of robotic agents, the designer should treat the mechanical system and the control with equal emphasis. Furthermore, the design process should consider the mechanical properties of the system to develop the desired behavior instead of consider solely the controller for this task [Pfeifer and Gómez, 2009]. Despite this appealing concept, it is still not well understood how the mechanical system should be designed such that useful functionalities like stability, adaptability, etc emerge.

The growing interest in the field of Embodiment identified a set of guidelines that can be used to design embodied systems (regarding the exploitation of morphology and material properties and sensorimotor interaction [Dickinson et al., 2000, Cham et al., 2004, Kimura et al., 2007, Blickhan et al., 2007, Tschacher and Bergomi, 2011]). First, models of locomotion can be used to design a body that appropriately mediates the interaction with the environment [Collins et al., 2005]. Second, the information-theoretic implication of embodiment indicates that when a system is engaged in a coordinated interaction with the environment the system can reduce its dimensionality by exploiting the statistical regularities encountered in the sensorimotor loop [Lungarella and Sporns, 2006].

Based on the previous findings, on how to design machines with human like locomotion capabilities, we have to understand the morphological properties that allow a human being to jump, run, walk and gallop. In the area of bipedal locomotion, researchers have proposed several math-

ematical models to understand the principles governing the gait dynamics. Some of these models use mechanical elements such as springs, dampers and multi-segmented legs to represent different leg components or neuromuscular structures [Siegler et al., 1982, Pandy, 2003, Zajac et al., 2003, Valero-Cuevas et al., 2009]. However, their mathematical complexity prevent their extensive use. In contrast, simpler mathematical models have been adopted as conceptual models of bipedal locomotion [Holmes et al., 2006]. These models provide an extensive exploration of their parameters and an easier visualization of the results due to their low dimensionality.

Experimental results ([Moritz and Farley, 2003, Ferris and Farley, 1997, Ferris et al., 1998]) show that the conceptual models not only explain the coordinated action of many muscles, tendons, and ligaments, but also provide new ideas of how the locomotion process can be controlled. These studies provide empirical results that support the idea of a hierarchical control architecture in which local control strategies tune morphological properties to compensate for external disturbances. In this case, the conceptual model is a desired template of dynamic behavior and the goal of the compensation is to bring the system closer to the template.

The most common conceptual models used to represent locomotion are the inverted pendulum (IP) model [Mochon and McMahon, 1980] and the spring-loaded inverted pendulum (SLIP) [Blickhan, 1989]. The Former is used to represent walking, and its detailed analysis have been a conceptual cornerstone for the development of mechanical devices capable of stable walking without any actuators or controllers [Collins, 2001]. Running is commonly represented with the SLIP model. This model has been successfully used for the control of running machines [Andrews et al., 2011]. The SLIP model has also been extended to reproduce the mechanics of human walking by adding an extra massless spring representing the second leg [Geyer et al., 2005]. Based on the theories of embodiment we assessed these models regarding the interaction process as it is shown in Ch. 2. Herein, we define the ground reaction forces as the biomechanical observables of the interaction process in human locomotion. Thus, our study is based on the SLIP model because this is the conceptual model that appropriately reproduces this observable.

The main contributions of this thesis are as follows. First, the development of a new mathematical framework to represent different human gaits based on the SLIP model. The SLIP model represents each gait using several phases. Each phase is described with a sub-model. These submodels represent the motion of a point mass under the influence of: only gravity, gravity and a linear spring, gravity and two linear springs. The point mass stands for the body of the agent and the massless linear springs model the forces from the legs. We studied this nonlinear and multiphase system using a return map in midstance. Results from a simulation study show that this system can produce gait transitions at the same energy level. In addition, the mechanisms to induce the gait transition exploit the natural dynamics of the system. We also identified a new periodic gait, namely, hopping. This gait is a combination of running and walking. In our simulation studies we showed that robustness can play an important role in inducing gait transitions, complementing the usual view that is focused solely in energy expenditure. The robustness measures the tolerable imprecision in the selection of the action. We assume that an agent spends more resources to calculate a highly precise action, and we call these resources attentional demand. The robustness is inversely related to the attentional demand because the higher the robustness of the system performing a gait, the lower the attentional demand on the action required.

The second contribution is an experimental study that shows how a change of mass affects the human gait while keeping the locomotion speed constant. For the data analysis, we used the SLIP model to represent human gaits using three dimensionless parameters: non-dimensional stiffness, non-dimensional time, and non-dimensional length. We observed a compensation of the change of the mass that can be explained in terms of the dimensionless SLIP model parameters. A direct consequence of the mass compensation is that the control strategy of the gaits does not have to change. The previous results show that the SLIP model can be the desired template of locomotion behavior. Thus, we may use this model to design bipedal machines.

The third contribution is a simulation study to understand the effect of legs with mass on locomotion. We extended the SLIP model and added masses in the legs. In simulations, we identified the leg features such that a system with mass behaves like the SLIP model. First, we used the SLIP model to generate all the possible symmetric gaits. Second, we modeled a pendulum constraint to the trajectories generated by the SLIP. With this model, we found the appropriate pendulums that can reproduce the SLIP trajectories under the assumption that the leg dynamics does not affect the trajectory of the hip. Then, we proposed the rod-SLIP model, in which we consider mass in the legs. With this model we found in simulation the limit mass ratio between the legs and the body that makes valid the predictions with the constraint pendulum. We found that there is a pendulum for which the system runs and walks. In addition, assuming a pendulum with human like mass distribution, we found that the length of the pendulum resembles the human leg length. All these results can also be interpreted from the control perspective which brings new ideas about plausible mechanisms that biped creatures could use to carry out gait transitions and stable locomotion. These mechanisms exploit the passive dynamics of the system, thus reducing the amount of energy to control the system.

This thesis is organized as follows. First we present a succinct introduction of conceptual models for locomotion in Sec. 2.1 and Sec. 2.2. Later in Sec. 2.3 and Sec. 2.4, we introduce some controllers for walking and running. These controllers are not only based on the conceptual models from previous sections but also on different mathematical frameworks. In Sec. 2.5, we apply the guidelines of embodiment design to study locomotion. In this effort, we introduce our definition of interaction. This definition motivates the selection of the SLIP model as a conceptual model to explain the different human gait patterns. In addition, we also introduce some important aspects that can be relevant in the control design from the perspective of embodiment.

In Ch. 3 we present the research approach used in this thesis. Based on the models and control strategies introduced in Ch. 2 we define four research questions. First, what are the conditions to induce gait transitions in the SLIP model and what mathematical representation can be used to visualize and study the gaits and gaits transitions? Second, what constraints in the model can improve the similarity of the results to experimental data? Third, is it possible that in human locomotion the SLIP model can serve as a template and how the perturbations are handled? And fourth, what are the leg features that allow a system to behave like the SLIP model?. In the following chapters Ch. $4-7$ we develop each of these questions and comment the results of physical and simulation experiments. In Ch. 8, the implications of these results for robot design and control are shown. In Ch. 9, we discuss the results introduced in this thesis, the conclusions and the future work.

Chapter 2

Conceptual models and control strategies of locomotion from the view point of theories of embodiment

In this chapter we introduce the conceptual models for locomotion behavior and control strategies for biped machines. Some of the controllers are based on the results of the conceptual models shown in Sec. $2.1 - 2.2$. Other controllers are developed based on a different mathematical framework such as the linear inverted pendulum or the zero moment criterion. We present these control strategies emphasizing their strengths and weaknesses. In Sec. 2.5 we assess these models and control strategies in the light of the embodiment theories based on our definition of interaction. As a result, we selected the SLIP model as a conceptual model for locomotion and used to develop our mathematical framework (Ch. 4). We finalize this chapter with relevant aspects for the control design from the perspective of embodiment.

2.1 Conceptual models of walking

Locomotion models have been inspired by the interplay between kinetic and potential energies [Cavagna et al., 1976]. In walking, the center of mass is in the highest position when the hip is over the ankle of the stance leg (mid-stance). Hence, in walking changes of kinetic and potential energies are out of phase. The inverted pendulum (IP) model proposed by Mochon et al. [Mochon and McMahon, 1980] is inspired by this idea. This model has been used to study and identify the principal features of walking. The simplest special case of this model has two rigid massless legs hinged at the hip, a point-mass at the hip, and infinitesimal point-masses at the feet (Fig. 2.1a). This two dimensional uncontrolled system can walk down a shallow slope powered only by gravity [Garcia et al., 1998].

Detailed analysis of this system (Fig. 2.1a) shows that the walking speed is proportional to the stance angle (i.e. the angle between the vertical and the stance angle after the heel strike), and the stance angle is proportional to the slope angle. The gravitational power used to keep the system walking is proportional to the velocity of the system along the slope [Garcia et al., 1998]. This model has been used to demonstrate stable one-period gaits, period doubling phenomenon, and bifurcations leading to chaos [Garcia et al., 1998, Goswami et al., 1998]. This model has been

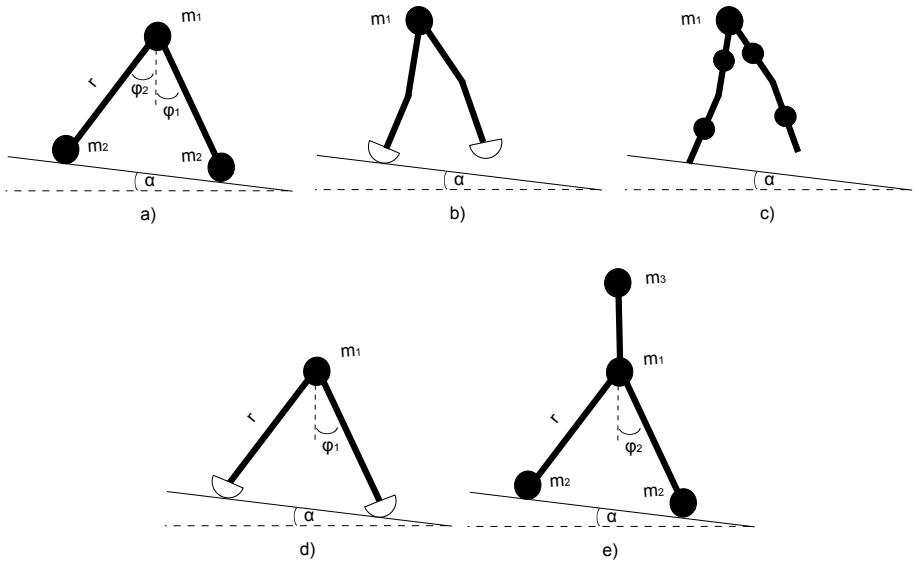

Figure 2.1: Inverted pendulum model and its extensions. The simplest walking model is shown in a). In this system the mass at the foot (m_2) is infinitesimal and the mass at the hip (m_1) represents the body. The angle of the slope α is used to compensate with potential gravitational energy the energy losses at heel strike. McGeer [McGeer, 1990b] introduced the model shown in b) to study the effect of knees in locomotion. Chen et al. [Chen et al., 2007] developed the model in c) to find the conditions in which the model with knees can reproduce the results of the simplest walking model. The effect of rolling feet [Garcia et al., 2000] have also been explored with the model shown in d). Wisse et al. [Wisse et al., 2004] introduced the model shown in e) to explain the effect of the trunk in locomotion.

extended to study different important parts of the body involved in the walking gait such us the knee, foot, and trunk.

McGeer in his seminal work about passive dynamic walkers [McGeer, 1990b] introduced a system with round feet and knees (Fig. 2.1b). This study analyzed the stability of the walking cycle and introduced a simple sensitivity calculation of the stability to parameter variations. Furthermore, in some cases the knees can improve the stability of the system [McGeer, 1990c]. This study has been extended in [Chen et al., 2007] to identify the mass distribution in the system to reproduce the stability of the compass walker (Fig. 2.1c). The result from simulations showed that the mass should be concentrated in the hip and close to the knee joints. The mass at the hip should be also comparable to the mass in the upper segment of the leg, and the ratio of mass between the upper and the lower segment of the leg should be at least 1:10. Under these conditions the walker with knees approximates the compass gait dynamics in the limiting case.

Simulation results from the IP model with round feet (Fig. 2.1d) and with point contact show that the a semi-circular foot contact softens the impact resulting in much smaller energy losses than point-foot walkers [Garcia et al., 2000]. Collisional losses are also lower if a single impulse is broken up into a series of smaller impulses that gradually redirect the velocity of the center of mass [Ruina et al., 2005]. Based on these findings Kwan [Kwan and Hubbard, 2007] proposed an anthropometric foot shape for the IP model which reduces the impact losses in walking. Adamczyk et al. [Adamczyk et al., 2006] used the IP model with roller feet to show that the work needed to redirect the COM velocity at each step decreases quadratically with the arc radius of the foot. The model was validated experimentally and the experiments show that when the arc radius was 0.3L (leg length) the net metabolic rate decreased to a minimum.

The IP model has also been extended to understand the effect of the upper body. Wisse et

al. [Wisse et al., 2004] introduced the simplest walking model with an upper body (Fig. 2.1e). This model has a kinematic coupling that keeps the upper body midway between the two legs. Simulation results showed that this model produces walking patterns and it can handle disturbances of 8% of the initial conditions. A robotic validation of this model confirmed that a higher center of mass provides a better robustness against disturbances and energy efficiency [Wisse, 2005].

These models have been useful to understand more about bipedal locomotion. However, they only explain partially aspects of the walking gait. In Sec. 2.5, we are going to extend these ideas together with the control strategies inspired by the results of this model.

2.2 Conceptual models of running

The spring-loaded inverted pendulum (SLIP) was proposed by [Blickhan, 1989] to study the mechanics of running. This model has been motivated by the in-phase interplay between kinetic and potential energies produced by this gait [Cavagna et al., 1976], i.e. the center of mass is in the lowest position at mid-stance. This model uses a massless spring to represent the legs and a point mass at the hip to represent the body (Fig. 2.2a). Given that the leg does not have mass the swinging dynamics cannot be described by Newton's equations. Thus, the model needs a policy which indicates the angle of attack. This is the angle between the leg and the ground produced at heel strike or touchdown.

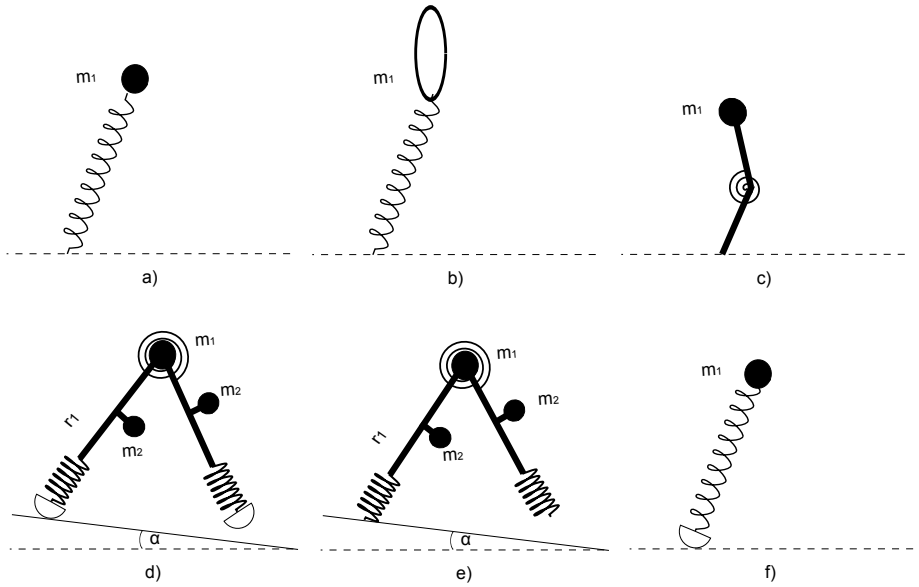

Figure 2.2: Spring-loaded inverted pendulum and its extensions. The SLIP model is shown in a). The model uses linear massless springs to represent the legs and a mass at the hip to represent the body. This model has been extended to consider the effects of the trunk as it is depicted in b). Rummel et al. [Rummel and Seyfarth, 2008] introduced the model in c) to consider the effect of nonlinear springs. This model uses a two-segmented leg with a linear torsional spring. In this system the segments of the leg are considered massless. McGeer [McGeer, 1990a] used the model shown in d). This model assumes mass in the legs, round feet, and a coil spring at the hip. Owaki et al. [Owaki et al., 2008] follow a similar model but with point feet as it is shown in e). To compensate the impact losses induced by the impacts of legs with mass the models depicted in d) and e) considered a slope with angle α for energy restitution. The effect of rolling foot in locomotion [Whittington and Thelen, 2009] has also been addressed with the model shown in f).

Blickhan [Blickhan, 1989] and McMahon and Cheng [McMahon and Cheng, 1990] showed that the SLIP model can reproduce the ground reaction forces of many types of fast animal and human locomotion. Seyfarth et al. [Seyfarth et al., 2002] found that the selection of constant angles of attack not only was useful to reproduce the experimental data of human running (Fig. 2.3) but also produced in the model a self-stabilized behavior (for a proper selection of stiffness and forward velocity). The predicted stable running proved to be in agreement with experimental studies. This model has been extended to understand the importance of other aspects involved in the locomotion process such as feet, the upper body, biarticular legs and mass in the legs.

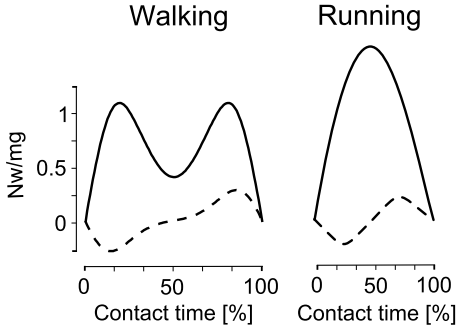

Figure 2.3: Characteristic ground reaction forces (GRF) observed in human locomotion. The dashed line represents the horizontal GRF, and the solid line represents the vertical GRF. The figure in the left shows the stance phase in walking and the figure in the right shows running.

The SLIP model has been extended to the Asymmetric Spring Loaded Inverted Pendulum (ASLIP) model [Hyon and Mita, 2002]. In the latter the trunk is a rigid body and its center of mass is not at the joint (Fig. 2.2b). The model is used to generate a finite state machine controller. The controller is based on the dynamics of the model and was successfully tested in a robotic platform. This model has also been used to generate a controller that induces stable running gaits exploiting the results of the SLIP model [Poulakakis and Grizzle, 2009]. The control has two objectives: the first is to keep the desired torso posture and the second to stabilize the system according the periodic orbit of the SLIP dynamics. The ASLIP has also been used to study the passive stabilization of the trunk in locomotion [Rummel and Seyfarth, 2010]. In this simulation study, springs at the hip apply torques during locomotion to keep the torso around midstance. The results from simulation reveal that the springs allow robust locomotion and the function of mono-articular muscles surrounding the hip.

The linear spring in the SLIP model has also been replaced by a nonlinear one [Rummel and Seyfarth, 2008]. The nonlinear stiffness is the result of a linear torsional spring in the knee joint of a two-segmented leg (Fig. 2.2c). In contrast to the linear leg springs, the segmented leg is capable of running at lower speeds and the stable locomotion can be produced with a bigger range of angles of attack. However, the model does not predict well fast running due to the mechanical disadvantage of larger compressions.

McGeer [McGeer, 1990a] considered mass in the legs, round feet, and a coil spring at the hip to help the swinging motion of the leg (Fig. 2.2d). In this simulation study, the stability properties of this system were shown. A similar model but with point feet (Fig. 2.2e) was introduced later by Owaki [Owaki et al., 2008, Owaki et al., 2009]. In these studies it was shown that the relation between the leg spring constant and the hip coil spring constant defines the locomotion pattern. In addition, this research explained the stabilization mechanism present in this system using a Poincaré map.

The SLIP model has also been extended to study the center-of-pressure excursion. In the SLIP model, the foot is a fixed contact point with the ground. Thus, the center of pressure and the foot are the same. However, in human locomotion, the center of pressure moves along the foot at each step. The SLIP model with roller feet accounts for this effect [Whittington and Thelen, 2009]. Simulation studies of this model (Fig. 2.2f) have shown that it reproduces the experimental data of human subjects. The model explains the center of mass motion, center-of-pressure excursions, and ground reaction forces. In addition, the model produces stable patterns of locomotion for a set of constant angles of attack similar to the SLIP model without roller feet.

2.3 Control strategies for walking

Kajita et al. [Kajita et al., 1992] introduced a 2D mathematical model of a walking system in which the center of gravity of the body moves only in the horizontal direction. Under this assumption the equation of motion of the system can be written as a linear differential equation. Thus, this model is called Linear Inverted Pendulum (LIP). As a difference from the conceptual models introduced in previous sections, the LIP model has an analytical solution. In this study, Kajita proposed a scalar function of the velocity and the position of the center of mass (orbital energy) to represent any trajectory of the system. The trajectory can be changed with the foot placement position calculated from the orbital energy function. Using this control law, the system can start walking, continue walking at different horizontal velocities, and stop walking. All the control strategy based on the LIP model require ideal sources of force or torque to keep the center of mass at the same height at any moment of the locomotion process. For this reason the velocity of locomotion is limited by the bandwidth of the force control.

The LIP model has been extended to the 3D LIP model [Kajita et al., 2001]. This study showed a walking system in which the center of gravity of the body moves in a plane. The 3D LIP model showed that the orbital energy function has two components. One component represents the trajectory in the frontal direction and the other represents the trajectory in the lateral direction. The implementation of the control law was tested in a simulation of a humanoid robot. In this simulation, the robot was capable of walking in a circular trajectory.

The LIP model has also been extended by Pratt et al. [Pratt et al., 2006] to solve the humanoid push and recovery problem. This proposed method is based on the computation of capture points and capture regions. The former are the points on the ground where a humanoid must step in order to come to a complete stop. The latter is the collection of all Capture Points. In this study the LIP model was extended to include a flywheel body. The rotational inertia enables the humanoid to control its centroidal angular momentum. The extended model proved to be useful to compute exact solutions of the capture region. The results of this study have been tested successfully in simulation experiments.

Another control strategy for walking robots is based on the zero moment point (ZMP) [Vukobratovic and Borovac, 2004]. The zero moment point is the place on the ground where the summation of torques produced by gravity and the inertial forces is equal to zero. The ZMP criterion states that if the ZMP is inside the support polygon described by the robot's feet then the robot is stable (the robot will not rotate on an edge of its feet and fall). The robots that use this criterion need to be fully actuated to be able to control the position of the ZMP. This very widely applied control strategy selects the trajectory of locomotion such that the ZMP criterion is satisfied.

Kajita et al. [Kajita et al., 2003] showed how the 3D LIP model with external torques resembles the a cart-pole system. The equation of motion of this system can be rewritten to consider the ZMP. With this mathematical framework, it is possible to combine both approaches the LIP and the ZMP control strategy. Moreover, it is possible to reduce the complexity of the robotic model to generate the walking pattern due to faster calculations. With this method, the designer needs only

to focus on static or quasi-static patterns of locomotion. As a result the gait patterns developed with this approach are slow.

In the field of computer animation, different control strategies to enable human like characters have been proposed. SIMBICON [Yin et al., 2007] is one representative example of this kind of controllers. This strategy is based on a finite state machine. Each state consists of a body pose representing target angles with respect to their parent links for all joints. Proportional derivative (PD) controllers drive the joints to the target angles. The transition between states occurs after a fixed period of time or an event, such as foot contact. With this strategy it is possible to generate controllers for several gaits that produce robust locomotion, and the information of motion capture systems can be used as a basis to develop the controller. This strategy assumes ideal torque and force sources.

The conceptual model IP provided the basic mathematical formulation for the passive dynamic walkers. Tad McGeer [McGeer, 1990b] developed these mechanical machines which were capable of stable locomotion without feedback control or energy input aside from gravity. To build machines based on these principles it is necessary to introduce an actuator that can replace the energy lost in each heel strike. The actuation can be either on the hip [Wisse and Frankenhuyzen, 2006, Geng et al., 2006] or in the ankle [Collins et al., 2005, Collins, 2001]. However a detailed analysis of this model suggested that adding energy with a push-off impulse from the stance leg just before heel strike is four times as effective as restoring energy after the collision has occurred [Kuo et al., 2002], because it simultaneously restores energy and reduces the ensuing collision. Robots based on this approach are energy efficient, but they are not robust to external perturbations

The idea of natural dynamics has motivated the formulation of new analytical control systems which can increase the basin of attraction of the one-period gaits [Westervelt et al., 2001, Tedrake et al., 2010, Tobenkin et al., 2010]. In this regard, one method that has been applied satisfactorily to cope with bipedal locomotion is the Hybrid Zero Dynamics (HZD) [Westervelt et al., 2001]. This method is based on the generation of holonomic constraints. In the case of low energy bipedal machines, these constraints are a function of the state variables evaluated when the machine is in the one-periodic gait. Using those constraints the system uses low energy actuation to continue the locomotion process. However, this method needs a complete description of the dynamics to be applied.

2.4 Control strategies for running

Some of the controllers introduced in the previous section have been extended for running. The control strategy based on simple rules and a finite state machine SIMBICON [Yin et al., 2007] can be used to generate robust running gaits. The ZMP control strategy in [Kajita et al., 2007] shows a mathematical framework to produce a running gait, although the ground clearance in the flight phase is very small and the duration is very short.

ASIMO [Sakagami et al., 2002] is one of the most famous and notable robots that uses this control framework. The last version of this platform has 57 controllable degrees of freedom, weights $48\ \mathrm{kg}$, and is $130\ \mathrm{cm}$ tall. It can run with a speed of $9\ \mathrm{km/h}$ and has a maximum walking speed of $2.7\ \mathrm{km/h}$. ASIMO has batteries of Lithium ion $51.8\ \mathrm{V}$ for an autonomy of one hour. The running behavior has been achieved thanks to highly-responsive and high-power motor drive units and light-weight highly-rigid leg structure.

QRIO [Geppert, 2004] is a robot developed by Sony that uses also the ZMP control strategy. It has 38 controllable degrees of freedom, weights $7\ \mathrm{kg}$, and is $61\ \mathrm{cm}$ tall. QRIO has an extremely advanced sense of balance that allows it to navigate unstable terrain or stand on wobbly surfaces. This robot achieved a maximum running speed of $23\ \mathrm{cm/s}$, and had an autonomy of one hour

thanks to a rechargeable battery.

As a difference with the previous robots, HRP3 [Akachi et al., 2005] only has implemented a control strategy for walking. This robot has 42 controllable degrees of freedom, weights $68\ \mathrm{kg}$, and is $160\ \mathrm{cm}$ tall. It can achieve a maximum walking speed of $2\ \mathrm{km/h}$, and it has autonomy for two hours. Even though these examples show impressive results, the gait pattern developed with this controller is not robust to external perturbations, and the energy efficiency is low [Collins and Ruina, 2005].

The Hybrid Zero Dynamics has also been extended [Sreenath, 2011] to control the compliant robot Mabel. This robot is a planar bipedal machine comprised of a torso and two legs with knees. Mabel weighs $65\ \mathrm{kg}$, and is $100\ \mathrm{cm}$ tall. The robot is mounted on a boom of radius $2.25\ \mathrm{m}$. Unlike most bipedal robots, all actuators are located in the torso to keep lightweight legs and facilitate rapid leg swinging for running. The actuated degrees of freedom of each leg do not correspond to the knee and hip angles. Instead, using a set of cable-differentials to connect two motors to the hip and knee joints, one motor controls the angle of the line connecting the hip to the toe, and the second motor controls the length or shape of the system. This controller based on the SLIP model finds the appropriate angle of attack of the leg and controls the attitude of the trunk. Preliminary results using this approach have been tested successfully on the robot showing walking, running and transitions.

The SLIP model has also been useful to generate simple rules for running controls [Raibert, 1986, Blum et al., 2010, Schmitt, 2007]. In the 1980's, Raibert introduced the idea of decoupled control laws in running robots [Raibert and Brown, 1984]. The balance and forward velocity were achieved with the development of different control laws which independently stabilized the apex height, the forward velocity, and the body attitude. The apex height controller compensates for energy losses with an impulse at each stride. The forward velocity was controlled with an angle control law, and finally the attitude controlled the position of the hip based on gyroscope and torque sensor. Schmitt [Schmitt, 2007] proposed the active energy removal control inspired by the feed-forward muscle activation utilized by cockroaches. In this approach, the energy is removed from the system by leg actuation during leg compression and is added to the system during leg extension.

The simulation study of the SLIP model presented in [Seyfarth and Geyer, 2002] showed a deadbeat control that guarantees running stability for comparably large disturbances in the ground level. This research studied how the angle of attack affects the resulting Poincaré map of the SLIP in running. An extension of this work is presented in [Ernst et al., 2012] in which besides the leg orientation, the controller changes the leg stiffness. This controller improves the robustness of the system against unforeseen ground level disturbances.

These results motivated the development of the robot Atrias [Grimes and Hurst, 2012]. This planar bipedal robot was designed to closely match the key features of the SLIP model. Each leg is a four-bar mechanism composed of lightweight carbon fiber tubes to decrease the mass. As a consequence, the total mass on the legs is around 10% of the total mass of the system. The actuation of the system is performed using two brushless DC motors placed at the hip. The motors actuate two bars of the four-bar mechanism through a large series spring. Using these motors the controller can set the leg length and the leg angle.

The deadbeat controllers found in the SLIP model have motivated the development of more theoretical approaches to generate similar results without extensive simulation of the system. In [Dai and Tedrake, 2012] a direct collocation method is proposed for designing nominal periodic trajectories that maximize a measure of robustness against uncertainty in the geometry of the ground. The application of this method produces the same deadbeat controller introduced in [Ernst et al., 2009].

2.5 Conceptual models and control strategy from the perspective of theories of embodiment

In sections 2.3, and 2.4, we introduced some of the most widely used control strategies in locomotion. The reader can identify two tendencies. One is to define a simple mathematical system in which the designer can calculate an analytical solution for the controller. The second option is a conceptual model that can reproduce a given gait. In the former, the design challenge is translated to the controllers and actuators that are going to maintain the constraints of the simple mathematical systems. In the case of the LIP model, the legs have to maintain the center of mass always at the same level above the ground even when the system is moving forward. In this control model, the leg actuators are considered as ideal force sources, and in practice this condition is satisfied only for slow speed responses.

Assuming a conceptual model for locomotion brings some challenges to the design of the controller. First, the system is nonlinear, multi-phase and with impacts. Hence, its analysis is nontrivial. Second, the controllers developed are not robust against external disturbances (i.e. control strategies based on the IP model). However the natural dynamics of the system is the most important aspect to be exploited. As it is presented in theories of embodiment, the correct selection of the morphology reduces the necessity of control [Pfeifer et al., 2007, Pfeifer and Gómez, 2009].

The other conceptual model for locomotion, the SLIP model, shows robust control strategies for running. While the SLIP model represents the basic mechanics of running the IP model cannot recreate the mechanics of walking [Full and Koditschek, 1999]. For instance, the IP model cannot reproduce the oscillatory motion of the hip [Lee and Farley, 1998] or the ground reaction forces in Walking [Pandy, 2003]. Furthermore, Geyer [Geyer et al., 2005] showed that the SLIP model can also represent walking, and demonstrated that the compliant leg is the key to reproduce the mechanics of walking and running.

From the perspective of the embodiment theory, we have to first understand the interaction between the creature and the environment. In the case of locomotion, this interaction occurs between the foot and the floor. Based on these ideas and the research results, we strongly believe that the ground reaction force is the observable we should use to explain the interaction in locomotion.

Following these arguments, we use the SLIP model as the conceptual model of locomotion. In this thesis, we show that this model can be used from the perspective of theories of embodiment to understand the interaction process, and bring light to the role of morphology in locomotion. One of the biggest challenges in this approach is the strategy to analyze the SLIP model. We need a unified mathematical framework to study the different gaits and gait transitions. Given that the SLIP model is nonlinear and multi-phase system finding such a mathematical framework is not trivial.

Besides the morphology, the embodiment theories also take information into account. Lungarella [Lungarella et al., 2005] showed a methodology to study the interaction of an embodied agent based on the quantification of information flow. Using this framework, Lungarella [Lungarella and Sporns, 2006] found that an embodied agent through coordinated and dynamically coupled sensorimotor activity, induces decreased entropy, increased mutual information, integration, and complexity. Additionally, simulated experiments on retinal cells (modeled as log-polar geometry) showed that their density and distribution work as a filter to reduce the number of inputs, and highlight information structure in sensorimotor activity.

These findings are aligned to new developments in the area of robust control. Elia [Elia and Mitter, 2001] demonstrated that when a linear control system is limited by a communication channel there is an optimal discretization of actions that is based on a logarithmic law and keeps

the system stable. This study demonstrates that the discretization of actions can be seen as a discretization in the sensor space. This implies that there is a discrete sensory system which can optimally provide good information to the controller.

This property could be exploited in the field of developmental robotics in which systems with high dimensional, multi-modal sensorimotor data are supposed to learn from the interaction with the environment. The sensory system would take into account the interrelations among the body, the control system, and the environment to implement information preprocessing that can effectively reduce the dimensionality of the control problem without decreasing the quality of the information in the sensorimotor loop.

Chapter 3

Thesis contributions

In this chapter, we present a concise introduction of the research approach used in this thesis. We discuss the models and the control strategies introduced in Ch. 2 and based on previous contributions we define four research questions. In the last section, we use the results obtained to answer the research questions from the perspective of design and control of bipedal locomotion. In the following chapters we develop each of the sections introduced herein and show the results of physical and simulation experiments.

3.1 Mathematical framework

As we mentioned in Sec. 2.5, based on theories of embodiment, we have to understand the interaction process to be able to exploit the morphology appropriately for the locomotion process. We defined the interaction process as the ground reaction forces (GRF), and we selected the SLIP model as the conceptual model for locomotion because it nicely reproduces the mechanics of walking and running [Geyer et al., 2005].

The IP model and the SLIP model have been used to describe separately walking and running. For this reason, the control schemes based on them are not easily integrable. In addition, previous studies of the SLIP model to explain both gaits (walking and running) have been performed using different Poincaré maps [Geyer, 2005]. These approaches impose boundaries between the control strategies based on its mathematical formulation.

In this thesis, we developed a new mathematical framework based on return maps in which running and walking can be analyzed using the same parameters (e.g. the state in midstance and the action selection). This representation allows us to study different periodic gaits and gait transitions in a unified perspective. We identified control strategies that can be used to endow the system with rich locomotion skills (symmetric locomotion and transitions), and its relation to morphological features. In Ch. 4, the reader can find a succinct presentation of this mathematical framework. For a more mathematical detail the reader can look at Appx. A and Appx. B.

3.2 Constraints for human like locomotion

The SLIP model has a very rich behavior. From its simulation, we even can identify gait patterns that are not supported by human experimental data [Rummel et al., 2009a]. The analyses of this model based on return maps have proven to be useful to generate robust controllers in running i.e. the deadbeat controller [Ernst et al., 2012]. This control strategy is more robust than the control strategies based on the limit cycles introduced in Sec. 2.3 such as the HZD and the simple

actuation on passive dynamic walkers. The controllers developed for walking based on HZD or passive dynamics cannot successfully maintain the gait under big disturbances.

Based on the previous results, we performed a nonperturbative analysis on the SLIP model. We look for strategies that could keep the system robust. Instead of applying robust control techniques [Dai and Tedrake, 2012], we did a study similar to [Ernst et al., 2012, Ernst et al., 2009, Seyfarth and Geyer, 2002] but with a the return map defined at midstance in which different gaits and gait transitions are assessed. With this analysis, we identified robust gaits and transitions. In our analysis we found the initial conditions in which the system can locomote. At each step the system performs a step by selecting an angle of attack from a valid continuous interval. The set of initial conditions where the system can indefinitely locomote are the robust regions. Instead of adding perturbations to the terrain to measure the robustness of the system as in [Byl and Tedrake, 2009], we considered the length of a range of valid angles of attack to produce a qualitative measure of the robustness. The robustness of a gait can be understood as inversely related to the attentional demand. If highly precise inputs are needed to continue with a gait the system must spend more resources to select an adequate action (e.g. use of detailed models, better estimation of states from noisy sensory data, more processing time; i.e. cognitive load or attention).

The selection of this control strategy reduces the possible selection of locomotion gaits and gait transitions. However the remaining gaits and transitions reproduce biomechanical observables such us the GRF, hip excursion, and gait duty factor. A consequence of this study is that the development of a transition can be explained as a result of the trade-off between robustness and energetic cost. In Ch. 5, the reader can find a concise summary of the mathematical definitions and the results of this nonperturbative analysis of the SLIP model. For a more mathematical detail the reader can look at Appx. C.

3.3 Compensation of disturbances with variation of morphological properties

Because the SLIP model is a nonlinear and multi-phase system, its analysis is hard. Based on the results of the model analysis, the generation of control strategies is strongly dependent on its parameters. For this reason any change in the parameters of the model will drastically affect the control strategy. However, experimental evidence [Moritz and Farley, 2003, Ferris and Farley, 1997, Ferris et al., 1998] shows that morphological properties are tuned to compensate for external disturbances.

Based on these ideas we studied the control strategies employed in human locomotion to compensate changes in mass. We redefine the SLIP model in terms of three non-dimensional variables. This reformulation generalizes the equation of motion, and enables comparisons of experimental data across human subjects. We performed experiments on a treadmill, and collected data for three loading conditions during walking and running for each subject. We increased the mass up to 34% for all the subjects. Experimental results confirm the idea of morphological compensation of the mass disturbance. The compensation strategy is developed based on the gait used by the subject. We show that this strategy maintains the same nondimensional SLIP model. We also show that equal nondimensional SLIP models have the same angle of attack selection. In Ch. 6, the reader can find a concise summary of the experiment, data analysis and experimental results. For a more detail description the reader can look at Appx. D.

3.4 Leg selection based on the SLIP model

Unlike the IP model, SLIP has no mass in the legs. For this reason in the SLIP model the Newton's equations do not describe the swinging dynamics of the leg. This limitation imposes the necessity of a control strategy to define the angle of attack at each touchdown or heel strike. Given that the SLIP model explains the mechanics of walking and running [Geyer et al., 2005], we assume that the SLIP model can be used as a template for the design of bipedal machines. With this purpose in mind, we analyze in simulation the effect of mass on the model.

We implemented a new model the rod-SLIP which has mass in the legs. We showed with a simulation study that when the legs have less than 5% of the total mass the SLIP predicts the leg features to induce symmetric gaits without control. In addition, assuming a human-like leg mass distribution the model predicts the total length of a human leg. In Ch. 7, the reader can find a concise summary of the models used in this simulation study. For a more detail description of the mathematical models the reader can look at Appx. E.

3.5 Implications for design and control

In Ch. 1, we introduced different control strategies used in bipedal locomotion. From this concise review we identified two different tendencies. One based on a simple mathematical system with analytical solution (LIP model and its extension to ZMP control), and another based on a simple but nonlinear multi-phase and hybrid system (IP and SLIP model). While the controllers proposed based on the SLIP model predictions of the running gait produce robust locomotion in a wide range of the phase space, the IP model has not been able to generate such robust control strategies. For this reason, the control strategies supported in the LIP model have been widely accepted and implemented in spite of the their high energy consumption and limitations in the bandwidth of the controllers (i.e. the actuators are ideal sources of force or torque only for low speed actuation).

With the new mathematical framework introduced in this thesis, we show that it is possible to generate a robust controller for running and walking using an analysis similar to [Ernst et al., 2012, Ernst et al., 2009, Seyfarth and Geyer, 2002]. In the phase space, we identify regions for robust locomotion and regions in which the system cannot stay but can go to a robust gait in one step. The models also let us define the features of the legs that we need in a system in order to reproduce the dynamics of the SLIP model.

We identify a control strategy in human locomotion based on the careful tuning of the natural length and the stiffness of the spring in the legs. In principle these features can be constant but in presence of disturbances they should change to compensate and let the same control strategy effectively drive the locomotion.

We also perform studies of information theory in linear systems and in a robotic platform. In these studies we show that we can decrease the dimensionality of a sensory input without decreasing the performance of the agent. These experiments lead to ideas on how the system should sample its state variables in order to acquire more information about its state in the most efficient manner. These ideas are going to be extended in Ch. 8. Herein, the reader can see how the results of the previous research questions bring new strategies to design and control a bipedal machine which exploits its natural dynamics to produce robust locomotion.

Chapter 4

Mathematical framework

This chapter refers to the publications [Martínez Salazar and Carbajal, 2011a, Martínez Salazar and Carbajal, 2011b] which are enclosed in Appendix A and B respectively. Herein, we show the solution to the first research question.

1. *How to study the SLIP model under the same representation to be able to tackle different gaits as well as gait transitions?*

4.1 Return Map

In the SLIP model, we represent a gait as a set of sub-models. We will call these sub-models *charts* [Guckenheimer and Johnson, 1995] or phases. Each chart represents the motion of a point mass under the influence of: only gravity (ff-chart or flight phase), gravity and a linear spring (s-chart or single stance phase), gravity and two linear springs (d-chart or double stance phase). The body of the agent is represented with a point mass, and the forces from the legs with massless linear springs. The equations of motion of these charts are introduced in [Martínez Salazar and Carbajal, 2011a]. The trajectory switches from one chart to another when an event function (a real valued function) is zero [Guckenheimer and Johnson, 1995, Piiroinen and Kuznetsov, 2008]. We define a running gait as a trajectory that switches from the s-chart to the ff-chart and back to the s-chart. A walking gait is defined as a trajectory that switches from the s-chart to the d-chart and back again to the s-chart (Fig. 4.1).

We studied the model using a return map in midstance i.e the support leg forms a right angle with the ground ($\mathcal{S} : \theta = \pi/2$). The return map based on the state of the system, the selection of the angle of attack and the gait, transforms an initial condition in the section $\mathcal{S}$ to a final condition in the section $\mathcal{S}$ if possible (Fig. 4.2). In this way, the map $\mathcal{R}_\alpha : \mathcal{S} \to \mathcal{S}$ transforms points through the evolution of the system from the s-chart to the ff-chart and back again to the s-chart using an angle of attack α. Similarly, the map $\mathcal{W}_\alpha : \mathcal{S} \to \mathcal{S}$ transforms points through the evolution of the system from the s-chart to the d-chart and back again to the s-chart using only one angle of attack α.

The study of these return maps showed that the system might not be able to intersect the section $\mathcal{S}$ i.e. the system can go from single stance phase to flight phase before the leg forms a right angle with the ground. In this situation the trajectory can cross the section $\mathcal{S}$ after the selection of a second angle of attack which is used to let the system switch from the flight phase to the single stance phase. In [Martínez Salazar and Carbajal, 2011b], the trajectories considered used only one angle of attack while in [Martínez Salazar and Carbajal, 2011b] we considered two angles of attack. In the later, we introduced the map $\mathcal{H}_{\beta,\alpha} : \mathcal{S} \to \mathcal{S}$ which transforms points

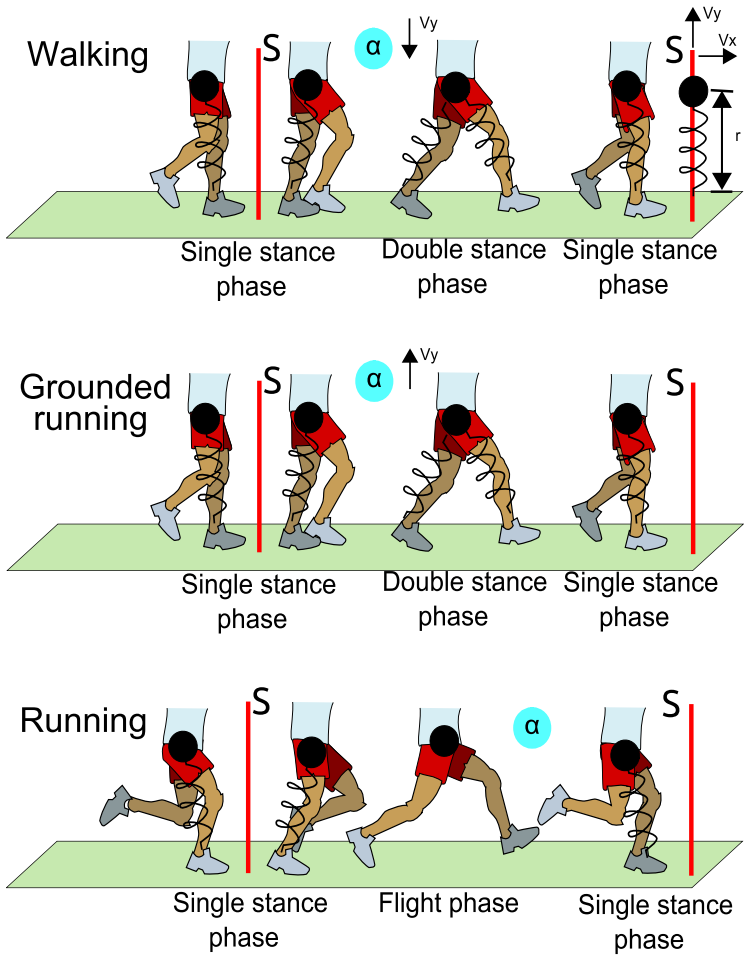

Figure 4.1: Evolution of the SLIP model for walking, grounded running and running. The different phases are indicated as well as the section S where the system is observed. The possible initial conditions in the section S are given by the total energy of the system at midstance. The evolution of the gait depends on the selection of the angle of attack α. This is the angle between the leg and the ground at touch down. Walking and grounded running share the same phases. The difference between these gaits is the direction of the vertical velocity at touch down. Walking is produced by a negative velocity while grounded running by a positive.

through the evolution of the system from the s-chart to the d-chart, using an angle of attack β, and from the ff-chart to the s-chart using an angle of attack α. This new switch during walking revealed a new gait. We named this emerging locomotion pattern *hopping gait*, since it resembles the gait used by children while running playfully (Fig. 4.3).

The state of the system in the section $\mathcal{S}$ is given by the height r and the vertical and horizontal velocity v_y and v_x respectively. For a given value of total energy E, all possible values of r, v_y and v_x lie on an ellipsoid. All initial conditions used in the simulation study have the same total energy, and given that the SLIP model is conservative, all the initial and final conditions are on the same surfaces defined by the total energy. Assuming a given total energy, we need two parameters to visualize the information from the return map. In this case, we used r and v_y.

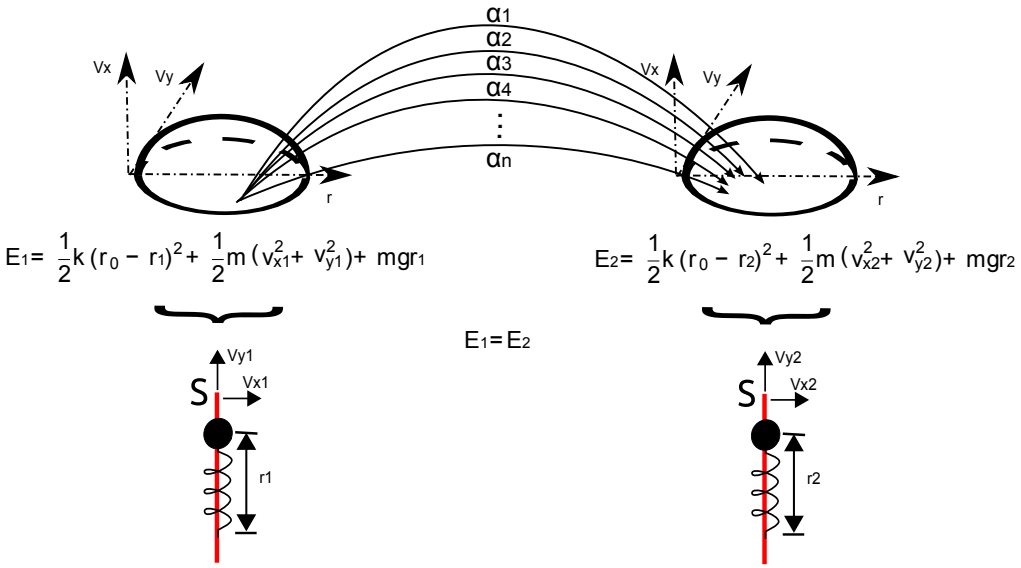

Figure 4.2: Return maps in midstance. The system is observed in the section S and the energy defines the set of possible initial conditions. The evolution of the locomotion depends on the selection of the angle of attack α and the gait pattern.

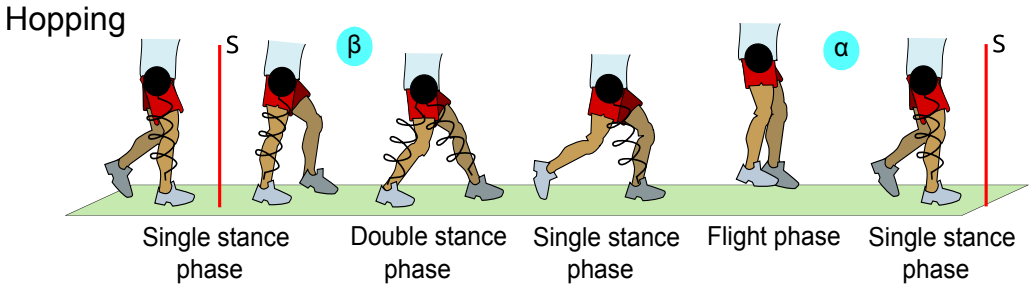

Figure 4.3: Evolution of the SLIP model for hopping. The different phases are indicated as well as the section S where the system is observed. The evolution of the gait depends on the selection of the angle of attack β, and α. The angle β is used for the system to go from the single stance phase to the double stance phase. The angle α is selected to let the system switch from the flight phase to the single stance phase.

4.2 Viability

In a physical platform the sensors and actuators have a finite resolution and are affected by noise. Thus, it is required that the angle of attack exists for a define interval. The return maps introduced in Sec. 4.1 are used to identify the initial conditions in the section $\mathcal{S}$, in which the system can take another step, selecting an angle of attack from an interval of reasonable length. The collection of points that satisfy this condition is called the viability region of a gait. Viability intuitively describes how easy it is to choose the future angle of attack. The level of ease is measured in terms of the size of the interval of angles that can be chosen to avoid a failure in the following step. In this thesis, we consider that a gait is possible for a given initial condition only if the initial condition is inside of the viability region of that gait.

4.3 Gaits and gait transitions

We identify running, walking, grounded running and hopping using the mathematical framework proposed in this thesis. Walking and grounded running have the same phases but not the same switching mechanisms. In grounded running, the vertical component of the velocity in the switch from single stance phase to double stance phase is positive while in walking is negative. For this reason, the vertical ground reaction force of grounded running does not have the "M" shape characteristic of human walking.

With this representation, we can also identify symmetric and non-symmetric gaits. The former can be produced when an initial condition in the section $\mathcal{S}$ with $v_y = 0$ can be mapped back to itself through the careful selection of an angle of attack. This symmetric gait will produce the same ground reaction force with both legs. The non-symmetric gaits in contrast do not have the same ground reaction forces with both legs. As it is shown in [Martínez Salazar and Carbajal, 2011a] with this representation we can propose control laws to bring the system from a non-symmetric gait to a symmetric gait by selecting the angle of attack. In addition, the regions where this control strategy can be used cover nearly the entire phase space. Thus, control policies with variable angle of attack can render stable almost any initial condition.

The transitions are possible in the SLIP model under this representation. To produce gait transitions the system has to leave the current symmetric gait. In this process the system performs a few steps with the same gait but non-symmetric until the system is in a region in the section $\mathcal{S}$ in which it is possible to perform another non-symmetric gait. In this condition, the system performs the new non-symmetric gait until there is a valid angle of attack that brings the system to the symmetric new gait. We showed some examples of this process in [Martínez Salazar and Carbajal, 2011a].

We extended the repertoire of gaits represented by the SLIP model, when we redefined the conditions for valid locomotion and permit the switch from single stance phase to flight phase before the leg forms a rectangular angle with the ground. Within these new conditions, we show that hopping is a periodic pattern of locomotion with two alternating angles of attack. Moreover, the representation of this new gait is compatible with the definition of *viability*. The hopping gait can be seen as alternating between walking and running.

4.4 Conclusion

All together we have shown that the SLIP model can be easily controlled to induce transitions between gaits. To find transitions we must search for an intersection between the future of the starting region and the desired objective region. Depending on how these regions are defined, it may be the case that multiple steps are required to achieve a successful transition. This has provided a better understanding of the biomechanics of several gaits [Dickinson et al., 2000] and the advantages of compliant legs in locomotion ([Geyer et al., 2005], [Rummel et al., 2010,Rummel et al., 2009b]).

We extended this analysis to different energies as it is presented in Ch. 5. There we look at the transitions in more detail and compare them with the results of human transitions. We select different biomechanical observables to assess the quality of the predictions that the model can offer using this new mathematical framework. We also identified the set of initial conditions in which the locomotion is robust against an imprecise selection of the angle of attack. These mathematical definitions are the core of the control strategy introduced in Ch. 8.

Chapter 5

Constraints for human like locomotion

This chapter refers to the article [Martínez Salazar and Carbajal, 2013] submitted to the Journal of the Royal Society Interface, which is enclosed in Appendix C. In this study we tackle the second research questions defined in this thesis.

2. *What constraints in the model can improve the similarity of the results to experimental data?*

Harold Roberto Martínez Salazar and Juan Pablo Carbajal

Robustness: a new SLIP model based criterion for gait transitions in bipedal locomotion

Abstract *Bipedal locomotion is a phenomenon that still eludes a fundamental and concise mathematical understanding. Conceptual models that capture some relevant aspects of the process exist but their full explanatory power is not yet exhausted. In the current study, we introduce the robustness criterion which defines the conditions for stable locomotion when steps are taken with imprecise angles of attack. Intuitively, the necessity of a higher precision indicates the difficulty to continue moving with a given gait. We show that the spring-loaded inverted pendulum model, under the robustness criterion, is consistent with previously reported findings on attentional demand during human locomotion. This criterion allows transitions between running and walking, many of which conserve forward speed. Simulations of transitions predict Froude numbers below the ones observed in humans, nevertheless the model satisfactorily reproduces several biomechanical indicators such as hip excursion, gait duty factor and vertical ground reaction force profiles. Furthermore, we identify reversible robust walk-run transitions, which allow the system to execute a robust version of the hopping gait. These findings foster the spring-loaded inverted pendulum model as the unifying framework for the understanding of bipedal locomotion.*

5.1 Robustness

In Sec. 4.2 we introduced the notion of *Viability*. With this definition, we define the easiness of taking a further step during locomotion (the wider the range of angles of attack that can be used to take a step the easier it is to take that step). The concept of *robustness* is defined on top of that of viability. A robust region in the section $\mathcal{S}$ is a set of viable states that can always be mapped back into the robust region (Fig. 5.1) by the selection of a viable angle (i.e. it must be selected from an interval of at least $\Delta\alpha$). This assumes that the controller can select an angle of attack for each step. In particular, this includes constant angle of attack policies and some of the self-stable regions identified in [Seyfarth et al., 2002] belong to a robust region. However, this does not mean that

the system remains in the self-stable region for each step, since that would imply that the angle of attack is selected precisely. Instead, robustness implies that if the system was in that region at time t, it can remain close to it, even if the angles are selected with finite resolution.

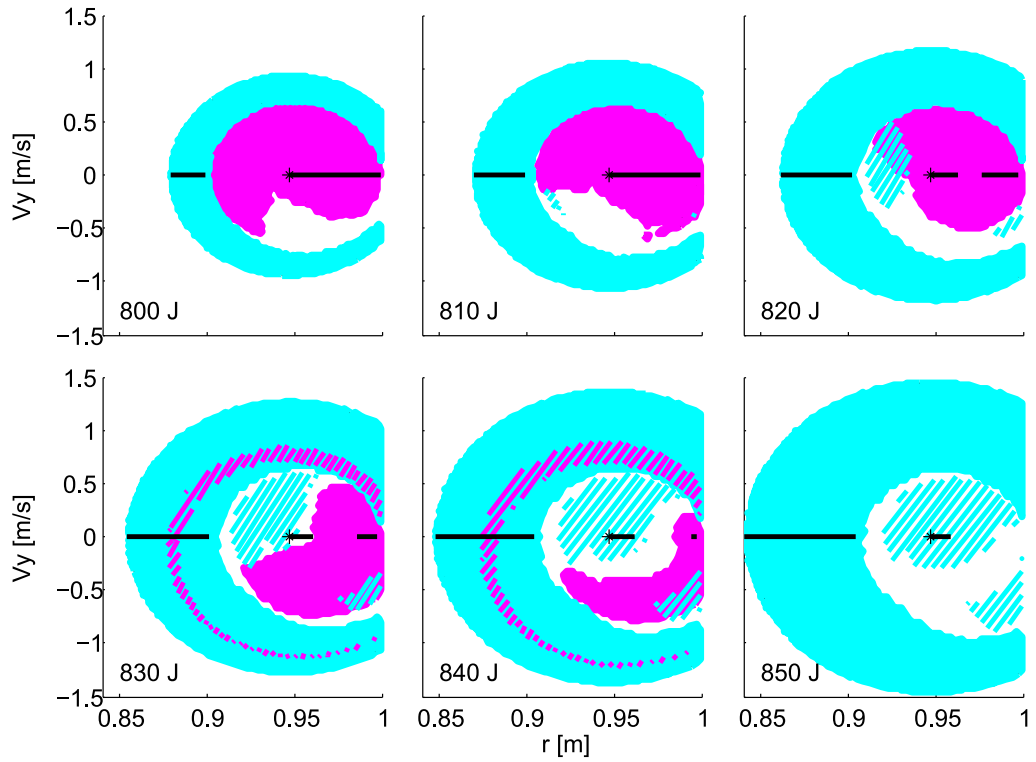

Figure 5.1: (Color online) Robust regions in the section $\mathcal{S}$. In all panels, the black star in the center of the sphere represents the maximum horizontal velocity. The solid line shows the set of initial conditions in which a gait can be periodic and symmetric. The (blue) light gray color represents the robust region of running. The (magenta) dark gray color represents the robust walking region. The shaded regions are one step robust transitions regions. The (blue) light gray shaded area is the region that using walking let the system to go to the robust running region. The (magenta) dark gray shaded area is the region that using running let the system to go to the robust walking region. The robust regions and robust transitions are calculated using intervals of at least 1° for the angle of attack.

With this approach, we performed a nonperturbational analysis of the SLIP model similar to [Ernst et al., 2012, Ernst et al., 2009, Seyfarth and Geyer, 2002] but with the return map introduced in 4.1. With this analysis, we look for a set of intervals of angles of attack that maintain the system performing a gait indefinitely. Our analysis is different from the one in [Byl and Tedrake, 2009], because we do not add perturbations to the terrain to produce a qualitative measure of the robustness of a limit cycle. Instead, we used the angles of attack interval size as a measure of robustness: the bigger the interval the more robust the gait for that initial condition. The robustness of a gait can also be understood as inversely related to the attentional demand.

5.2 Gaits and gait transitions with robustness

The SLIP model can generate several gaits. Some of them are not supported by human experimental data such as grounded running [Rummel et al., 2009a]. The Robustness criterion reduces the possible gaits to the ones that are supported by human experimental data (running, walking and hopping). In addition, robust walking exists only at low locomotion energies, while running increases robustness for higher energies. These observations are consistent with the experimental results reported in [Abernethy et al., 2002], where it was shown that imposed fast walking required higher attention than running at similar speeds. Furthermore, normal switching between gaits did not require high attentional demand.

As shown in [Martínez Salazar and Carbajal, 2013] the symmetric gait region is not continuous. Based on the energy, we can identify one, two or no regions in the section $\mathcal{S}$ where a symmetric gait can be performed. Furthermore, the robust region does not enclose all the different symmetric regions. For high energy levels in the walking gait the robust region contains the symmetric walking with the lowest forward speed. Due to these facts, at energies close to 840 J, the speed of symmetric robust walking and running match. For higher energies the gait transition is imminent, since the only robust gait remaining is symmetric running.

Assuming that during locomotion the fastest robust gait patterns are preferred over slower or non-robust ones, we see that for energies below 840 J walking is the gait of choice and for energies above that value running would be chosen. Therefore, we study viable transitions at 840 J and compare them with results from an experiment on human gait transition. We define admissible transitions using the concept of viability (Sec. 4.2) (only when all angles of attack used in the process can be chosen from an interval of length $\Delta\alpha$).

The biomechanical observables used to compare our results with experimental data are: *Froude number*, *hip excursion*, *gait duty factor*, and *vertical ground reaction forces*. The Froude number is the ratio between the weight and the centripetal force ${}^{w^2 l_o}/_{g}$, where g is the acceleration due to gravity, l_o is the natural length of the leg and w is the angular velocity of the body around the foot in contact with the ground. Hip excursion denotes the amplitude of vertical oscillations of the hip. The gait duty factor is the fraction of the total duration of a gait cycle in which a given foot is on the ground. The vertical ground reaction force is the vertical component of the normal force exerted by the ground. We compare all our simulations against the experimental data reported in Figure 2 of [Ivanenko et al., 2011], we will refer to this data as "experimental data" or "the experiment".

Ground reaction forces prior to the transition from walking to running have three main characteristics [Li and Hamill, 2002]. Firstly, they present an asymmetric double bell-shaped profile. Secondly, the earlier peak becomes bigger than the later one and, thirdly the depression between the peaks becomes more accentuated in the last step of walking, exactly before the transition. In the case of the transition from running to walking, it was reported that the vertical ground reaction forces decrease during the steps prior to the transition. The simulation experiments show transitions that match the change in amplitude that was observed in the experiment. All cases qualitatively match the characteristics of the ground reactions reported in [Li and Hamill, 2002]. The decrement in the force of the last running step is due to the support of the second foot. A reduction of the peak in more than one step appears only in the case where we matched the hip excursion of the experimental data.

In the simulations of this model, the Froude number of all these transitions are lower than 0.5, this reflects the fact that the simulations have lower forward speeds (v_x) than those observed in humans. The transitions that can be simulated, permit the matching of the relative change in hip excursion (Δr) measured in the experiment. In all simulated transitions the duty factor is qualitatively well reproduced. The selection of the angle of attack is qualitatively similar to what we found in the experimental case: the system moves progressively from one gait to the other,

changing the angle of attack at each step. However, the oscillation of the hip before and after the simulated transitions presents a change of phase ($\Delta\phi$) that not always coincide with what is observed in reality.

We identify a transition region in robust walking where the system can go in one step to robust running. Among the states in this transition region, there are some that are mapped directly into the transition region of robust running. By selecting alternatively the right angles of attack, the system can sequentially walk and run, producing the hopping gait.

5.3 Conclusion

Our findings indicate that robustness can play an important role in inducing gait transitions, complementing the usual view focused solely on energy expenditure. The robustness criterion is analogous to the attentional demand during locomotion and may play an important role in deciding the gait transition events. To our knowledge this is the first time such a criterion is included in a numerical model of locomotion. The SLIP model can be used as a conceptual model to explain many aspects of bipedal locomotion such as the mechanics of running, walking, hopping and gait transitions. The mathematical definitions introduced in this chapter are used to calculate the controller presented in Ch. 8. In Ch. 6 we introduce new ideas in how to use the morphology to compensate for changes in the system and therefore exploit the same control strategy. In Ch. 7, we show the conditions in which a leg with mass can be used to produce trajectories similar to the ones found in the SLIP model.

Chapter 6

Compensation of disturbances with variation of morphological properties

This chapter refers to the article [Martínez Salazar, 2013a] submitted to the Journal of Experimental Biology, which is enclosed in Appendix D. In this study we address the third research questions defined in this thesis.

3. *Is it possible that in human locomotion the SLIP model is a template and how are the perturbations handled?*

Harold Roberto Martínez Salazar

Covariation of Body Parameters Compensates for Mass Disturbances in Human Locomotion

Abstract *In this paper, we introduce an experimental study with human subjects. We performed the experiment on a treadmill, and collected data for three loading conditions during walking and running. We adopted the Spring Loaded Inverted Pendulum (SLIP) model as a mathematical framework to realize the data analysis. This model has been used in the literature to explain the dynamics of a wide variety of gaits. In contrast with previous studies, we redefine the SLIP model in terms of three non-dimensional variables related to the stiffness, the time and the distance. This reformulation generalizes the equation of motion, and allows comparisons across subjects. Results show that there is a compensation for the change of mass that can be explained in terms of the dimensionless parameters of the model. A direct consequence of the mass compensation is that the control strategy of the gaits does not have to change. We strongly believe that this analysis can be extended to study other important aspects of human gaits.*

6.1 Experiment and data analysis

We measured kinetic data using a split-belt force treadmill. The force plates underneath the frame measured GRFs and moments in three axes for four subjects. For all subjects, we collected data during three treadmill walking and running trials. In the walking condition the speed was held constant at $1.5\ \mathrm{m/s}$ for all trials. In the first trial all subjects walked normally on the treadmill for $60\ \mathrm{s}$. In the second trial all subjects walked with a weighted belt with $9.3\ \mathrm{kg}$ for $60\ \mathrm{s}$. In the third trial all subjects walked with a weighted belt and a weighted vest with $20.5\ \mathrm{kg}$ for $60\ \mathrm{s}$. In the running condition the speed was held constant at $2.5\ \mathrm{m/s}$ for all trials. In the running experiment

we followed the same mass variations and locomotion time used in the walking experiment. Subjects were given rest periods of up to 3 minutes between trials in both conditions.

We can define the non-dimensional distance $\hat{l}$ as $\hat{l} = l/r_0$, where l is a dimensional distance and r_0 is the natural length of the spring, and the dimensionless time $\hat{t}$ as $\hat{t} = t\sqrt{g/r_0}$, where t is time, g is gravity and r_0 is the natural length of the spring. Using these relations we can convert the velocities ($\dot{\hat{l}} = \dot{l}/\sqrt{gr_0}$), and accelerations ($\ddot{\hat{l}} = \ddot{l}/g$) to the non-dimensional space. With these definitions we can rewrite all the previous differential equations of the SLIP model in the dimensionless space. The result of the reformulated system is that the single stance phase and the double stance phase require the same dimensionless parameters. Therefore, we need only three parameters (non-dimensional stiffness $\hat{k} = \frac{kr_0}{gm}$, non-dimensional time $\hat{t} = t\sqrt{g/r_0}$, and non-dimensional length $\hat{l} = l/r_0$) to represent any gait based on the SLIP model.

6.2 Results

In the non-dimensional space the GRF of each subject in the walking experiment is similar. For each subject the three different trials seem to overlap showing the same profile of force in the vertical and horizontal direction. In the running experiment the result is not the same. For all the subjects, the bigger the mass the shorter the flight phase. For this reason, the duty factor increases as a function of the weight. Furthermore, the dimensionless vertical GRF magnitude changes as a function of the mass: the bigger the mass the smaller the peak force.

We selected as a quality measure of the fitting the squared error between the experimental GRF and the GRF generated by the model. The fitting procedure shows that the model can represent the experimental data with an error lower than 1%. The change in the mass for all the subjects through the experiments is around 33%, however the angle of attack (control strategy) changes less than 2.67% in walking and less than 4.58% in running. The fitting procedure assumes a symmetric gait, for this reason the same angle of attack is used for both legs. The experimental data of subject two shows that this assumption is close to the reality even when the human locomotion is clearly asymmetric. In addition, in the running gait, the vertical GRF sometimes has a notch. However, despite these sources of error, the SLIP model can reproduce the experimental data with an average error of 0.45% for walking and 0.63% for running.

We use the parameters from the fitting procedure to measure the similarity between the experimental trials. To analyze the results across all subjects, we compare the changes of the dimensionless SLIP parameters against the changes of mass. Results show that in the walking experiment the dimensionless constant of elasticity $\frac{kr_0}{gm}$ is maintained constant even when there are increments in the mass m. In general the stiffness compensates for the changes on the mass. This occurs because the constant of elasticity grows almost in the same proportion as the mass. However, the compensation can also be produced by the joint action of the stiffness and natural length r_o.

In the running experiment, there is a compensation for the changes in mass however this compensation is not as strong as in walking. Furthermore, the compensation is not carried out by the stiffness but by an increment in the natural length of the leg. The stiffness in the running trials do not increase, on the contrary it is reduced when the subject has a bigger mass. The combination of these two effects, on the one hand decreases the stepping frequency, and on the other hand increases the contact time of the foot with the ground. For this reason, the increment of mass in running increases the duty factor.

6.3 Conclusion

The SLIP model can be used to represent human gaits using the general representation of three dimensionless parameters (e.g non-dimensional stiffness $\hat{k} = \frac{kr_0}{gm}$, non-dimensional time $\hat{t} = t\sqrt{g/r_0}$, and non-dimensional length $\hat{l} = l/r_0$). The combination of these quantities allows us to convert other important physical quantities to the dimensionless space like energy or force. Results showed that a compensation of the change of the mass can be explained in terms of the dimensionless SLIP model parameters. A direct consequence of the mass compensation is that the control strategy of the gaits does not have to change.

Chapter 7

Leg selection based on the SLIP model

This chapter refers to the article [Martínez Salazar, 2013b] submitted to the Journal of Theoretical Biology, which is enclosed in Appendix E. In this study we tackle the fourth research question defined in this thesis.

4. *What are the leg features that allow a system to behave like the SLIP model?*

Harold Roberto Martínez Salazar

Features of the right leg for a system based on the SLIP model

Abstract *The spring loaded inverted pendulum (SLIP) model is a conceptual model of bipedal locomotion. This model has been proposed as a unified framework to explain the dynamics of a wide variety of gaits. In this study we extend the SLIP model to the rod-SLIP model in which we consider mass in the legs. Results show that under certain conditions the rod-SLIP model can reproduce the symmetric gaits identified in the SLIP model. These conditions explain the length of a human leg and give mathematical support to the leg contraction control strategies in running. From the control perspective, the results show plausible mechanisms that biped creatures can probably use to carry out gait transitions and stable locomotion with energy efficiency, given that these mechanisms exploit the passive dynamics of the system.*

7.1 SLIP model extensions

In this study, we extend the SLIP model to study the main features of a system with mass in the legs. We look for the conditions in which the system with mass in the legs can closely reproduce the SLIP model behavior. We assumed that a leg is a rigid planar pendulum. To test our hypothesis we develop three different models. The Compound Pendulum Constraint to the SLIP model (CPC-SLIP model), the Rod Pendulum Constraint to the SLIP model (RPC-SLIP model), and the SLIP model with masses in the legs (Rod-SLIP model).

For the models with a constraint pendulum we assumed that the mass on the legs is much lower than the point mass at the hip. With this assumption, the dynamics of a legged system is basically described by the SLIP model, and the pendulum dynamics is negligible in terms of changes in the position of the center of mass. For this reason, the trajectories can be estimated from the symmetric gaits found in the SLIP model. Thus, the dynamics of the system can be described as a pendulum that moves constrained to a predefined trajectory. Using this model, we

found the appropriate pendulum which can passively match the angle of attack of the symmetric gaits. The difference between the CPC-SLIP model and the RPC-SLIP model is that the former has a pendulum that approximates the mass distribution of an extended human leg while in the latter the pendulum is a rod. The equations of motion of the system are introduced in detail in [Martínez Salazar, 2013b]. We used optimization algorithms to identify the features of the leg that allow the system to produce the symmetric gaits present in the SLIP model.

We developed another mathematical model the rod-SLIP in which the spring has a pendulum inside. With this model we investigated the relation between the mass of the leg and the point mass at the joint, which allows a SLIP model behavior. in this model we simplified the leg structure and assume a planar rod pendulum. As the SLIP model, the rod-SLIP model has three different phases. Single stance phase, double stance phase, and flight phase. The equation of motion of each phase was obtained using the Lagrangian of the system. As a difference with the SLIP model the rod-SLIP model produces impacts when it switches from single stance phase to double stance phase or from flight phase to single stance phase i.e. the leg hits the ground. We generated the model transition assuming totally inelastic conditions. In the case of a switch from single stance phase to double stance phase, we use two equations to calculate the new state of the system after the impact. One is the conservation of the linear momentum along the landing leg, and the other is the conservation of the linear momentum along the rear leg. To describe the switch from the flight phase to the single stance phase we use three equations. The conservation of the linear momentum along the landing leg, and the conservation of the angular momentum on the landing foot and on the hip. To compensate the energy losses produced by the impacts of the leg with ground the system walks and runs on an incline plane with angle α. With the rod-SLIP model, we investigated to what extent a leg with mass allows a similar behavior to the SLIP model. With this model we also applied optimization algorithms to identify the leg features that allow the rod-SLIP model to produce symmetric gait. The optimization criterion is that the gait pattern must be able to contain more than five steps. We used the results from the optimization process with the RPC-SLIP model as a first guess for the identification of the leg features in the rod-SLIP model.

7.2 Leg features based on the SLIP model

The simulation results show that the CPC-SLIP model is able to produce symmetric gaits similar to the SLIP model. In addition, symmetric walking can be produced with several pendulums whose total length is in the range of $[0.2\mathrm{m}\ 0.64\mathrm{m}]$ for most of the valid energies. In the case of symmetric running, the pendulums have two possibilities. For all the range of valid energies, the pendulum can have a value around $0.2\mathrm{m}$ and for lower energies the length of the pendulum can be bigger than $0.6\mathrm{m}$. We found a total length that allows the system to perform both gaits that is around $0.64\mathrm{m}$. This length resembles the length of the thigh and shank in the human body.

Simulation results from the rod-SLIP model show that the RPC-SLIP model accurately predicts the length of the pendulum until the mass at the legs is around 5% of the total mass in the walking and running gait. The results from walking show that the more mass in the legs, the smaller the vertical height of the hip to produce stable locomotion. Furthermore when the mass in the legs is bigger than 20% of the total mass, the bigger the total energy of the system the smaller the total length of the pendulum. In the case of running, for a mass bigger than 10% of the total mass, the total length of the pendulum is restricted to the lower bound of $0.2\mathrm{m}$.

7.3 Conclusion

In this study, we used three different models to study the role of the legs in locomotion. First, we used the SLIP model to generate all the possible symmetric gaits in the energy range $[780, 900]$J. The second model assumed a pendulum constraint to the trajectories generated by SLIP. With this model, we found the appropriate pendulums that can reproduce the SLIP trajectories. Then, we proposed the rod-SLIP model, in which we consider mass in the legs. With this model we found in simulation the mass relation between the legs and the body that reproduces the SLIP model results. We found that there is a pendulum that can be used to generate both gaits running and walking. Assuming a pendulum with human like mass distribution, we found that the pendulum resembles the human leg length. The results from this study can also be interpreted from the control perspective which brings new ideas about plausible mechanisms that biped creatures could use to carry out gait transitions and stable locomotion. These mechanisms exploit the passive dynamics of the system, thus reducing the amount of energy to control the system.

Chapter 8

Implications for control

This chapter refers to the articles [Martínez Salazar and Carbajal, 2011a,Martínez Salazar and Carbajal, 2013, Martínez Salazar, 2013a, Martínez Salazar, 2013b, Martínez Salazar et al., 2010] which are enclosed in Appendix A, C, D, E, F. In this chapter we comment on the implication of the results of this studies in the design and control of bipedal machines.

8.1 Morphological properties for locomotion

The results shown in Ch. 4, 5, and 7 are based on the SLIP model with parameters that feature the human body. The total mass of the system is $80\ \mathrm{kg}$, the elastic constant of the linear springs k is $15\ \mathrm{kNm}$, and the rest length of the linear springs r_0 is $1\ \mathrm{m}$. As introduced in Ch. 6, the SLIP model can be represented with three different dimensionless parameters (i.e. non-dimensional stiffness $\hat{k} = \frac{kr_0}{gm}$, non-dimensional time $\hat{t} = t\sqrt{g/r_0}$, and non-dimensional length $\hat{l} = l/r_0$). All the systems with identical nondimensional parameters have the same trajectories in the nondimensional space. For this reason, an effective control strategy from one of these systems can be easily adapted for any other system with the same dimensionless parameters.

The robustness criterion introduced in Ch. 5 restricts the gaits in the SLIP model. We identified that when it is consider an imprecise selection of the angle of attack the robust grounded running gait overlaps with robust walking and robust running. The imprecise action reduces the set of initial conditions in which the system can perform a robust gait. For errors of 0.5° around 92% of the initial conditions between 790J and 800J can be used to keep the system in robust locomotion. Figure 8.1 shows the control strategy computed assuming intervals of at least 0.5° for the angle of attack. The controller takes the angle in the middle of the interval used to define the robust region and the robust transitions.

The selection of the control strategy needs intensive computational simulation. For that reason, it cannot be calculated in real time. Instead of that, it is better to have the controller as a look up table that the robot can check to make a decision at each step. Bipedal machines must be able to adapt to changes in the environment and perform different tasks (e.g. carry different loads). In these cases, the template model used to develop the controller can be significantly different. To avoid a recalculation of the controller, we can use the same strategy found in humans. We can use variable compliance actuators to change the compliance of the leg and/or the natural length of the spring. This local control strategy has to maintain the dimensionless parameters of the model at a constant level. Hence, this local control only acts on the system when the mass changes or when the stiffness of the ground is comparable to the one in the leg. When these conditions are not present, the control strategy is the one presented in Fig. 8.1.

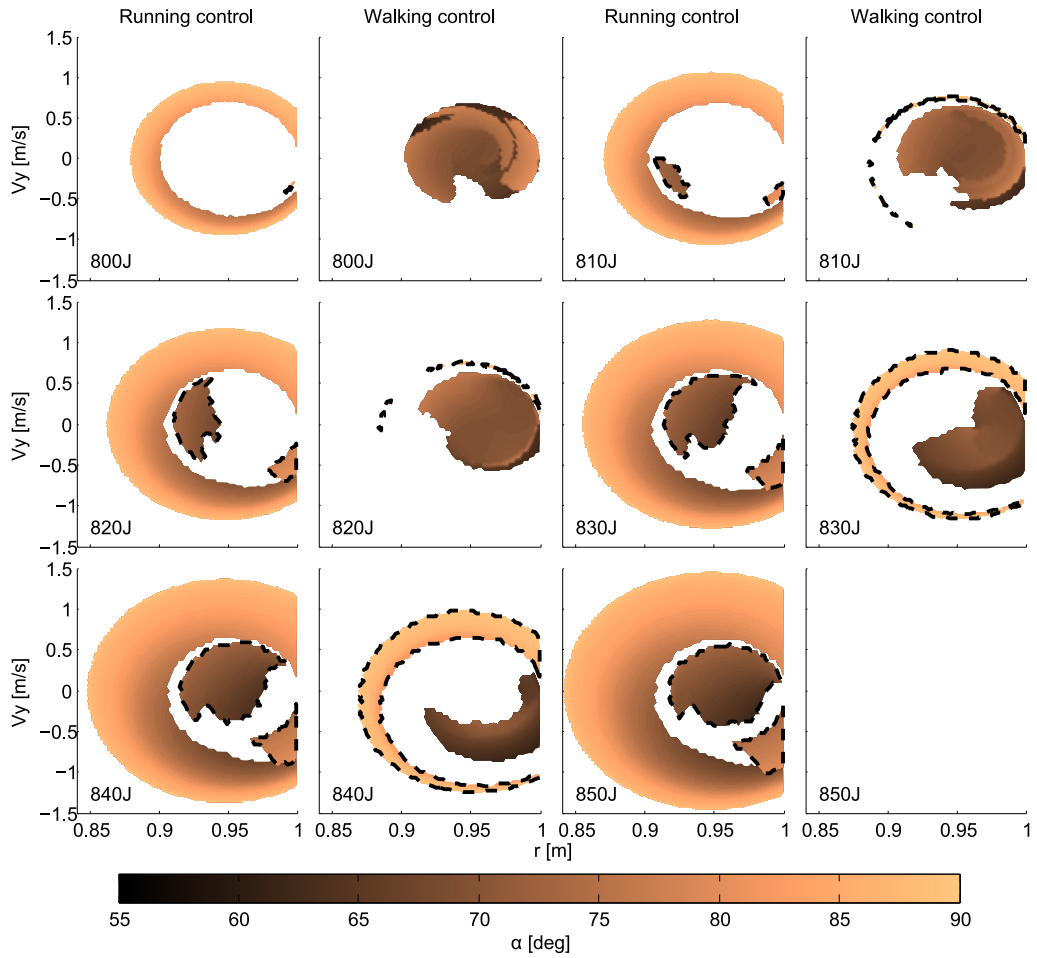

Figure 8.1: (Color online) Controller. The panels show the angle of attack for each initial conditions in the section $\mathcal{S}$. For each energy there are two different controllers. Each control presents a policy to keep the system in robust running or walking as it is indicated in the title of column. For the controller in the column running control the system should use the running gait for all the initial conditions except the ones in the region enclosed with the shaded lines. In this region the system should use walking to bring the system to the robust running region. Similarly, for the controller in the column walking control the system should use always walking except in the region enclosed with the shaded lines in which the running gait will bring the system to the walking robust region

When we used the SLIP model as a template for design, we found that for small leg masses (less than 5% of the total mass) the SLIP model can be used to predict the behavior of the system. In addition, the SLIP model can be used to define the features of the leg to exploit the passive dynamics. In this way, the energy required to keep the system in the gait can be reduced. The mass on the legs introduces impacts in the system. To compensate for these energy losses we can actuate either the hip or the ankle to restore the energy of the system [Wisse and Frankenhuyzen, 2006, Geng et al., 2006, Collins et al., 2005, Collins, 2001]. Once the energy is restored the system can use the controller proposed in Fig. 8.1 which takes into account all the phase space where the system exists. As a difference with other control strategies that exploit the passive dynamics, with this approach it is not necessary a previous identification of a limit cycle. Furthermore, the system can recover from disturbances in almost all the possible initial conditions.

From the perspective of theories of embodiment the information processing is also important. The appropriate measure of the environment can reduce the dimensionality of the system and increase the quality of the information processed by the agent [Martínez Salazar et al., 2010]. In the case of locomotion, the state information used for the action selection is the state in the midstance. In this region the small changes in height can affect drastically the policy selection. A system that implements these ideas in a real platform has to be able to estimate this state with a very high precision.

8.2 Conclusions

By taking advantage of the nondimensional parameters, we can define the machine for different dimensions using the same controller introduced in this chapter. The robot has to be able to change its morphological properties such as the stiffness or the natural length of the legs in order to compensate for changes without the necessity of recalculating the controller which is computationally expensive. The control strategy endows the system with a strategy to perform running, walking and gait transitions. The gaits and transitions allow a level of noise in the action selection, and under this condition the controller is robust in almost all the set of possible initial conditions. If the level of precision is not physically implementable, the mathematical framework introduced in Ch. $4-5$ can be used to explore how different morphological properties such as non-linear stiffness or round foot can reduce the level of precision needed for the machine.

Chapter 9

Discussion, future work and conclusions

In Table 9.1, we show a succinct description of the models we used in this study and the research questions we addressed with them. In this chapter, we present a summary of the contributions of this work to the area of biomechanics and robotics and discuss the results obtained from the analyses of these models. Finally, we show different future research questions that can be developed upon these results.

9.1 Summary of the results

The viability regions are useful to indicate where it is possible to perform a gait. The area of the viability region depends on the range of the angle of attack, the bigger the range, the smaller the viability region. The viability regions show that walking and running do not intersect.This makes the gait transition more difficult. In order to cope with this situation, we perform transitions using several steps. We found that there are some initial conditions, that under a set of angles of attack, are mapped from the viability region of one gait to the viability region of another gait.

A controller based on the proposed return map has to select the gait and the angle of attack for any initial condition in the section $\mathcal{S}$. The controller needs the data of the maps generated for each gait to select an angle of attack capable of stabilizing the system. The controller based on this representation is able to produce gait transition when it is needed. Hence, the transition regions should be known by the controller and with a model of the gait, the angle of attack required can be selected. We expect that this approach can be used to handle uneven terrain, given that these irregularities can be modeled (under certain restrictions) as a change in energy.

We proposed the robustness criterion, and with it we explore the possibility of generating locomotion patterns. The Robustness intuitively can be seen as the level of attention required to take a step; the more robust a gait is, the less attention is needed to take the next step. Our results show that the selection of the gait can be based on two criteria: efficiency, which is the selection of the gait with the highest forward speed; and robustness, which defines how easy it is to maintain the given gait. This second criterion is consistent with the experimental results of attentional demand in locomotion reported in [Abernethy et al., 2002]. Based on these criteria, walking is the best choice for energies below 840J, and running is more appropriate for higher energies. This resembles what is observed in human locomotion.

Using robustness as the leading criterion, we identify transition regions that allow the system to go from one gait to the other even in the case of imprecise angle selection. These transition

Table 9.1: Models. The table shows the models used in this thesis and the research questions they addressed.

Models	Description
SLIP 	*Unified mathematical framework:* we defined a mathematical representation to study bipedal gaits and gait transitions. *Compensation for mass disturbances:* we used the model to reproduce the ground reaction forces of a experiment. Results showed two compensation mechanisms that kept the dimensionless stiffness almost constant.
CPC-SLIP 	*Pendulum that features the human mass distribution:* with this model, we predict the human leg length. We assume that the trajectory of the center of mass is not affected by the motion of the pendulum. The trajectory of the center of mass is calculated from the SLIP-model.
RPC-SLIP 	*Rod pendulum constrained to the SLIP-model trajectory:* with this model we select the length of the rod pendulum that could generate the angle of attack necessary for symmetric gaits. This length was used as a first guess in the rod-SLIP model.
rod-SLIP 	*Effect of the mass on the leg:* with this model we studied the effect of the mass on the leg compared with the results of the RPC-SLIP model. We found the range of mass in which both models reproduce the same data.

regions are present when the symmetric robust running and walking share all the possible velocities, facilitating gait transitions. The transitions connecting robust regions are reversible and the system can oscillate between the two gaits robustly. It is in this situation where the hopping gait emerges. The robustness criterion reduces the set of possible gaits that the system can perform. Grounded running is not feasible as a locomotion pattern because it needs more precision.

The SLIP model can be written using three different non-dimensional parameters. The dimensionless analysis allows for a more general study of human locomotion based on the relations of a small set of variables that describe the dynamics. Under this representation we can study how a change of one of these variables can affect locomotion. We studied how changes in mass affect the human gait at constant speed of locomotion. We identified a compensation of the change of mass for walking and running that tries to keep the non-dimensional stiffness constant. In the case of walking, the mechanism is to increase the stiffness of the leg. With this strategy, the dimensionless stiffness is practically constant. The compensation in running uses the natural length of the leg instead of the stiffness. The findings in physiology showed that there are neural strategies to control the length and tension of muscles. These control strategies have motivated the development of muscle servo models [Houk and Rymer, 2011] to show how these fundamental aspects are carefully varied by our nervous system.

One consequence of keeping the same non-dimensional constant of elasticity in the SLIP model is that the strategy of control (constant angle of attack) does not have to change. This idea is supported by the results of the fitting process, which show that even when the change of

the mass is around 33% the constant angle of attack changes less than 4%. This is true even for the running experiment, in which the compensation of the change of the mass is about 50%.

Non-dimensional analysis using the SLIP model allow us to compare the relevant variables that describe the dynamics of human locomotion. Furthermore, we can analyze across several subjects. However, we have to remember that this is an abstraction and that the natural length r_0 is not the length of the leg but the natural length of the equivalent spring that represents the leg. The same happens with the angle of attack which is not the same as the angle between the human leg and the ground, but between the equivalent spring and the ground. We believe that a similar analysis as the one presented in this study can be developed to understand the control strategy adopted in human locomotion in the presence of other disturbances.

We extended the SLIP model and generated three new models to study the roll of a leg with mass in locomotion. The Compound Pendulum Constraint to the SLIP model (CPC-SLIP model), the Rod Pendulum Constraint to the SLIP model (RPC-SLIP model), and the SLIP model with masses in the legs (Rod-SLIP model). The CPC-SLIP model has a leg with human-like mass distribution. Simulation results show that the pendulum that can be used for running and walking has a similar length to a human leg ($0.64\mathrm{m}$) [Springs et al., 1988].

The results from the RPC-SLIP model and CPC-SLIP model indicate that in the case of symmetric walking there are several compound pendulums that can be used. This suggest that the swing controller of the leg can be calculated based on the total energy of the system and the height of the hip. Given these parameters, the controller can tune the swinging of the leg to match a pendulum with the given total length. This strategy allows for robust walking for a broad range of energies without changing the dimension of the leg. This control strategy can also be applied to the running gait and gait transitions. The results show that different lengths of a pendulum can be used to produce the same running pattern. At low energies the running gait can use a similar pendulum to the one needed in walking. For high energy levels the compound pendulum is smaller. From the perspective of a control strategy, high energy running requires a swinging controller that actuates the leg with a higher frequency emulating a reconfiguration of the leg (leg contraction). For lower energies the swinging control can select a lower frequency which emulates an extension of the leg. This can appropriately facilitate a gait transition from running to walking because in the walking gait the swinging strategy is the same.

9.2 Implications of the mathematical framework

The SLIP model is a multiphase nonlinear system. We proposed the section $\mathcal{S}$ to create return maps to study the model and propose new hypothesis about bipedal gaits and gait transitions. This strategy has proven to be powerful, however we are restricting the observation of the system to one point in the whole trajectory. The results showed that in some regions the trajectories of different gaits are very close. It would not be a surprise if trajectories of these gaits (i.e running, walking, grounded running) were crossing each other along their continuous evolution, but given that we are looking just at the section $\mathcal{S}$, this cannot be anticipated.

The definition of the switches that allow the transition from one phase to the other increase or decrease the alternatives for gait transitions. An example of this is the switch from s-chart to ff-chart before crossing the section $\mathcal{S}$. The new switch increases the range of valid angles of attacks that can be selected while the system is running. In addition, it is possible to run in regions that before where restricted to walking. At the same time, this can be interpreted as a one-step transition from walking (or grounded running) to running. It is also important to note that with these new switches the system has to select two angles of attack before it reaches the section $\mathcal{S}$ again.

The return maps used to study the SLIP model can be used to study the impact on robustness

of other morphological variables. Assuming a massless leg we can add a foot or change the nature of the spring. These changes are going to affect the dynamical system but they are not going to increase the number of state variables of the system. For that reason, we can still use the section $\mathcal{S}$ to create the return maps. In previous studies, the comparison of new morphological features was possible only after linearizations and it is not possible to compare different gaits or gait transitions [Rummel et al., 2009a]. Our proposed mathematical framework offers a better alternative to compare the performance of the system under different morphologies.

9.3 Biomechanical predictions

All transitions found using the robustness criterion produce similar results concerning the duty factor. Walking has a duty factor around 0.7 and running has a duty factor around 0.4, in accordance with experimental data. Furthermore, in all transitions from walking to running the model predicts a progressive change in the vertical component of the reaction forces, i.e. the relation between the first and the second peak of the force during the transition. This also applies to the transitions from running to walking. In particular, the ground reaction forces corresponding to transitions matching the hip excursion of the experimental data introduces a progressive reduction of the force peak in more than one step. All these results qualitatively reproduce the experimental results reported in [Li and Hamill, 2002].The robustness criterion induces an underestimation of the forward speed at gait transitions. The highest Froude number achieved using this transition strategy is around one third of the one observed in humans (0.5). This is due to the assumption of a static center of pressure. To generate a center of pressure that moves on the ground in the stance phase, we need to let the spring penetrate the ground up to 50% of its length. With this artifact the model can reproduce similar Froude numbers.

The SLIP model has proven its capability to represent several different features of human locomotion, for this reason is not surprising that it approximates the results from the experiment with different loads. The approximation errors are small, however in the running experiment the approximation error is bigger than that in the walking experiment. This happens because the SLIP model assumes a spring with a linear constant of elasticity.

The predictions of the RPC-SLIP model are supported by the simulation results from the rod-SLIP model. In the case of legs with less than 5% of the total mass, the rod-SLIP model can reproduce similar gait patterns to the ones find in the SLIP model. However, a bigger mass affects the stability and the system cannot perform the minimum number of steps required to reproduce the data from the SLIP model. In humans the thigh and the shank of both legs have around 17% of the total mass [Springs et al., 1988]. In the rod-SLIP model the increment of mass in the legs restrict the pendulum that can be selected. In the case of walking, the bigger the energy, the lower the pendulum. This is different from the results from the SLIP model, in which most of the energies can use a variety of pendulums. We believe that the possibility of selecting a wide range of pendulums can also be seen as possible swinging frequencies. For this reason, if the human walking gait follows the CPC-SLIP model we would be able to identify different stepping frequencies for a given forward velocity. If this is the case, then the selection of these frequencies can be disturbed by adding more mass in the legs. We can measure the attention demand as the effort to compensate this disturbance similar to [Abernethy et al., 2002]. We expect that when adding more mass in the legs, the range of possible stepping frequencies is going to be reduced and the attention demand to produce the gait has to increase.

To reduce the gap between simulated and experimental data we believe that the model can be extended to include the displacement of the point where the leg is in contact with the ground during the stance phase [Adamczyk et al., 2006, Whittington and Thelen, 2009]. We can do that by adding rolling feet. In addition, experimental studies have shown that human legs have a

nonlinear constant of elasticity [Dumke et al., 2010, Blum et al., 2009]. The model can be extended with biarticular springs or torsional springs similar to [Rummel and Seyfarth, 2008] or [Iida et al., 2008]. The results from this analysis can provide the appropriate morphology to the rod-SLIP model. These aspects can be a key factor to increase the stability of the system even when the mass in the legs is around 17% of the total mass.

9.4 Implication for robot design

In this thesis, we presented a mathematical framework that allows us to study bipedal locomotion using the unified view of the SLIP model. Based on the selection of a return map we are able to propose a controller that keeps the system in a robust gait for most of the phase space of the system. With the same representation we can also produce gait transitions. We exploit the natural dynamics to formulate this control strategy, and based on experimental studies we also propose how the morphology can be used to compensate for disturbances.

The SLIP model can also be used to define the appropriate legs for bipedal locomotion. Our simulation studies show new alternatives to define the controller that matches the angle of attack and the range of masses in which it is valid. However, results show that a precise action is required in order to produce a robust gait capable of recovering the system from almost any initial conditions in the phase space. In the best case, around 2% of the initial conditions cannot produce a robust gait and the system will fail. This control strategy performs close to the controllers based on the LIP model which ensures a stable walking.

The mathematical framework that has been introduced in this thesis can be used to explore other morphological properties such as the rolling foot, the nonlinear springs, other SLIP model parameters, and new switches between the phases. These exploratory studies can offer the correct conditions to produce robust locomotion over the whole phase space, exploiting the natural dynamics of the system and reducing the complexity of the control architecture.

9.5 Conclusion

In this thesis we took advantage of the perspective of hybrid dynamical systems to represent locomotion as a process generated by several charts. We introduce a return map to study the system and with this approach we discover new gaits, namely hopping and alternatives to perform gait transitions. The reported gaits and transitions exploit the passive dynamics of the system, which potentially reduces the amount of energy needed to control it. Our findings indicate that robustness can play an important role in inducing gait transitions, complementing the usual view focused solely in energy expenditure. The robustness criterion is analogous to the attentional demand during locomotion and may play an important role in inducing the gait transition events. To our knowledge this is the first time such a criterion is included in a numerical model of locomotion.

The SLIP model can be represented with three dimensionless parameters: non-dimensional stiffness $\hat{k} = \frac{kr_0}{gm}$, non-dimensional time $\hat{t} = t\sqrt{g/r_0}$, and non-dimensional length $\hat{l} = l/r_0$. The Combination of these quantities allow us to convert other important physical quantities to the dimensionless space like energy or force. We studied how the change of mass affects the human gait while keeping the locomotion speed constant. We identified a compensation of the change of the mass that can be explained in terms of the dimensionless SLIP model parameters. A direct consequence of the mass compensation is that the control strategy of the gaits does not have to change. We strongly believe that this analysis can be extended to study other important aspects of the human gait.

The SLIP model can be used to study the roll of the legs in locomotion. Based on the trajectories of symmetric gaits developed with the SLIP model, we found the appropriate pendulums that can reproduce the SLIP trajectories. Then, we proposed the rod-SLIP model, in which we consider mass in the legs. With this model, we found in simulation the mass relation between the legs and the body that reproduces the SLIP model behavior. We found a pendulum which can be used in both gaits running and walking. In addition, assuming a pendulum with human like mass distribution, we found that this pendulum resembles the human leg length. This study brings new ideas about plausible mechanisms that biped creatures could use to carry out gait transitions and stable locomotion into the research field.

Bibliography

[Abernethy et al., 2002] Abernethy, B., Hanna, A., and Plooy, A. (2002). The attentional demands of preferred and non-preferred gait patterns. *Gait Posture*, 15(3):256 – 265.

[Adamczyk et al., 2006] Adamczyk, P. G., Collins, S. H., and Kuo, A. D. (2006). The advantages of a rolling foot in human walking. *Journal of Experimental Biology*, 209(20):3953–3963.

[Akachi et al., 2005] Akachi, K., Kaneko, K., Kanehira, N., Ota, S., Miyamori, G., Hirata, M., Kajita, S., and Kanehiro, F. (2005). Development of humanoid robot hrp-3p. In *Humanoid Robots, 2005 5th IEEE-RAS International Conference on*, pages 50 –55.

[Andrews et al., 2011] Andrews, B., Miller, B., Schmitt, J., and Clark, J. (2011). Running over unknown rough terrain with a one-legged planar robot. *Bioinspir Biomim*, 6(2):026009.

[Blickhan, 1989] Blickhan, R. (1989). The spring-mass model for running and hopping. *Journal of Biomechanics*, 22(11-12):1217–1227.

[Blickhan et al., 2007] Blickhan, R., Seyfarth, A., Geyer, H., Grimmer, S., Wagner, H., and Günther, M. (2007). Intelligence by mechanics. *Philosophical Transactions of the Royal Society A: Mathematical, Physical and Engineering Sciences*, 365(1850):199–220.

[Blum et al., 2010] Blum, Y., Lipfert, S. W., Rummel, J., and Seyfarth, A. (2010). Swing leg control in human running. *Bioinspiration and Biomimetics*, 5(2):026006.

[Blum et al., 2009] Blum, Y., Lipfert, S. W., and Seyfarth, A. (2009). Effective leg stiffness in running. *Journal of Biomechanics*, 42(14):2400 – 2405.

[Byl and Tedrake, 2009] Byl, K. and Tedrake, R. (2009). Metastable walking machines. *The International Journal of Robotics Research*, 28(8):1040–1064.

[Cavagna et al., 1976] Cavagna, G. A., Thys, H., and Zamboni, A. (1976). The sources of external work in level walking and running. *Journal of Physiology*, 262:639–657.

[Cham et al., 2004] Cham, J. G., Karpick, J. K., and Cutkosky, M. R. (2004). Stride period adaptation of a biomimetic running hexapod. *The International Journal of Robotics Research*, 23(2):141–153.

[Chen et al., 2007] Chen, V., of Technology. Dept. of Electrical Engineering, M. I., and Science, C. (2007). *Passive Dynamic Walking with Knees: A Point Foot Model*. Massachusetts Institute of Technology, Department of Electrical Engineering and Computer Science.

[Collins and Ruina, 2005] Collins, S. and Ruina, A. (2005). A bipedal walking robot with efficient and human-like gait. In *Robotics and Automation, 2005. ICRA 2005. Proceedings of the 2005 IEEE International Conference on*, pages 1983 – 1988.

[Collins et al., 2005] Collins, S., Ruina, A., Tedrake, R., and Wisse, M. (2005). Efficient bipedal robots based on passive-dynamic walkers. *Science*, 307(5712):1082–1085.

[Collins, 2001] Collins, S. H. (2001). A three-dimensional passive-dynamic walking robot with two legs and knees. *Int. J. Robot. Res.*, 20(7):607–615.

[Dai and Tedrake, 2012] Dai, H. and Tedrake, R. (2012). Optimizing robust limit cycles for legged locomotion on unknown terrain. In *Decision and Control (CDC), 2012 IEEE 51st Annual Conference on*, pages 1207–1213. IEEE.

[Dickinson et al., 2000] Dickinson, M. H., Farley, C. T., Full, R. J., Koehl, M. A. R., Kram, R., and Lehman, S. (2000). How animals move: An integrative view. *Science*, 288(5463):100–106.

[Dumke et al., 2010] Dumke, C. L., Pfaffenroth, C. M., McBride, J. M., and McCauley, G. O. (2010). Relationship between muscle strength, power and stiffness and running economy in trained male runners. *Int J Sports Physiol Perform*, 5(2):249–61.

[Elia and Mitter, 2001] Elia, N. and Mitter, S. (2001). Stabilization of linear systems with limited information. *Automatic Control, IEEE Transactions on*, 46(9):1384 –1400.

[Ernst et al., 2009] Ernst, M., Geyer, H., and Blickhan, R. (2009). Spring-legged locomotion on uneven ground: a control approach to keep the running speed constant. In *International Conference on Climbing and Walking Robots (CLAWAR)*, pages 639–644. World Scientific.

[Ernst et al., 2012] Ernst, M., Geyer, H., and Blickhan, R. (2012). Extension and customization of self-stability control in compliant legged systems. *Bioinspiration & Biomimetics*, 7(4):046002.

[Ferris and Farley, 1997] Ferris, D. P. and Farley, C. T. (1997). Interaction of leg stiffness and surfaces stiffness during human hopping. *Journal of applied physiology (Bethesda, Md. : 1985)*, 82(1).

[Ferris et al., 1998] Ferris, D. P., Louie, M., and Farley, C. T. (1998). Running in the real world: adjusting leg stiffness for different surfaces. *Proceedings of the Royal Society of London. Series B: Biological Sciences*, 265(1400):989–994.

[Full and Koditschek, 1999] Full, R. J. and Koditschek, D. E. (1999). Templates and anchors: neuromechanical hypotheses of legged locomotion on land. *Journal of Experimental Biology*, 202(Pt 23):3325–3332.

[Garcia et al., 2000] Garcia, M., Chatterjee, A., and Ruina, A. (2000). Efficiency, speed, and scaling of two-dimensional passive-dynamic walking. *Dynamics and Stability of Systems*, 15(2):75–99.

[Garcia et al., 1998] Garcia, M., Chatterjee, A., Ruina, A., and Coleman, M. (1998). The simplest walking model: Stability, complexity, and scaling. *ASME Journal of Biomechanical Engineering*, 120:281–288.

[Geng et al., 2006] Geng, T., Porr, B., and Worgotter, F. (2006). A reflexive neural network for dynamic biped walking control. *Neural Comput.*, 18(5):1156–1196.

[Geppert, 2004] Geppert, L. (2004). Qrio, the robot that could. *Spectrum, IEEE*, 41(5):34 – 37.

[Geyer, 2005] Geyer, H. (2005). *Simple models of legged locomotion based on compliant limb behavior*. PhD thesis.

[Geyer et al., 2005] Geyer, H., Seyfarth, A., and Blickhan, R. (2005). Spring-mass running: simple approximate solution and application to gait stability. *Journal of theoretical biology*, 232(3):315–28.

[Goswami et al., 1998] Goswami, A., Thuilot, B., and Espiau, B. (1998). A study of the passive gait of a compass-like biped robot: Symmetry and chaos. *INTERNATIONAL JOURNAL OF ROBOTICS RESEARCH*, 17:1282–1301.

[Grimes and Hurst, 2012] Grimes, J. A. and Hurst, J. W. (2012). The design of atrias 1.0 a unique monopod, hopping robot. In *Proceedings of the 2012 International Conference on Climbing and walking Robots and the Support Technologies for Mobile Machines*, pages 548–554.

[Guckenheimer and Johnson, 1995] Guckenheimer, J. and Johnson, S. (1995). Planar hybrid systems. In *Hybrid Systems II*, pages 202–225, London, UK. Springer-Verlag.

[Holmes et al., 2006] Holmes, P., Full, R. J., Koditschek, D., and Guckenheimer, J. (2006). The dynamics of legged locomotion: Models, analyses, and challenges. *SIAM Rev.*, 48(2):207–304.

[Houk and Rymer, 2011] Houk, J. C. and Rymer, W. Z. (2011). *Neural Control of Muscle Length and Tension*. John Wiley and Sons, Inc.

[Hyon and Mita, 2002] Hyon, S.-H. and Mita, T. (2002). Development of a biologically inspired hopping robot. In *Robotics and Automation, 2002. Proceedings. ICRA'02. IEEE International Conference on*, volume 4, pages 3984–3991. IEEE.

[Iida et al., 2008] Iida, F., Rummel, J., and Seyfarth, A. (2008). Bipedal walking and running with spring-like biarticular muscles. *Journal of Biomechanics*, 41(3):656–667.

[Ivanenko et al., 2011] Ivanenko, Y. P., Labini, F. S., Cappellini, G., Macellari, V., McIntyre, J., and Lacquaniti, F. (2011). Gait transitions in simulated reduced gravity. *J. Appl. Physiol.*, 110(3):781–8.

[Kajita et al., 2003] Kajita, S., Kanehiro, F., Kaneko, K., Fujiwara, K., Harada, K., Yokoi, K., and Hirukawa, H. (2003). Biped walking pattern generation by using preview control of zero-moment point. In *Robotics and Automation, 2003. Proceedings. ICRA'03. IEEE International Conference on*, volume 2, pages 1620–1626. IEEE.

[Kajita et al., 2001] Kajita, S., Kanehiro, F., Kaneko, K., Yokoi, K., and Hirukawa, H. (2001). The 3d linear inverted pendulum mode: A simple modeling for a biped walking pattern generation. In *Intelligent Robots and Systems, 2001. Proceedings. 2001 IEEE/RSJ International Conference on*, volume 1, pages 239–246. IEEE.

[Kajita et al., 2007] Kajita, S., Nagasaki, T., Kaneko, K., and Hirukawa, H. (2007). Zmp-based biped running control. *Robotics & Automation Magazine, IEEE*, 14(2):63–72.

[Kajita et al., 1992] Kajita, S., Yamaura, T., and Kobayashi, A. (1992). Dynamic walking control of a biped robot along a potential energy conserving orbit. *Robotics and Automation, IEEE Transactions on*, 8(4):431–438.

[Kimura et al., 2007] Kimura, H., Fukuoka, Y., and Cohen, A. H. (2007). Adaptive dynamic walking of a quadruped robot on natural ground based on biological concepts. *Int. J. Rob. Res.*, 26:475–490.

[Kuo et al., 2002] Kuo, A. D. et al. (2002). Energetics of actively powered locomotion using the simplest walking model. *TRANSACTIONS-AMERICAN SOCIETY OF MECHANICAL ENGINEERS JOURNAL OF BIOMECHANICAL ENGINEERING*, 124(1):113–120.

[Kwan and Hubbard, 2007] Kwan, M. and Hubbard, M. (2007). Optimal foot shape for a passive dynamic biped. *Journal of theoretical biology*, 248(2):331–339.

[Lee and Farley, 1998] Lee, C. R. and Farley, C. T. (1998). Determinants of the center of mass trajectory in human walking and running. *Journal of Experimental Biology*, 201(21):2935–2944.

[Li and Hamill, 2002] Li, L. and Hamill, J. (2002). Characteristics of the vertical ground reaction force component prior to gait transition. *RQES*, 73(3):229–237.

[Lungarella et al., 2005] Lungarella, M., Pegors, T., Bulwinkle, D., and Sporns, O. (2005). Methods for quantifying the informational structure of sensory and motor data. *Neuroinformatics*, 3:243–262. 10.1385/NI:3:3:243.

[Lungarella and Sporns, 2006] Lungarella, M. and Sporns, O. (2006). Mapping information flow in sensorimotor networks. *PLoS Comput Biol*, 2(10):e144.

[Martínez Salazar, 2013a] Martínez Salazar, H. R. (2013a). Covariation of body parameters compensates for mass disturbances in human locomotion.

[Martínez Salazar, 2013b] Martínez Salazar, H. R. (2013b). The slip model predicts an anthropometric leg for walking and running.

[Martínez Salazar and Carbajal, 2011a] Martínez Salazar, H. R. and Carbajal, J. P. (2011a). Exploiting the passive dynamics of a compliant leg to develop gait transitions. *Phys. Rev. E*, 83:066707.

[Martínez Salazar and Carbajal, 2011b] Martínez Salazar, H. R. and Carbajal, J. P. (2011b). From walking to running a natural transition in the slip model using the hopping gait. In *Robotics and Biomimetics (ROBIO), 2011 IEEE International Conference on*, pages 2163 – 2168.

[Martínez Salazar and Carbajal, 2013] Martínez Salazar, H. R. and Carbajal, J. P. (2013). Robustness: a new slip model based criterion for gait transitions in bipedal locomotion.

[Martínez Salazar et al., 2010] Martínez Salazar, H. R., Lungarella, M., and Pfeifer, R. (2010). On the influence of sensor morphology on eye motion coordination. In *Development and Learning (ICDL), 2010 IEEE 9th International Conference on*, pages 238 –243.

[McGeer, 1990a] McGeer, T. (1990a). Passive Bipedal Running. *Proceedings of The Royal Society of London. Series B, Biological Sciences (1934-1990)*, 240:107–134.

[McGeer, 1990b] McGeer, T. (1990b). Passive dynamic walking. *The International Journal of Robotics Research*, 9(2):62–82.

[McGeer, 1990c] McGeer, T. (1990c). Passive walking with knees. pages 1640–1645.

[McMahon and Cheng, 1990] McMahon, T. A. and Cheng, G. C. (1990). The mechanics of running: how does stiffness couple with speed? *Journal of Biomechanics*, 23:65–78.

[Mochon and McMahon, 1980] Mochon, S. and McMahon, T. A. (1980). Ballistic walking. *Journal of Biomechanics*, 13(1):49–57.

[Moritz and Farley, 2003] Moritz, C. T. and Farley, C. T. (2003). Human hopping on damped surfaces: strategies for adjusting leg mechanics. *Proceedings. Biological sciences / The Royal Society*, 270(1525):1741–6.

[Owaki et al., 2008] Owaki, D., Osuka, K., and Ishiguro, A. (2008). On the embodiment that enables passive dynamic bipedal running. In *Robotics and Automation, 2008. ICRA 2008. IEEE International Conference on*, pages 341–346.

[Owaki et al., 2009] Owaki, D., Osuka, K., and Ishiguro, A. (2009). Understanding the common principle underlying passive dynamic walking and running. In *Intelligent Robots and Systems, 2009. IROS 2009. IEEE/RSJ International Conference on*, pages 3208–3213.

[Pandy, 2003] Pandy, M. G. (2003). Simple and complex models for studying muscle function in walking. *Philosophical Transactions of the Royal Society of London. Series B: Biological Sciences*, 358(1437):1501–1509.

[Pfeifer et al., 2007] Pfeifer, R., Al, E., Pfeifer, R., Lungarella, M., and Iida, F. (2007). Self-organization, embodiment, and biologically inspired robotics. *Science*, pages 1088–1093.

[Pfeifer and Gómez, 2009] Pfeifer, R. and Gómez, G. (2009). Creating brain-like intelligence. chapter Morphological Computation — Connecting Brain, Body, and Environment, pages 66–83. Springer-Verlag, Berlin, Heidelberg.

[Piiroinen and Kuznetsov, 2008] Piiroinen, P. T. and Kuznetsov, Y. A. (2008). An event-driven method to simulate Filippov systems with accurate computing of sliding motions. *ACM T. Math. Software*, 34(3):1–24.

[Poulakakis and Grizzle, 2009] Poulakakis, I. and Grizzle, J. W. (2009). The spring loaded inverted pendulum as the hybrid zero dynamics of an asymmetric hopper. *Automatic Control, IEEE Transactions on*, 54(8):1779–1793.

[Pratt et al., 2006] Pratt, J., Carff, J., Drakunov, S., and Goswami, A. (2006). Capture point: A step toward humanoid push recovery. In *Humanoid Robots, 2006 6th IEEE-RAS International Conference on*, pages 200–207. IEEE.

[Raibert, 1986] Raibert, M. H. (1986). *Legged robots that balance*. Massachusetts Institute of Technology, Cambridge, MA, USA.

[Raibert and Brown, 1984] Raibert, M. H. and Brown, Jr., H. B. (1984). Experiments in balance with a 2D one-legged hopping machine. *ASME Transactions Journal of Dynamic Systems and Measurement Control B*, 106:75–81.

[Ruina et al., 2005] Ruina, A., Bertram, J. E., and Srinivasan, M. (2005). A collisional model of the energetic cost of support work qualitatively explains leg sequencing in walking and galloping, pseudo-elastic leg behavior in running and the walk-to-run transition. *Journal of theoretical biology*, 237(2):170–192.

[Rummel et al., 2010] Rummel, J., Blum, Y., Maus, H. M., Rode, C., and Seyfarth, A. (2010). Stable and robust walking with compliant legs. In *2010 IEEE International Conference on Robotics and Automation*, pages 5250–5255. IEEE.

[Rummel et al., 2009a] Rummel, J., Blum, Y., and Seyfarth, A. (2009a). From walking to running. In *Autonome Mobile Systeme 2009*, pages 89–96. Springer.

[Rummel et al., 2009b] Rummel, J., Blum, Y., and Seyfarth, A. (2009b). From walking to running. In *Autonome Mobile Systeme*, pages 89–96, Berlin, Heidelberg. Springer Berlin Heidelberg.

[Rummel and Seyfarth, 2008] Rummel, J. and Seyfarth, A. (2008). Stable running with segmented legs. *The International Journal of Robotics Research*, 27(8):919–934.

[Rummel and Seyfarth, 2010] Rummel, J. and Seyfarth, A. (2010). Passive stabilization of the trunk in walking. In *International Conference on Simulation, Modeling and Programming for Autonomous Robots*, pages 127–136.

[Sakagami et al., 2002] Sakagami, Y., Watanabe, R., Aoyama, C., Matsunaga, S., Higaki, N., and Fujimura, K. (2002). The intelligent asimo: system overview and integration. In *Intelligent Robots and Systems, 2002. IEEE/RSJ International Conference on*, volume 3, pages 2478 – 2483 vol.3.

[Schmitt, 2007] Schmitt, J. M. (2007). Incorporating energy variations into controlled sagittal plane locomotion dynamics. *ASME Conference Proceedings*, 2007(4806X):1627–1635.

[Seyfarth and Geyer, 2002] Seyfarth, A. and Geyer, H. (2002). Natural control of spring-like running-optimized self-stabilization. In *Proceedings of the Fifth International Conference on Climbing and Walking Robots (CLAWAR 2002), Professional Engineering Publishing Limited, London*, pages 81–85.

[Seyfarth et al., 2002] Seyfarth, A., Geyer, H., Günther, M., and Blickhan, R. (2002). A movement criterion for running. *Journal of biomechanics*, 35(5):649–655.

[Siegler et al., 1982] Siegler, S., Seliktar, R., and Hyman, W. (1982). Simulation of human gait with the aid of a simple mechanical model. *J. Biomech.*, 15(6):415 – 425.

[Springs et al., 1988] Springs, Y., Project, A. R., Army, U. S., Force, U. S. A., Navy, U. S., Panel, T.-S. A. R., and Committee, T.-S. (1988). *Anthropometry and Mass Distribution for Human Analogues: Military male aviators*. Number v. 1. Anthropology Research Project.

[Sreenath, 2011] Sreenath, K. (2011). *Feedback control of a bipedal walker and runner with compliance*. PhD thesis, The University of Michigan.

[Tedrake et al., 2010] Tedrake, R., Manchester, I. R., Tobenkin, M., and Roberts, J. W. (2010). LQR-trees: Feedback Motion Planning via Sums-of-Squares Verification. *The International Journal of Robotics Research*, 29(8):1038–1052.

[Tobenkin et al., 2010] Tobenkin, M. M., Manchester, I. R., and Tedrake, R. (2010). Invariant funnels around trajectories using sum-of-squares programming. Technical Report arXiv:1010.3013. Comments: 7 pages, 3 figures.

[Tsagarakis et al., 2007] Tsagarakis, N. G., Metta, G., Sandini, G., Vernon, D., Beira, R., Becchi, F., Righetti, L., Santos-Victor, J., Ijspeert, A. J., Carrozza, M. C., and et al. (2007). icub: the design and realization of an open humanoid platform for cognitive and neuroscience research. *Advanced Robotics*, 21(10):1151–1175.

[Tschacher and Bergomi, 2011] Tschacher, W. and Bergomi, C. (2011). *The Implications of Embodiment: Cognition and Communication*. Imprint Academic.

[Valero-Cuevas et al., 2009] Valero-Cuevas, F., Hoffmann, H., Kurse, M., Kutch, J., and Theodorou, E. (2009). Computational models for neuromuscular function. *Biomedical Engineering, IEEE Reviews in*, 2:110 –135.

[Vukobratovic and Borovac, 2004] Vukobratovic, M. and Borovac, B. (2004). Zero-moment point - thirty five years of its life. *I. J. Humanoid Robotics*, 1(1):157–173.

[Westervelt et al., 2001] Westervelt, E. R., Grizzle, J., and Koditschek, D. E. (2001). Hybrid zero dynamics of planar biped walkers. *IEEE Transactions on Automatic Control*, 48:42–56.

[Whittington and Thelen, 2009] Whittington, B. R. and Thelen, D. G. (2009). A simple mass-spring model with roller feet can induce the ground reactions observed in human walking. *J Biomech Eng*, 131(1):011013.

[Wisse, 2005] Wisse, M. (2005). Three additions to passive dynamic walking: actuation, an upper body, and 3d stability. *International Journal of Humanoid Robotics*, 2(04):459–478.

[Wisse and Frankenhuyzen, 2006] Wisse, M. and Frankenhuyzen, J. V. (2006). Design and construction of mike; a 2-d autonomous biped based on passive dynamic walking. In *Adaptive Motion of Animals and Machines*, pages 143–154, Tokyo. Springer-Verlag.

[Wisse et al., 2004] Wisse, M., Schwab, A., and Van Der Helm, F. (2004). Passive dynamic walking model with upper body. *Robotica*, 22(6):681–688.

[Yin et al., 2007] Yin, K., Loken, K., and van de Panne, M. (2007). Simbicon: simple biped locomotion control. In *ACM Transactions on Graphics (TOG)*, volume 26, page 105. ACM.

[Zajac et al., 2003] Zajac, F. E., Neptune, R. R., and Kautz, S. A. (2003). Biomechanics and muscle coordination of human walking: Part ii: Lessons from dynamical simulations and clinical implications. *Gait & Posture*, 17(1):1 – 17.

Appendix A

Exploiting the Passive Dynamics of a Compliant Leg to Develop Gait Transitions

Reprinted from:

Martínez, H. R. , and Carbajal, J. P. (2011). *Exploiting the passive dynamics of a compliant leg to develop gait transitions*, In Physical Review E, 83(6), 066707.

Exploiting the Passive Dynamics of a Compliant Leg to Develop Gait Transitions

Harold Roberto Martinez Salazar* and Juan Pablo Carbajal†
Artificial Intelligence Laboratory, Department of Informatics,
University of Zurich
Andreasstrasse 15 8050 Zurich Switzerland
(Dated: April 20, 2013)

Abstract: In the area of bipedal locomotion, the spring loaded inverted pendulum (SLIP) model has been proposed as a unified framework to explain the dynamics of a wide variety of gaits. In this paper, we present a novel analysis of the mathematical model and its dynamical properties. We use the perspective of hybrid dynamical systems to study the dynamics and define concepts such as partial stability and viability. With this approach, on the one hand, we identified stable and unstable regions of locomotion. On the other hand, we found ways to exploit the unstable regions of locomotion to induce gait transitions at a constant energy regime. Additionally, we show that simple non-constant angle of attack control policies can render the system almost always stable.

I. INTRODUCTION

One of the most accepted mathematical models for bipedal running is the spring loaded inverted pendulum (SLIP, for an extensive review see[1]). In a similar fashion, the rigid inverted pendulum has been extensively used to model bipedal walking[2]. In 2006, Geyer et al.[3] propose the SLIP model as a unifying framework to describe walking as well as running. The unified perspective proves useful for accurately explaining data from human locomotion[3]. Additionally, it allows describing both gaits (walking and running) in terms of dynamical entities observed in a discrete map, obtained by intersecting the trajectories of the system with a predefined section of lower dimension. Geyer associates these entities with limit cycles of the *hybrid dynamical system*[4, 5] and named their attracting behavior as *self-stabilization*. Though the nature of the observed dynamical properties is not yet clarified, those results emphasize that bipedal locomotion may be dictated solely by the mechanics of the system. As a consequence, the control necessary for locomotion is thus reduced to the swing phase of the leg, showed in Fig. 1 between points A and B. The most popular control policy is to produce touchdowns at constant angle of attack α (CAAP (α)), i.e. the angle spanned by the landing leg and the horizontal.

In the last decade, many energy-efficient bipedal walking machines have been developed. Through careful design, they exploit the passive dynamics of their own body to move forward, requiring little control or none[6–10]. However, the construction of bipedal machines capable of exploiting passive dynamics in different gaits remains an unsolved engineering challenge. In this context, Geyer et al.[3] report that, in the SLIP model, it is not possible to have multiple gaits at the same energy. The results are based on simulations that do not cover all possible initial conditions of the system. In addition, Rummel et al.[11] prove that walking and running is possible at the same energy level. They use a new map that allows comparing different gaits with ease. The map is defined at the vertical plane crossing the landing point of the foot (Fig. 1). In this way, they find the self-stable regions, but their intersection is empty. To concretize these ideas, let us describe this region for the running map $\mathcal{R}$.

$$E^R_\infty = \{x |\ x \in \mathcal{S} \wedge (\exists \alpha |\ x = \mathcal{R}_\alpha(x))\}, \tag{1}$$

where the subscript in $\mathcal{R}_\alpha$ denotes running using CAAP (α) and $\mathcal{S}$ denotes the section where the map is defined. Therefore, if for different gaits these stable regions do not intersect, e.g. $E^R_\infty \cap E^W_\infty = \emptyset$, we conclude that a transition between the two gaits cannot occur if the system is to remain in these regions. In other words,

$$\begin{aligned} x \in E^R_\infty \wedge y \in E^W_\infty \quad &\Rightarrow \\ \mathcal{R}_\alpha(y) \notin E^R_\infty \ \wedge\ \mathcal{W}_\beta(x) \notin E^W_\infty \quad &\forall\, \alpha,\, \beta. \end{aligned} \tag{2}$$

In this study, we will show how transitions between gaits are found at points outside these stable regions. The transitions require the selection of the angle of attack; therefore CAAP's are not suitable for this task. We will also show evidence indicating that it is possible to find an angle of attack θ that maps a point into a stable region, e.g. $x \notin E^R_\infty \wedge \big(\exists\, \theta, y \mid y \neq x,\ y \in E^R_\infty,\ y = \mathcal{R}_\theta(x)\big)$. Additionally, we introduce the concepts of *partial stability* and *viability* that will be useful in the construction of the transitions presented herein.

This paper is organized as follows. In section II, we describe the models used for our simulations, their representation in state variables and the definition of the discrete map. Next, in section III, we introduce the new concepts, and we show the regions where the transitions between gaits exist. Later, in section IV, we discuss about the requirements of a controller for the system and the implications for robot design and bipedal locomotion. We conclude the paper in section V with our conclusion.

*http://ailab.ifi.uzh.ch/martinez/; martinez@ifi.uzh.ch
†http://ailab.ifi.uzh.ch/carbajal/; carbajal@ifi.uzh.ch, both authors can be contacted regarding the content of the paper

II. METHODS

As explained previously, we use the SLIP model to study bipedal gaits. We adopt the framework in [12], which is described in the language of hybrid dynamical systems. Therefore, we reintroduce some notation and definitions.

To represent the different phases of a gait, the model is segmented into three sub-models. We will call these sub-models *charts*[4] or phases see Fig.1. Each chart represents the motion of a point mass under the influence of: only gravity (ff-chart or flight phase), gravity and a linear spring (s-chart or single stance phase), gravity and two linear springs (d-chart or double stance phase). The point mass represents the body of the agent and the massless linear springs model the forces from the legs (Fig.1). A trajectory switches from one chart to another when some real valued functions evaluated on it cross zero (*event functions*[4, 13]). We define a running gait as a trajectory that switches from the s-chart to the ff-chart and back to the s-chart. A walking gait is defined as a trajectory that switches from the s-chart to the d-chart and back again to the s-chart. Switches from the ff-chart to d-chart or vice versa are not included in this study.

A. Equations of motion in each chart

The motion in all the charts is governed by a system of ordinary differential equations:

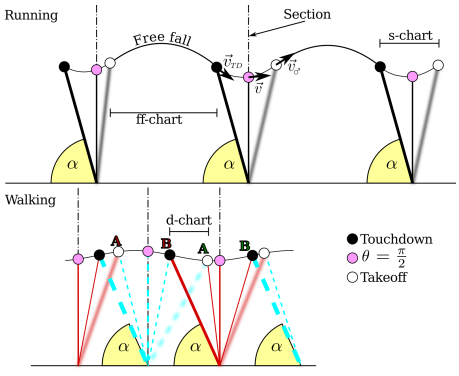

FIG. 1. (Color online) Illustration of the evolution of the SLIP model for running and walking. The mass is represented with a filled circle. The color of the fill indicates touchdown event (black), takeoff event (white), and the crossing of the section (pink (grey)). The landing leg is pictured with a thick solid line, and the leg at takeoff is represented with a blurred line. Due to the passive properties of these models, control is necessary only during the swing of the leg, i.e. during free fall while running and from point A to B while walking.

$$\dot{\vec{X}} = \vec{F}_i\left(\vec{X}\right), \tag{3}$$

where $\vec{X}$ is the vector of state variables and $\vec{F}_i$ is a force function characteristic of each chart. Since all forces are conservative, the energy of the system is constant. For the ff-chart the state is described by the Cartesian coordinates of the position of the point mass and its velocity $\vec{X}_{ff} = (x, y, v_x, v_y)^T$,

$$\dot{\vec{X}}_{ff} = \begin{pmatrix} v_x \\ v_y \\ 0 \\ -g \end{pmatrix}, \tag{4}$$

where g is the acceleration due to gravity.

The state in the s-chart is represented in polar coordinates $\vec{X}_s = \left(r, \theta, \dot{r}, \dot{\theta}\right)^T$, where r is the length of the spring and θ is the angle spanned by the leg and the horizontal, growing in clockwise direction. Thus, the equations of motion are:

$$\dot{\vec{X}}_s = \begin{pmatrix} \dot{r} \\ \dot{\theta} \\ \frac{k}{m}(r_0 - r) + r\dot{\theta}^2 - g\sin\theta \\ -\frac{1}{r}\left(2\dot{r}\dot{\theta} + g\cos\theta\right) \end{pmatrix}. \tag{5}$$

It is important to note that $\theta(t_{TD}) = \alpha$, i.e. the angular state at the time of touchdown is equal to the angle of attack. The parameter r_0 defines the natural length of the spring.

In the d-chart the state is also represented in polar coordinates $\vec{X}_d = \left(r, \theta, \dot{r}, \dot{\theta}\right)^T$, with the origin of coordinates in the new touchdown point. The motion is described by:

$$\dot{\vec{X}}_d = \begin{pmatrix} \dot{r} \\ \dot{\theta} \\ \frac{k}{m}\left[(r_0 - r) + \left(1 - \frac{r_0}{r_{\sigma}}\right)(x_{\sigma}\cos\theta - r)\right] \\ \qquad + r\dot{\theta}^2 - g\sin\theta \\ -\frac{1}{r}\left[\frac{k}{m}\left(1 - \frac{r_0}{r_{\sigma}}\right)x_{\sigma}\sin\theta + 2\dot{r}\dot{\theta} + g\cos\theta\right] \end{pmatrix} \tag{6}$$

$$r_{\sigma} = \sqrt{r^2 + x_{\sigma}^2 - 2r x_{\sigma}\cos\theta}, \tag{7}$$

where x_{σ} is the horizontal distance between the two contact points and r_{σ} is the length of the back leg.

B. Event functions

Event functions are functions on the phase space of the system. An event occurs when the trajectory of the system intersects a level curve of the event function. At the time of the event, the current state of the system

is mapped to the state of another chart. Some event functions are parameterized with the angle of attack and the natural length of the springs.

Switches from the ff-chart to the s-chart are defined by:

$$\mathcal{F}_{ff\to s}\left(\vec{X}_{ff},\alpha,r_0\right):\begin{cases} y-r_0\cos\alpha=0 \\ v_y<0 \end{cases}, \tag{8}$$

which means that the mass is falling and the leg can be placed at its natural length with angle of attack α. Therefore, the motion is now defined in the s-chart. The switch in the other directions is simply:

$$\mathcal{F}_{s\to ff}\left(\vec{X}_s,r_0\right): r-r_0=0. \tag{9}$$

These are the only two event functions involved in the running gait. The map from one chart to the other is defined by:

$$x=-r\cos\theta \qquad y=r\sin\theta. \tag{10}$$

It is important to have in mind that the origin of the s-chart is always at the touchdown point.

For the walking gait, we have to consider switches between single and double stance phases. From the s-chart to the d-chart, we have:

$$\mathcal{F}_{s\to d}\left(\vec{X}_s,\alpha,r_0\right):\begin{cases} r\sin\theta-r_0\cos\alpha=0 \\ \theta>\frac{\pi}{2} \end{cases}, \tag{11}$$

which is similar to (8) with the additional condition that the mass is tilted forward. Additionally, if we consider the sign of the radial speed, we differentiate between walking gait $\mathcal{W}$ with $\dot{r}<0$ and Grounded Running gait $\mathcal{GR}$, with $\dot{r}>0$.

The switch from the double stance phase to the single stance phase is defined by:

$$\mathcal{F}_{d\to s}\left(\vec{X}_d,r_0\right): r_{\mathscr{s}}-r_0=0, \tag{12}$$

with $r_{\mathscr{s}}$ as defined in (7). The map from the d-chart to the s-chart is the identity. In the other direction we have:

$$r_d=r_0 \quad \theta_d=\alpha, \tag{13}$$

$$x_{\mathscr{s}}=r_0\cos\alpha-r_s\cos\theta_s, \tag{14}$$

where the subscripts indicate the corresponding chart.

If the system falls to the ground ($y\leq 0$), attempts a forbidden transition (e.g. d-chart to ff-chart), or renders $v_x<0$ (motion to the left,"backwards"), we consider that the system fails.

C. Simulation of the dynamics

The state of the model is observed when the trajectory of the system intersects the section defined by $\mathcal{S}:\theta=\pi/2$. In this way, the map $\mathcal{R}_\alpha:\mathcal{S}\to\mathcal{S}$ transforms points through the evolution of the system from the s-chart to the ff-chart and back again to the s-chart using an angle of attack α. Similarly, the map $\mathcal{W}_\alpha:\mathcal{S}\to\mathcal{S}$ transforms points through the evolution of the system from the s-chart to the d-chart and back again to the s-chart using an angle of attack α.

All initial conditions are given in the $\mathcal{S}$ section and in the s-chart, i.e. only one leg touching the ground and oriented vertically. Moreover, all the initial conditions are given at the same total energy. The results are visualized using the values of the length of the spring r and the radial component of the velocity which, in $\mathcal{S}$, equals the vertical speed $\dot{r}=v_y$ (v_x is obtained from these values and the equation of constant energy). It is important to note that all possible values of r, v_y and v_x, for a given value of the total energy E, lay on an ellipsoid. Besides, there is a transformation that maps the ellipsoid to a sphere. This can be shown as follows: the total energy in the section is,

$$E=\frac{1}{2}k\left(r_0-r\right)^2+\frac{1}{2}m\left(v_x^2+v_y^2\right)+mgr \tag{15}$$

Defining the parameters

$$L=\sqrt{\frac{2}{k}\left[E-mg\left(r_0-\frac{mg}{2k}\right)\right]}, \tag{16}$$

$$\omega=\sqrt{\frac{k}{m}}, \tag{17}$$

the new variables

$$\hat{v}_x=\frac{v_x}{\omega}, \tag{18}$$

$$\hat{v}_y=\frac{v_y}{\omega}, \tag{19}$$

$$\hat{r}=r-\left(r_0-\frac{mg}{k}\right), \tag{20}$$

transform equation (15) into,

$$L^2=\hat{v}_x^2+\hat{v}_y^2+\hat{r}^2 \tag{21}$$

which defines a sphere. Therefore, all initial conditions of $\hat{r}$ and $\hat{v}_y$ with constant energy, are defined inside a circle. A Delaunay triangular mesh was created in the circle with 65896 initial conditions as vertices (131245 triangles). Each vertex was transformed using $\mathcal{R}_\alpha$, $\mathcal{GR}_\alpha$ and $\mathcal{W}_\alpha$ with 400 values of $\alpha\in[55°,90°]$. To compute the evolution of an arbitrary initial condition, we used bilinear interpolation in the triangles of the mesh.

The model implementation and data analysis were carried out in MATLAB(2009, The MathWorks), GNU Octave[14] and Matplotlib[15]. Simulations were run for constant energy, using the step variable integrator ode45 (relative tolerance: 1×10^{-6} and absolute tolerance: 1×10^{-8}). Table I shows the values of the parameters used.

TABLE I. Values used for the simulations presented in this paper.

Description	Name	Value
Mass	m	80 kg
Elastic constant of linear springs	k	15 kNm
Rest length of linear springs	r_0	1 m
Total energy	E	820 J
Acceleration due to gravity	g	9.81 m/s^2
Angle of Attack	α	from 55°to 90°

III. RESULTS

In this section, we present the results of the analysis on the data collected from the models as described in section II C. Aiming to define a controller, we introduce some important properties of the dynamics of each gait, namely finite stability for a given CAAP and viability.

A. Finite stability and Viability

Finite stability describes the set of initial conditions where the system can do a maximum amount of steps (sequential applications of the map) before failing, using CAAP. For example, we can define for $\mathcal{W}$

$$E_n^W = \{x |\ x \in \mathcal{S} \wedge (\exists \alpha |\ y = \mathcal{W}_\alpha^n(x)\,,\ n \geq 1,\ y \in \mathcal{S})\}. \tag{22}$$

That is, at a given state $x = (r, v_y)$ in $\mathcal{S}$ there is a CAAP (α) such that the system can do at most n steps before failing. The region E_0^W are all the points in the section where applying $\mathcal{W}$ produces a failure. The existence of E_n^W implies that a controller of the system may not need to take a decision at each step. In addition, the controller may exploit this alleviation by planning future angles of attack. Viability describes how easy is to choose the future angle of attack. The level of ease is measured in terms of the size of the interval of angles that can be chosen to avoid a failure of the system. For the running gait this region is defined as:

$$\begin{aligned} V^R(\Delta\alpha) = &\{x |\ x \in \mathcal{S} \wedge \\ &(\exists \alpha \in I_\alpha,\ \|I_\alpha\| \geq \Delta\alpha \mid y = \mathcal{R}_\alpha(x)\,,\ y \in \mathcal{S})\}, \end{aligned} \tag{23}$$

where I_α denotes a real interval and $\|\cdot\|$ measures its length. In a real system, it is required that a viable angle of attack exists for a definite interval, since real sensors and actuators have a finite resolution and are affected by noise.

Fig. 2 shows the finite stability regions for each gait. The stable region of $\mathcal{R}$, as reported in [12] ($v_y = 0$) is not visible. Although E_∞^R may have some area of attraction, due to the resolution we used for the angles of attack (described in section II C) we do not see it in our results. Based on results not presented here, we estimate that the resolution in the angle of attack to detect such basin for the current energy is $\sim 10^{-4}$. In despite of the low resolution in the angles, the system can perform an average of 10 steps in $\mathcal{R}$, and at least 25 steps (maximum calculated) in $\mathcal{GR}$ and $\mathcal{W}$. This means that running is more difficult at this energy level than the other two gaits. Particularly for $\mathcal{GR}$ and $\mathcal{W}$, we see that there is a plateau with the maximum number of steps. This is the evidence of the self-stable regions of these gaits, and the plateau is related to the basing of attraction of that region.

Fig. 3 shows the $V^i(\Delta\alpha)$ regions for each gait i. Comparing with Fig. 2, we see that in general long partial stability implies wider options for the angle of attack. Particularly, transitions are found near these regions of high viability and long partial stability, as will be described in the next section.

Fig. 4 shows one of the strongest results presented here. For each gait i, there is at least one angle of attack that maps the current state of the system into E_∞^i, and this angle exists for an extense region of $\mathcal{S}$. This implies that if we consider control policies with variable angle of attack, almost any point in the section can be rendered stable. For this region the optimal control policy requires two angles: the first one maps the point to E_∞^i; the second angle, keeps the system in this region.

B. Transition regions

As it was shown in the previous section, the only way of producing transitions between gaits is to put the system in a region with finite stability (due to the empty intersection of the E_∞^i regions reported in [12], see Fig 4). In Fig. 5 we show transitions starting at E_n^i and arriving at $V^j(2°)$ for $i \neq j$ and $(i \to j) = \{(R \to GR), (GR \to W), (W \to GR), (W \to R)\}$. We show the transitions that will be used in the next example, however transitions between two any gaits are possible. It shall be noticed that wherever two regions of different gaits intersect, the transition is trivial.

Finally, Fig. 6 and Fig. 7 show one example of three transitions for a given initial condition. The trajectory has a total of 26 steps and the angle sequence is

$$\begin{aligned} \alpha = \big(&81.886^5, 88.500, 62.400, 72.350, 71.100^3, 71.000, \\ &74.400, 72.130, 74.000^4, 78.000^2, 76.500, 69.000, 81.728^4\big) \end{aligned} \tag{24}$$

where the exponent indicates how many times the angle was used. The path of the center of mass in the Cartesian plane is also shown in the figures.

All together we have shown that the SLIP model can be easily controlled to present transitions between gaits. To find transitions we must search for an intersection between the future of the starting region and the desired

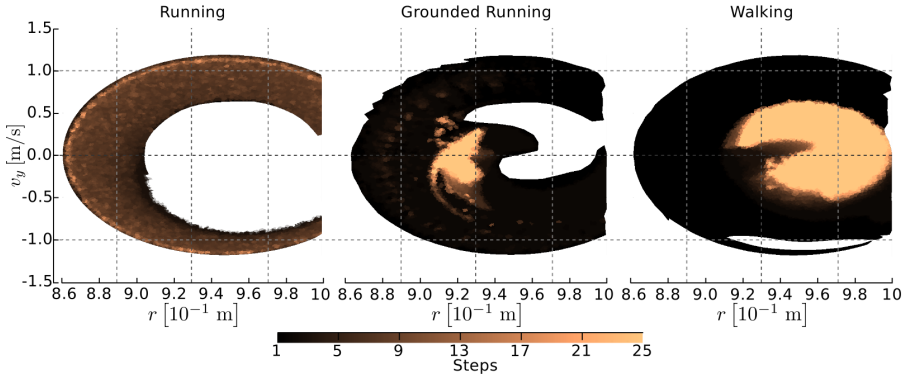

FIG. 2. (Color online) Finite stability regions. The figures show initial conditions for $\mathcal{R}$, $\mathcal{GR}$ and $\mathcal{W}$ that can do multiple steps under CAAP before failing. A region in white corresponds to E_0^i for gait i.

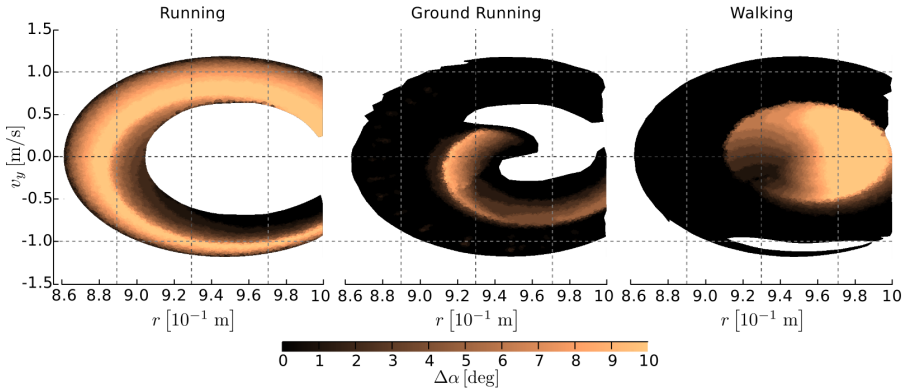

FIG. 3. (Color online) Viability regions for each gait. The figures show the range of angles of attack that can be selected in each initial condition that allows the system give at least one more step. Colors indicate the size of the window, spanning from 0°to 10°.

objective region. Depending how these regions are defined, it may be the case that multiple steps are required to achieve a successful transition.

IV. DISCUSSION

There are two important aspects regarding the viability regions. First, it is important to notice that $V^i(\Delta\alpha)$ enclose the E^i_∞ region, and the points that can be mapped to stable regions in one step (Fig. 4) . Second, as it can be seen in Fig. 3, the bigger the range of the angle of attack is, the smaller the viability region is. We can take advantage of these properties to stabilize the system more easily. The selection of an appropriate $\Delta\alpha$ e.g. 2° defines a set of $V^i(\Delta\alpha)$ inside the section $\mathcal{S}$, where the controller has at least a range of 2° to select an appropriate angle of attack. Moreover, the agent can select conservative angles, step by step, to bring itself to the E^i_∞ region (Fig. 5).

Despite the relief to the controller induced by the viability region, the selection of the $\Delta\alpha$ can generate regions that do not intersect; e.g. in Fig. 4 we can see that $V^i(2°)$ does not intersect any other region, which makes the gait transition more difficult to carry out. In order to cope with this situation, we look at the future of all the initial conditions in E^i_n. As it is presented in Fig. 5, we found that there are some initial conditions, that under a set of angles of attack, are mapped from E^i_n to E^j_n (e.g. E^R_n to E^{GR}_n). What is also important is that the region where we can find these initial conditions are inside the viability region (Fig. 5).

In these terms, the controller has two purposes. First, based on the state on the $\mathcal{S}$ section, it has to select the gait, and the angle of attack to keep the agent stable. Thus, the controller needs to have the knowledge of all the $V^R(\Delta\alpha)$, and the desired $\Delta\alpha$ to identify which gait has to be selected; the angle of attack can be selected based on the gait model. Second, the controller has to be

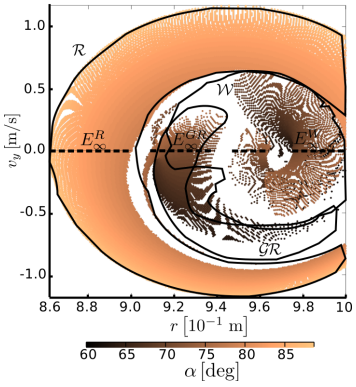

FIG. 4. (Color online) Points that can be mapped to stable regions in one step. The figures show the initial conditions that can be mapped to a small neighborhood of the stable region E^i_∞, $|v_y| < 1 \times 10^{-3}$ ($v_y = 0$, dashed horizontal lines). Color indicates the angle chosen. Regions $V^i(2°)$ are marked with solid lines.

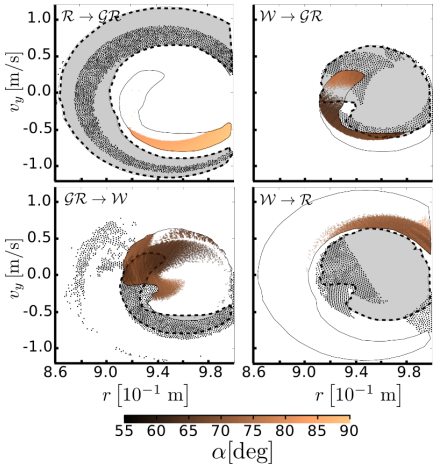

FIG. 5. (Color online) Transitions regions landing in $\Delta\alpha \geq 2°$. All the initial conditions that have a future inside the region with $\Delta\alpha \geq 2°$ of the objective gait are plotted with black dots. The same region of the starting gait is given as a reference and appears shaded. Colors in the objective region indicate the angle of attack used to perform the transition. Wherever two regions of different gaits intersect, the transition is automatically given.

able to produce gait transition when it is needed. Hence, the transition regions should be known by the controller and with a model of the gait, the angle of attack required can be selected. We expect that this approach can be used to handle uneven terrain, given that these irregularities can be modeled (under certain restrictions) as a change in energy.

All these results are conditioned to the selection of the

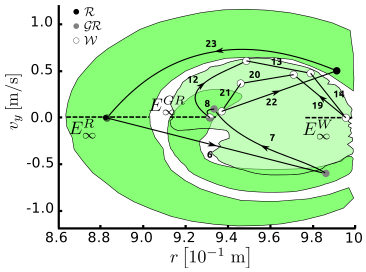

FIG. 6. (Color online) Transition sequence. The plot shows a trajectory with three transitions. The Regions $V^i(2°)$ are shown shaded with self-stable regions in dotted line. The arrows indicate the order of the sequence and the step number is given. The angle of attack sequence is given in (24).

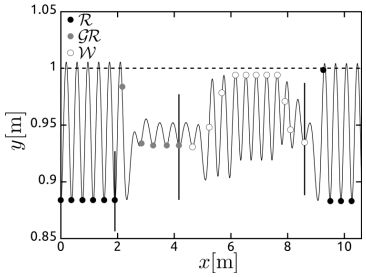

FIG. 7. Transition time series. The figure shows the motion of the point mass[a] in the plane is shown together with the crossing of the section (filled circles 6). Transition points are indicated with a vertical line.

[a] An animation of these transitions can be seen in http://www.ifi.uzh.ch/arvo/ailab/people/hamarti/GaitT.avi

$\mathcal{S}$ section. This means that we are analyzing the system in only one point in the whole trajectory. From what we see in these results, in some regions the trajectories are very close. It would not be a surprise that these trajectories of $\mathcal{R}$, $\mathcal{W}$, and $\mathcal{GR}$ cross each other in another point along their continuous evolution, but given that we are looking just at the $\mathcal{S}$ section, this cannot be anticipated. Nevertheless, the selection of this section establishes the angle of attack as a natural control action to stabilize the system and to generate the transitions.

V. CONCLUSION

In the present study we have taken advantage of the perspective of hybrid dynamical systems to represent locomotion as a process generated by several charts. Although, this view makes evident a bigger set of connections among the charts, in this paper we take into account a small subset (s-chart to ff-chart, and s-chart to d-chart) which allow us to discover new alternatives to perform gait transitions. The development of the maps

$\mathcal{W}^1_\alpha$, $\mathcal{GR}^1_\alpha$, $\mathcal{R}^1_\alpha$ is fundamental to identify important regions in the $\mathcal{S}$ section that bring the system to stable locomotion and to a gait transition. The present results bring new ideas about plausible mechanisms that biped creatures could use to carry out gait transitions and stable locomotion. These mechanisms exploit the passive dynamics of the system, which reduces the amount of energy needed to control the system. These features are also present in biped machines with compliant legs, and as suggested in this paper, these mechanisms can be exploited to develop stable gaits and gait transitions.

ACKNOWLEDGMENTS

Funding for this work has been supplied by SNSF project no. 122279 (From locomotion to cognition), and by the European project no. ICT-2007.2.2 (ECCEROBOT). Additionally, the research leading to these results has received funding from the European Community's Seventh Framework Programme FP7/2007-2013-Challenge 2-Cognitive Systems, Interaction, Robotics-under grant agreement No 248311-AMARSi.

[1] P. Holmes, R. J. Full, D. Koditschek, and J. Guckenheimer, SIAM Rev. **48**, 207 (2006), ISSN 0036-1445.

[2] S. Mochon and T. A. McMahon, J. Biomech. **13**, 49 (1980), ISSN 00219290.

[3] H. Geyer, A. Seyfarth, and R. Blickhan, P. Roy. Soc. B - Biol. Sci. **273**, 2861 (Nov. 2006), ISSN 0962-8452.

[4] J. Guckenheimer and S. Johnson, in *Hybrid Systems II* (Springer-Verlag, London, UK, 1995) pp. 202–225, ISBN 3-540-60472-3.

[5] J. Cortes, IEEE Contr. Sys. Mag. **28**, 36 (Jun. 2008), ISSN 0272-1708.

[6] T. McGeer, Int. J. Robot. Res. **9**, 62 (Apr. 1990), ISSN 0278-3649.

[7] S. H. Collins, Int. J. Robot. Res. **20**, 607 (Jul. 2001), ISSN 0278-3649.

[8] M. Wisse and J. V. Frankenhuyzen, in *Adaptive Motion of Animals and Machines* (Springer-Verlag, Tokyo, 2006) pp. 143–154, ISBN 4-431-24164-7.

[9] S. H. Collins, A. Ruina, R. Tedrake, and M. Wisse, Science **307**, 1082 (Feb. 2005), ISSN 1095-9203.

[10] T. Geng, B. Porr, and F. Worgotter, Neural Comput. **18**, 1156 (May 2006), ISSN 0899-7667.

[11] J. Rummel, Y. Blum, H. M. Maus, C. Rode, and A. Seyfarth, in *IEEE Int. Conf. Robot. (ICRA)* (IEEE, 2010) pp. 5250–5255, ISBN 978-1-4244-5038-1.

[12] J. Rummel, Y. Blum, and A. Seyfarth, in *Autonome Mobile Systeme* (Springer, Berlin, Heidelberg, 2009) pp. 89–96, ISBN 978-3-642-10283-7.

[13] P. T. Piiroinen and Y. A. Kuznetsov, ACM T. Math. Software **34**, 1 (May 2008), ISSN 00983500.

[14] J. W. Eaton, *GNU Octave Manual* (Network Theory Limited, http://www.octave.org, 2002) ISBN 0-9541617-2-6, `http://www.octave.org`.

[15] J. D. Hunter, Computing in Science and Engineering **9**, 90 (2007), ISSN 1521-9615.

Appendix B

From Walking to Running a Natural Transition in the SLIP Model Using the Hopping Gait

Reprinted from:

Martínez, H. R., and Carbajal, J. P. (2011, December). *From walking to running a natural transition in the SLIP model using the hopping gait*, In Robotics and Biomimetics (ROBIO), 2011 IEEE International Conference on (pp. 2163-2168). IEEE.

From Walking to Running a Natural Transition in the SLIP Model Using the Hopping Gait

Harold Roberto Martinez and Juan Pablo Carbajal

***Abstract*— In this paper we adopt the spring loaded inverted pendulum (SLIP) model as the mathematical framework to represent biped locomotion, but in contrast with previous studies, we redefine the conditions for valid locomotion. As a consequence we identify new ways to produce gait transitions (e.g. change from walking to running) through the control of the angle of attack, at a constant energy level. Moreover, we show that the new valid conditions of locomotion allow the representation of the hopping gait. This new gait requires two different angles of attack for its execution, hence constant angle of attack policies are not applicable. First, we show the regions of phase space where one step gait transitions exist. Next, we report the region where it is possible to generate a periodic hopping gait. Mainly, the two results imply that through the control of the angle of attack the system can exploit its passive dynamics to induce transitions between running, walking and hooping or keep the system stable in any of these gaits. Finally, we briefly discuss the relation between these findings and the use of complaints legs in robots.**

I. Introduction

The design and implementation of biped machines capable of human like gait locomotion remains a challenge in engineering. To cope with it, researchers have devoted their work to understand the main principles of locomotion through the development of mathematical models ([1], [2], [3], [4], [5]). This has provided a better understanding of the biomechanics of several gaits [6] and the advantages of compliant legs in locomotion ([7], [8], [9]). The technical knowledge generated with these models permitted the development of energy efficient biped robots ([10], [11], [12], [13], [14]). These machines exploit their passive dynamics to move forward with little control. Though these are impressive prototypes, they are built either for walking or for running, and no gait transition is possible. This is due to the incompatibility of the models used to build walking and running prototypes.

Geyer and his collaborators overcome this problem with a unified framework [5], which represents walking and running based on the spring loaded invert pendulum (SLIP) model. They looked for a set of initial conditions that allow a 2D biped agent to walk and run. The authors associated certain dynamical entities with limit cycles of the *hybrid dynamical system* [15], [16] and named their attracting behavior, *self-stabilization*. Their results showed that the stance face of bipedal locomotion is totally determined by the mechanics of the system, considerably reducing the control necessary for locomotion. The most popular control policy is to keep constant the angle spanned by the landing leg and the horizontal, i.e. to produce touchdowns at Constant Angle of Attack α ($\mathrm{CAAP}(\alpha)$). Following this representation, Rummel et al. [8] proved that the intersection of the so called self-stable regions of walking and running is empty, which means that it is not possible to go from a stable walking gait to a stable running gait or vice versa in one step. However, as reported in [17] as soon as it is possible to select the angle of attack at each step, it is possible to let the system transit unstable regions, allowing gait transitions at constant energy.

In the SLIP model, gaits are mainly defined by a sequence of discrete events. Running is defined as a single stance phase, i.e. one leg touching the ground, followed by a flight phase. Similarly, walking is determined by a single stance phase followed by a double stance phase. In this study we redefine the conditions for valid locomotion and consequently, we identify new mechanisms to induce gait transition, extending the repertoire of gaits represented by the SLIP model. Within these new conditions, we show that hopping is a periodic pattern of locomotion with two alternating angles of attack. Moreover, the representation of this new gait is compatible with the definitions of *partial stability* and *viability* introduced by Martinez and Carbajal in [17], as well as with the section proposed by Rummel et al. in [8], that allowed an easy comparison between different gaits. This section is defined at the vertical plane crossing the landing point of the foot (Fig. 1).

This paper is organized as follows. In Section II, we briefly describe the model used and the method to obtain the simulated data. The concepts of finite stability and viability are briefly reintroduced there as well. Next, in Section III, we show the regions where hopping is periodic and the region where it can be used to do transitions from walking to running. The controller naturally follows from these results. Subsequently, in Section IV, we discuss the policies generated by the controller, its requirements, and the implications for robot design and robotic biped locomotion. Conclusion are presented in section V.

II. Gait definition and methods

As explained previously, we used the SLIP model to study the hopping gait. We followed the framework described in [17] therefore herein we provide a succinct recapitulation;

The research leading to these results has received funding from the European Community's Seventh Framework Programme FP7/2007-2013 - Challenge 2 - Cognitive Systems, Interaction, Robotics - under grant agreement no. 231864 - ECCEROBOT. Additionally, Funding for this work has been supplied by the European Community's Seventh Framework Programme FP7/2007-2013 - Challenge 2 - Cognitive Systems, Interaction, Robotics - under grant agreement No 248311-AMARSi.

The authors are with the Artificial Intelligence laboratory, Department of Informatics, University of Zurich, Andreasstrasse 15 8050 Zurich Switzerland { martinez,carbajal } @ifi.uzh.ch

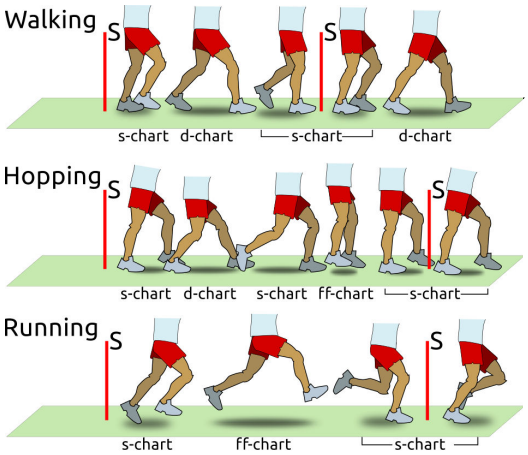

Fig. 1. Walking, Hopping and Running gaits depicted. The different charts are indicated as well as the section $\mathcal{S}$ where the system is observed. Note the new allowed switch, from s-chart to ff-chart without crossing the section $\mathcal{S}$, during hopping.

a complete description with full details can be obtained from that reference.

The different phases of a gait are represented with three sub-models. We will call these sub-models *charts* [15] or phases. Each chart represents the motion of a point mass under the influence of: only gravity (ff-chart or flight phase), gravity and a linear spring (s-chart or single stance phase), gravity and two linear springs (d-chart or double stance phase). The point mass stands for the body of the agent and the massless linear springs model the forces from the legs. A trajectory switches from one chart to another when some real valued functions evaluated on it cross zero (*event functions* [15], [18]). The event functions are parameterized with the angle of attack and the natural length of the springs and they also define the failure of the system, i.e. the agent falls to the ground, it moves backwards, or it makes a forbidden chart switch. The system is observed when it crosses a section $\mathcal{S}$, defined at the vertical position of the support leg in the single stance phase.

Previously only three gaits where allowed: running $\mathcal{R}$, walking $\mathcal{W}$ and grounded running $\mathcal{GR}$ (the difference between walking and grounded running is that in the latter, the vertical component of the velocity in the s-chart to d-chart switch is positive). The analysis of the forbidden switches showed that the system naturally attempts to change from the single stance to a flight phase before crossing the section $\mathcal{S}$. The difference with the results presented in [17] is that herein, we adopt as valid the transition from s-chart to ff-chart before crossing the section $\mathcal{S}$ (we refer to it as "the new switch"). This new switch during walking revealed a new gait. We named *hopping gait* to this emerging locomotion pattern, since it resembles the gait used by children while running playfully. In Table I we give the sequence of chart switches associated with each gait. Each sequence is ordered

TABLE I

SEQUENCES OF CHART SWITCHES ASSOCIATED WITH EACH GAIT. THE SECTION CROSSING IS INDICATED

Gait	Charts (ordered and cyclic)
Walking $\mathcal{W}$	$\mathcal{S}$(s-chart), d-chart, s-chart
Grounded Running $\mathcal{GR}$	$\mathcal{S}$(s-chart), d-chart, s-chart
Running $\mathcal{R}$	$\mathcal{S}$(s-chart), ff-chart, s-chart
Hopping $\mathcal{H}$	$\mathcal{S}$(s-chart), d-chart, s-chart, ff-chart, s-chart

and the last chart switches to the first one. The gaits are pictorially represented in Fig. 1. The evolution in the s-chart is broken in two parts to indicate the crossing of the section $\mathcal{S}$. Note that during hopping there are two s-chart, but the section $\mathcal{S}$ is crossed in just one of them. Hopping can be seen as alternating between walking and running.

A. Simulation of the dynamics

The state of the model is observed when the trajectory of the system intersects the section defined by the support leg forming a right angle with the ground, i.e. $\mathcal{S} : \theta = \pi/2$. In this way, the map $\mathcal{R}_\alpha : \mathcal{S} \to \mathcal{S}$ transforms points through the evolution of the system from the s-chart to the ff-chart and back again to the s-chart using an angle of attack α. Similarly, the map $\mathcal{W}_\alpha : \mathcal{S} \to \mathcal{S}$ transforms points through the evolution of the system from the s-chart to the d-chart and back again to the s-chart using only one angle of attack α. Likewise, the map $\mathcal{H}_{\beta,\alpha} : \mathcal{S} \to \mathcal{S}$ transforms points through the evolution of the system from the s-chart to the d-chart, using an angle of attack β, and from the ff-chart to the s-chart using an angle of attack α. All initial conditions are given in the $\mathcal{S}$ section and in the s-chart, i.e. only one leg touching the ground and oriented vertically. Moreover, all the initial conditions are given at the same total energy. The results are visualized using the values of the length of the spring r and the radial component of the velocity which, in $\mathcal{S}$, equals the vertical speed $\dot{r} = v_y$ (v_x is obtained from the equation of constant energy). All possible values of r, v_y and v_x, for a given value of the total energy E, lie on an ellipsoid. We transform the ellipsoid to a sphere to generate an uniform set of initial conditions using a Delaunay triangular mesh with 65896 initial conditions as vertices (131245 triangles). Each vertex was transformed using $\mathcal{R}_\alpha$, $\mathcal{GR}_\alpha$, $\mathcal{W}_\alpha$ and $\mathcal{H}_{\alpha,\beta}$ with 400 values of α and $\beta \in [55°, 90°]$. To compute the evolution of an arbitrary initial condition, we used bilinear interpolation in the triangles of the mesh. The model implementation and data analysis were carried out in MATLAB(2009, The MathWorks), GNU Octave [19] and Matplotlib [20]. Simulations were run for constant energy, using the step variable integrator ode45 (relative tolerance: 1×10^{-6} and absolute tolerance: 1×10^{-8}). Table II shows the values of the parameters used.

B. Finite stability and viability

We adopt the definitions of finite stability and viability presented in [17]. Finite stability E_n^i describes the set of initial conditions where the system can do at least n steps

with the gait $i \in \{\mathcal{R}_\alpha, \mathcal{GR}_\alpha, \mathcal{W}_\alpha\}$, using CAAP. As a consequence E_0^i represents the points in the section where a gait cannot be performed, and E_∞^i represents the point in the region where the system never falls using CAAP. If the system can select an angle of attack in each step (i.e. not CAAP), the region where it can locomote is inside the union of E_n^i, with $n \in [1, \infty)$. For the hoping gait, the definition is extended for two angles. That is, finite stability of hopping is defined when both angle, α and β are fixed.

In a physical platform it is required that the angle of attack exists for a definite interval, since real sensors and actuators have a finite resolution and are affected by noise. For this reason, the area of the section $\mathcal{S}$ where the system can take another step, selecting an angle of attack from an interval of reasonable length is important. This area is the viability region of a gait. The viability region is represented with $V^i(\Delta\alpha)$, where $i \in \{\mathcal{R}_\alpha, \mathcal{GR}_\alpha, \mathcal{W}_\alpha\}$, indicating that the angle can be selected from an interval with length $\Delta\alpha$ or greater, e.g. the region where the system can choose a viable angle of attack in an interval of two degrees or more is $V^i(\Delta 2^\circ)$. For the hopping gait we have two viability regions, one for each angle and a joint viability for the two angles $V^H(\Delta\alpha, \Delta\beta) = V^H(\Delta\alpha) \cap V^H(\Delta\beta)$.

Fig. 2 shows the viability regions $V^R(\Delta 2^\circ)$, $V^W(\Delta 2^\circ)$ and $V^{GR}(\Delta 2^\circ)$ together with the stable regions E_∞^R, E_∞^W and E_∞^{GR}. The identification of these regions in the section $\mathcal{S}$ allows the development of the controller proposed in [17] which exploits the dynamics of the system to keep it stable and induce gait transitions.

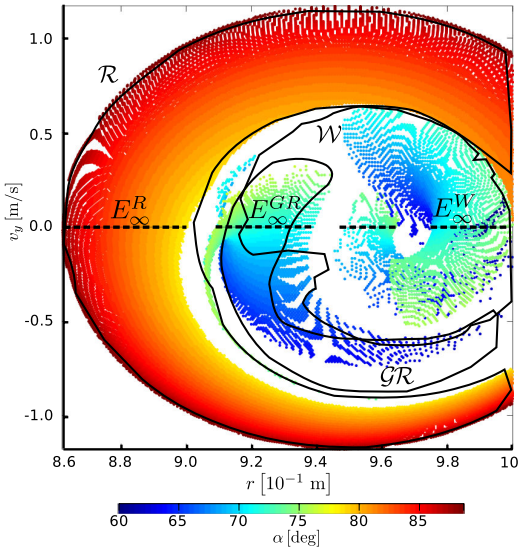

Fig. 2. Viability and one step stability regions for each gait at 820J. The figure show the angle of attack that can be selected in each initial condition to move the system to the E_∞^i region in one step. Colors indicate the angle of attack, spanning from 60°to 90°.

TABLE II

VALUES USED FOR THE SIMULATIONS PRESENTED IN THIS PAPER.

Description	Name	Value
Mass	m	80 kg
Elastic constant of linear springs	k	15 kNm
Rest length of linear springs	r_0	1 m
Total energy	E	820 J
Acceleration due to gravity	g	9.81 m/s^2
Angle of Attack	α	from 55°to 90°

TABLE III

GAIT SEQUENCES ALTERED BY ALLOWING THE NEW SWITCH. ANGLES AND NEW SWITCH ARE INDICATED WITH GREEK LETTERS AND •, RESPECTIVELY.

Gait	Charts
Walking $\mathcal{W}$	$\mathcal{S}$(s-chart), $_\beta$d-chart, s-chart,• ff-chart, s-chart
Running $\mathcal{R}$	$\mathcal{S}$(s-chart), ff-chart, $_\alpha$s-chart,• ff-chart, s-chart

III. RESULTS

As mentioned before, when the system is allowed to switch from the s-chart to the ff-chart without crossing the region new phenomena becomes evident. We have already described the hopping gait as composed of four different charts and it can be understood as an alternation between walking and running. Additionally, we show here that new gait transitions are made available.

During running and walking, we observed that the system was attempting to switch from the s-chart to the ff-chart before crossing the section. By allowing this switch, the running and walking gaits can be altered to the sequences shown in table III. For both altered sequences, during the last s-chart, the system can cross the section $\mathcal{S}$. If at the time of crossing the point defined by the vertical speed (v_y) and the length of the leg (r) lays inside the viability region of walking, then the system can walk; i.e. after the s-chart it switches to the d-chart and continues with the normal walking sequence (see table I). However, if this point falls inside the viability region of running, then the system can run; i.e. after the s-chart, it switches back to the ff-chart and continues with the normal running sequence. Thus, the future of the altered gait is defined by the crossing point in the section $\mathcal{S}$. Therefore, if the system makes a transition exploiting the new switch, this transition will take just one step. It is clearly visible from the table III that when walking is altered each time the system crosses section $\mathcal{S}$, the system is hopping.

These results are presented in Fig. 3. The solid contour line shows the region of initial conditions for which there exists an angle of attack that will produce the new switch and that can be selected from an interval of 2° or more. In running, this corresponds to the angle α indicated in table III. In walking (and grounded running), this region corresponds to the angle β indicated in the same table. The next crossing of the section is plotted with dots, these points are generated by choosing all possible angles of attack at touchdown after the new switch. Shaded areas represent the viability regions

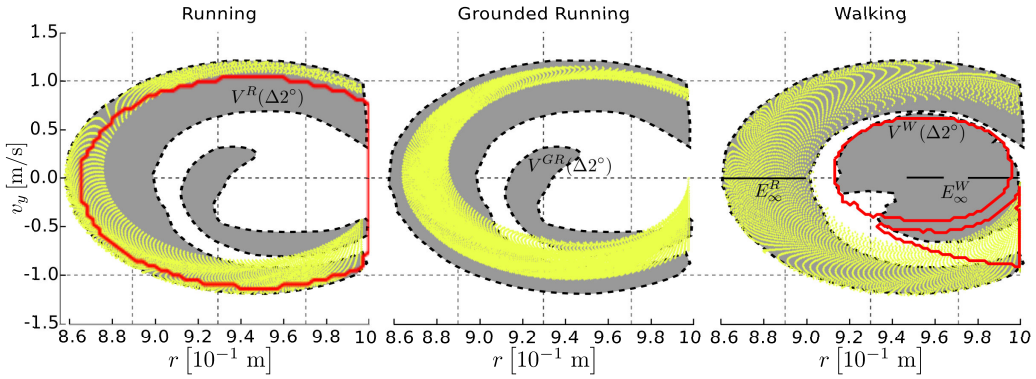

Fig. 3. Altered gait transitions. The viability region $V^i(\Delta 2^\circ)$ of the objective gait is shown shaded. The red solid contour line denotes regions of initial conditions that can generate the new switch with angles of attack selected from intervals of length greater than 2°. The yellow dots represent the crossings of the section for all possible angles of attack at landing after the new switch. Wherever dots are inside the viability region of the objective gait the transition is possible.

of the normal gaits. Wherever the dots are found inside the viability regions of the normal gaits, the transition is possible.

For altered running (left panel in Fig. 3), we see that the dots fall inside the viability region of running and grounded running. This means that the system could continue with normal running or transit to grounded running. Additionally we see that many of the initial conditions are outside of the running region. There, a running system will not cross section $\mathcal{S}$ and eventually fail. However, a controller can choose an angle of attack which leads the system to the new switch. From there, the controller would select another angle of attack that brings the system back to the viability region of running.

For grounded running (middle panel in Fig. 3), we observe that there is no initial condition in the section for which there is an angle of attack that can be selected from a reasonable interval (there is no solid line contour). Nevertheless, we present the crossing for angles selected with greater precision to show that almost all fall inside the viability region of running.

The transition is striking in the case of altered walking (right panel). Almost all crossing of the section occurs inside the viability region of running. This implies that after altered walking, it is straightforward to continue running. It is noteworthy the fact that we can produce a transition from stable walking to stable running, i.e. from E^W_∞ to E^R_∞. The angles can be selected from intervals spanning up to 16°.

Now we move on to describe the situation when the new switch occurs periodically, namely, the hopping gait. The shaded area in Fig. 4 is the region where the system can perform periodic hopping. The hopping is developed using two alternating angles of attack. The angle β takes the system to the new switch and angle α is used to switch from the free falling phase to the single support (s-chart). Using the extended notion of viability mentioned earlier, the shaded region in Fig. 4 represents the viability region of the hopping gait, i.e. $V^H(\Delta\alpha, \Delta\beta) = V^H(\Delta\alpha) \cap V^H(\Delta\beta)$. For the sake of comparison we added to the same figure the viability regions of the normal gaits, these are shown with dotted lines.

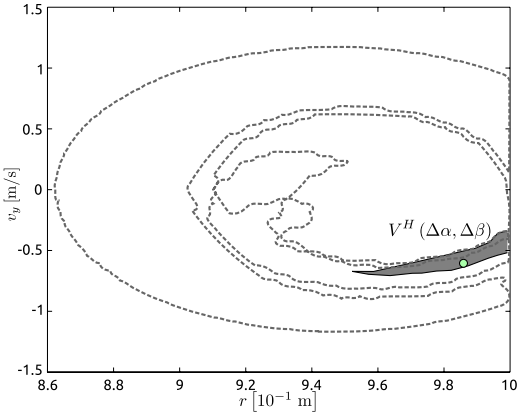

Fig. 4. Periodic hopping region. Dotted lines demark the viability regions $V^W(\Delta 2^\circ)$, $V^{GR}(\Delta 2^\circ)$ and $V^R(\Delta 2^\circ)$. The shaded area represent the region where it is possible to find a periodic hopping. The dot in this region corresponds to the initial condition selected to show the periodic trajectory of the hopping gait in Fig. 5.

Fig. 5 shows the trajectory of the center of mass in a periodic hopping gait. This trajectory corresponds to the initial condition marked with a dot in Fig. 4. The trajectory shows the switching between all the charts. The angle used for landing is 88.5975° (ff-chart to s-chart). The angle used to switch to the double support phase (s-chart to d-chart) is 68.2050°. To ease the reference to table I, we also show the crossing of the section and the new switch.

IV. Discussion

As reported, the hopping gait and the new alternatives for gait transitions are a direct consequence of allowing the system to switch from s-chart to ff-chart before crossing the

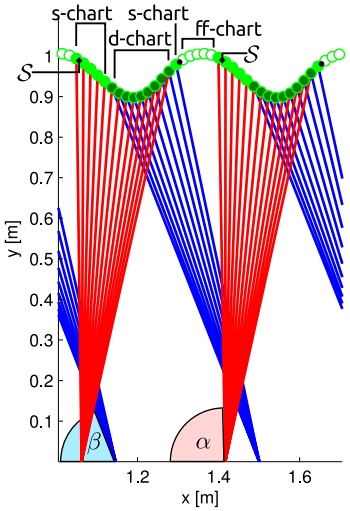

Fig. 5. Trajectory of a Periodic hopping gait. The angles of attack used are $\beta = 68.2050$ and $\alpha = 88.5975$. The figure shows two consecutive sequences of switches.

section $\mathcal{S}$. It was shown in the left panel of Fig. 3 that the new switch increases the range of valid angles of attacks that can be selected while the system is running. To do this, the controller of the system must set it into altered running for one step, and then bring it back to regions where running has higher finite stability. In this way, it is possible to run (with alterations) in regions that before where restricted to walking. At the same time, this can be interpreted as a one-step transition from walking (or grounded running) to running. That is, if the system is walking and chooses not to go into the d-chart, it switches to the ff-chart and enters altered running. From here, it can transit to any point in the viability region of running, depending on the angle of attack selected. In general, if the system crosses the section in any point inside the solid contour in the left panel of Fig. 3, it can do a transition to running by the mechanism just described.

The right most panel of Fig. 3 shows yet another one-step transition from walking to running. This transition is performed by choosing an angle β for the s-chart to d-chart switch, such that the next s-chart switches to the ff-chart without crossing the section. The intervals from which the latter angle can be selected are as large as $16°$. The system is now in altered walking and can land in any point of the region $V^R(\Delta 2°)$ by choosing the angle of attack. When compared with the walking to running transition reported in [17], we see that the new one-step transition covers a larger area of the viability region of running. Moreover, the transition can be executed anywhere inside the viability region of walking. Altogether, the transitions using altered gaits are a more suitable way to change between the locomotion patterns.

In the case of grounded running, we noted that there is no range of angles in $V^{GR}(\Delta 2°)$ and $V^W(\Delta 2°)$ that could let the system switch from s-chart to ff-chart, and allow it to come back to the section $\mathcal{S}$ as it was shown in Fig. 3(middle panel). In $V^{GR}(\Delta 2°)$ there is a very small range of angles that could allow the system to continue in the running region, but given the size of the range this could not be easy to implement in a real controller.

In Fig. 4, the region of periodic hopping gait is found inside the region of $V^{GR}(\Delta 2°)$. This is due to the fact that, in this region, the system can switch from s-chart to ff-chart and come back to s-chart, ad infinitum. An example was shown in Fig. 5.

All the features described herein are fundamental aspects in the design of biped robots. Particularly, it is important in the case of legged robots that can exploit their passive dynamics. If properly designed, these robots could easily accommodate all the different gaits that we find in biped locomotion.

V. Conclusion

In this work we have identified a new periodic gait in the SLIP model, namely, hopping. This gait adds to the previously known stable gaits of the SLIP model: running, walking and grounded running. Additionally, we found new ways to produce transitions between the existing gaits. These results are a direct consequence of allowing the system to switch from s-chart to the ff-chart without crossing the section $\mathcal{S}$, i.e. allowing the system to go from a single support phase to a flight phase, before the support leg is in a vertical position. The reported gaits and transitions exploit the passive dynamics of the system, which potentially reduces the amount of energy needed to control it. This exploitation is believed to be ubiquitous in nature and is the cornerstone in the development of biped robots with compliant legs. With this, we contribute to the corpus of plausible mechanisms used to explain stable locomotion of biped creatures and machines.

VI. Acknowledgments

We want to thank Dr. Hugo Gravato Marques and Dr. Hidenobu Sumioka for their review of the manuscript. We thank Prof. Dr. Rolf Pfeifer for his support to our research.

References

[1] P. Holmes, R. J. Full, D. Koditschek, and J. Guckenheimer, "The dynamics of legged locomotion: Models, analyses, and challenges," SIAM Rev., vol. 48, no. 2, pp. 207–304, 2006.

[2] T. A. McMahon and G. C. Cheng, "The mechanics of running: How does stiffness couple with speed?" Journal of Biomechanics, vol. 23, no. 1, pp. 65–78, 1990.

[3] R. Blickhan, "The spring-mass model for running and hopping," Journal of Biomechanics, vol. 22, no. 11-12, pp. 1217–1227, 1989. [Online]. Available: http://dx.doi.org/10.1016/0021-9290(89)90224-8

[4] S. Mochon and T. A. McMahon, "Ballistic walking," Journal of Biomechanics, vol. 13, no. 1, pp. 49–57, 1980. [Online]. Available: http://dx.doi.org/10.1016/0021-9290(80)90007-X

[5] H. Geyer, A. Seyfarth, and R. Blickhan, "Compliant leg behaviour explains basic dynamics of walking and running." Proceedings. Biological sciences / The Royal Society, vol. 273, no. 1603, pp. 2861–7, Nov. 2006. [Online]. Available: http://rspb.royalsocietypublishing.org/cgi/content/abstract/273/1603/2861

[6] M. H. Dickinson, "How animals move: An integrative view," Science, vol. 288, no. 5463, pp. 100–106, Apr. 2000. [Online]. Available: http://www.sciencemag.org/content/288/5463/100.abstract

[7] H. Geyer, A. Seyfarth, and R. Blickhan, "Spring-mass running: simple approximate solution and application to gait stability." Journal of theoretical biology, vol. 232, no. 3, pp. 315–28, Feb. 2005. [Online]. Available: http://dx.doi.org/10.1016/j.jtbi.2004.08.015

[8] J. Rummel, Y. Blum, H. M. Maus, C. Rode, and A. Seyfarth, "Stable and robust walking with compliant legs," in 2010 IEEE International Conference on Robotics and Automation. IEEE, May 2010, pp. 5250–5255. [Online]. Available: http://ieeexplore.ieee.org/xpl/freeabs_all.jsp?arnumber=5509500

[9] J. Rummel, Y. Blum, and A. Seyfarth, "From walking to running," in Autonome Mobile Systeme. Berlin, Heidelberg: Springer Berlin Heidelberg, 2009, pp. 89–96. [Online]. Available: http://www.springerlink.com/content/g490x3j552055v05/

[10] T. McGeer, "Passive dynamic walking," The International Journal of Robotics Research, vol. 9, no. 2, pp. 62–82, Apr. 1990. [Online]. Available: http://ijr.sagepub.com/cgi/content/abstract/9/2/62

[11] S. H. Collins, "A three-dimensional passive-dynamic walking robot with two legs and knees," The International Journal of Robotics Research, vol. 20, no. 7, pp. 607–615, Jul. 2001. [Online]. Available: http://ijr.sagepub.com/cgi/content/abstract/20/7/607

[12] M. Wisse and J. V. Frankenhuyzen, "Design and construction of mike; a 2-d autonomous biped based on passive dynamic walking," in Adaptive Motion of Animals and Machines. Tokyo: Springer-Verlag, 2006, pp. 143–154. [Online]. Available: http://www.springerlink.com/content/m4720323068452v6/

[13] S. Collins, A. Ruina, R. Tedrake, and M. Wisse, "Efficient bipedal robots based on passive-dynamic walkers." Science, vol. 307, no. 5712, pp. 1082–5, Feb. 2005. [Online]. Available: http://www.sciencemag.org/content/307/5712/1082.abstract

[14] T. Geng, B. Porr, and F. Worgotter, "A reflexive neural network for dynamic biped walking control," Neural Computation, vol. 18, no. 5, pp. 1156–1196, May 2006. [Online]. Available: http://www.mitpressjournals.org/doi/pdf/10.1162/neco.2006.18.5.1156

[15] J. Guckenheimer and S. Johnson, "Planar hybrid systems," in Hybrid Systems II. London, UK: Springer-Verlag, 1995, pp. 202–225. [Online]. Available: http://portal.acm.org/citation.cfm?id=646875.710001

[16] J. Cortes, "Discontinuous dynamical systems," IEEE Control Systems Magazine, vol. 28, no. 3, pp. 36–73, Jun. 2008. [Online]. Available: http://ieeexplore.ieee.org/xpl/freeabs_all.jsp?arnumber=4518905

[17] H. R. Martinez Salazar and J. P. Carbajal, "Exploiting the passive dynamics of a compliant leg to develop gait transitions," Phys. Rev. E, vol. 83, no. 6, p. 066707, Jun 2011.

[18] P. T. Piiroinen and Y. A. Kuznetsov, "An event-driven method to simulate Filippov systems with accurate computing of sliding motions," ACM Transactions on Mathematical Software, vol. 34, no. 3, pp. 1–24, May 2008. [Online]. Available: http://portal.acm.org/citation.cfm?doid=1356052.1356054

[19] J. W. Eaton, GNU Octave Manual. Network Theory Limited, http://www.octave.org, 2002. [Online]. Available: http://www.octave.org

[20] J. D. Hunter, "Matplotlib: A 2d graphics environment," Computing In Science & Engineering, vol. 9, no. 3, pp. 90–95, May-Jun 2007.

Appendix C

Robustness: a new SLIP model based criterion for gait transitions in bipedal locomotion

Reprinted from:

Martínez, H. R., and Carbajal, J. P. (2013). *Robustness: a new SLIP model based criterion for gait transitions in bipedal locomotion*, submited to the Journal of the Royal Society Interface.

Robustness: a new SLIP model based criterion for gait transitions in bipedal locomotion

Harold Roberto Martínez Salazar *[1], Juan Pablo Carbajal[1], and Yuri P. Ivanenko[2]

[1]Artificial Intelligence Laboratory, Department of Informatics, University of Zurich, Switzerland
[2]Laboratory of Neuromotor Physiology, Fondazione Santa Lucia, Italy,

July 18, 2013

Abstract

Bipedal locomotion is a phenomenon that still eludes a fundamental and concise mathematical understanding. Conceptual models that capture some relevant aspects of the process exist but their full explanatory power is not yet exhausted. In the current study, we introduce the robustness criterion which defines the conditions for stable locomotion when steps are taken with imprecise angle of attack. Intuitively, the necessity of a higher precision indicates the difficulty to continue moving with a given gait. We show that the spring-loaded inverted pendulum model, under the robustness criterion, is consistent with previously reported findings on attentional demand during human locomotion. This criterion allows transitions between running and walking, many of which conserve forward speed. Simulations of transitions predict Froude numbers below the ones observed in humans, nevertheless the model satisfactorily reproduces several biomechanical indicators such as hip excursion, gait duty factor and vertical ground reaction force profiles. Furthermore, we identify reversible robust walk-run transitions, which allow the system to execute a robust

*If you have queries relating to the content of the paper, please contact martinez@ifi.uzh.ch

version of the hopping gait. These findings foster the spring-loaded inverted pendulum model as the unifying framework for the understanding of bipedal locomotion.

Keywords SLIP model, gait transitions, bipedal locomotion, human locomotion, biomechanics

1 Introduction

The study of bipedal locomotion has motivated the development of several models that explain the most important principles governing the dynamics of the observed gaits. Some researchers have adopted models that include detailed representations of different leg components or that emulate neuromuscular structures using physical elements such as springs, dampers and multi-segmented legs. Although these models reproduce the dynamics of locomotion, their use as conceptual models is not widespread due to their complexity. In contrast, simpler models have been used extensively as conceptual models of bipedal locomotion [1].

Most of these simple models were developed to explain the exchange of kinetic and potential energy of the center of mass (CoM) of biological agents. During walking, kinetic and potential energy of the CoM are out of phase, i.e. the maximum height of the CoM corresponds with a minimum of its speed [2]. In consequence, the inverted pendulum (IP) model [3] is frequently used to represent walking, since in this model the exchanges of energy are also out of phase. Detailed analyses of the passive dynamics of the IP model constituted a conceptual cornerstone for the development of mechanical devices capable of stable walking without any actuators or controllers [4]. Despite its conceptual explanatory power, the IP model does not correctly reproduce several aspects of human walking [5], e.g. the vertical oscillations of the CoM experimentally observed are smaller than the ones predicted by the model. Inspired in this model Srinivasan and Ruina proposed a biped model with ideal actuators on the legs [6]. They determined the periodic gaits that minimized the work cost assuming that the leg forces are unbounded if necessary. They found that transitions from walking to running at constant Froude number and step length are possible only when the Froude number is one. As a result, they found an optimal walking gait that resembles the conditions of the walking gait at human walk to run transition, but at this condition they did not found an optimal running gait. In contrast, they identified a hybrid gait called pendular running which is not supported with the experimental data of human gait transitions. Further more, in this study the double support

phase in walking was not allowed.

Running is commonly represented with another model, the spring-loaded inverted pendulum (SLIP) [7]. The SLIP model consist of a point mass (the body) attached to a massless spring (the leg). During the stance phase the spring is fixed to the ground via an ideal revolute joint that is removed during flight phase. This model has been successfully used for the control of running machines [8]. In terms of combining multiple gaits, the explanatory power of the SLIP model surpasses that of the IP model, since the former can be extended to reproduce the mechanics of human walking by adding an extra massless spring representing the second leg, therefore unifying walking and runnig in a single model. However, the analyses carried out with the SLIP model had not yet explained gait transitions at constant forward speed, e.g. from walking to running at a characteristic Froude number. Previous studies suggested that transitions were only possible if the total energy was drastically increased or decreased to induce a considerable change in the forward speed of the system [9]. With a simulation study [10], Srinivasan explained gait transitions for springless bipeds model as a mechanism to minimize the energetic cost of the locomotion. However, in the case of springy biped systems the walk to run transition is not predicted by work minimization because for a certain range of stiffness it is possible to find work-free running at very low speeds.

Given that the legs in the SLIP model are massless, their swinging motion cannot be directly described using equations derived from Newton's laws. Therefore, a control policy that sets the angle of attack at touchdown (the angle spanned by the landing leg and the horizontal at the time the foot collides with the ground) must be defined a priori. Generally, the angle of attack at touchdown is kept constant. Herein, we assume a more general control policy: the system selects a new angle of attack at each step. The study of the system is based on a return map. With the return map, we can understand the evolution of the dynamical system as a function of the selection of the gait and the angle of attack. This analysis is similar to [11, 12, 13], but in our study we define the return map at midstance. With this analysis, we can identify the initial conditions that under this control policy can perform indefinitely a gait. Instead of adding perturbations to the terrain to measure the robustness of the system as in [14], we extended the concept of viability introduced in [15], and assume that all the initial conditions with a valid control policy must be able to select an angle of attack inside a range of an arbitrary minimum size. We considered the length of a range of valid angles of attack to produce a qualitative measure of the robustness. The regions in which this control policy is valid, we called them robust regions, and regions where the system can change from one gait to another are called

transition regions.

In this study, we propose this defined robustness as a criterion to explain the onset of gait transitions, complementing the classical energetic criterion [16, 17]. Intuitively, the robustness of a gait can be understood as inversely related to the attentional demand required to maintain it. If highly precise inputs are needed to continue with a gait the system must spend more resources to select an adequate action, e.g. use of detailed models, better estimation of states from noise sensory data, more processing time; i.e. cognitive load or attention.

This new perspective is accompanied with a trade-off between robustness and energetic cost. A similar trade-off have been observed in bees [18]: when flying in turbulent flows, the animal extends its lower limbs reducing the chances of rolling, but increases the drag force sacrificing forward speed. Furthermore, the transitions found under the newly included robustness criterion qualitatively reproduce experimental values of the changes in the amplitude of the oscillations of the hip, changes in the gait duty factor and variations of ground reaction forces. Incidentally, these transitions use a gait pattern that we identify with hopping.

This paper is organized as follows. In section 2, we define the models used for the simulation and introduce several concepts required for the understanding of the results. In section 3 we show the regions of robust locomotion and gait transition. In that section we also compare our results with biological data. Discussions are given in section 4 and we conclude the paper in section 5.

2 Definitions

The time evolution of a gait is segmented in several phases, each phase is described with a sub-model. These sub-models represent the motion of a point mass under the influence of: only gravity (flight phase), gravity and a linear spring (single stance phase), gravity and two linear springs (double stance phase). The point mass stands for the body of the agent and the massless linear springs model the forces from the legs. During walking, running and hopping the system always goes through the single stance phase, therefore all gaits can be studied and compared during this phase. We denote the maps defined by walking, running and hopping as $\mathcal{W}$, $\mathcal{R}$ and $\mathcal{H}$, respectively. Given an initial state x_i of the model, a walking step taken with angle of attack α is denoted $x_{i+1} = \mathcal{W}_\alpha(x_i)$ and similarly for running. As explained later a step of the hopping gait requires two angles, therefore it can be denoted with $x_{i+1} = \mathcal{H}_{\alpha\beta}(x_i)$.

The state of the system is observed when its continuous trajectory passes through a section, called $\mathcal{S}$. This section is defined by the support leg forming a right angle with the ground. At this section the state of the system is defined by the height of the hip (i.e. height of the CoM), r, and the velocity in the vertical direction, v_y (see Appendix A for more details).

All initial conditions are given in the $\mathcal{S}$ section and in the single stance phase, i.e. only one leg touching the ground and oriented vertically. (r, v_y) pairs were simulated for values of the total energy E in the range $[780, 900]$J at intervals of 10 J. The model was implemented is in MATLAB(2009, The MathWorks) and simulations were run using the step variable integrator ode45. Experimental data analysis was performed using GNU Octave.

2.1 Viability, Robustness, symmetric gaits and biomechanical observables

Viability, as presented in [15], defines the easiness of taking a further step during locomotion. That is, the wider the range of angles of attack that can be used to take a step the easier is to take that step. In a physical platform it is required that a valid angle of attack exists for a definite interval, since real sensors and actuators have a finite resolution and are affected by noise. A viability region in the section $\mathcal{S}$ contains all the states for which at least one step can be taken selecting an angle of attack from an interval of at least $\Delta\alpha$, i.e. states for which if at least one iteration of the gait is applied map into states of the same gait. For example, for the running gait, this can be expressed as,

$$\begin{aligned} V^R(\Delta\alpha) = &\{x |\ x \in \mathcal{S} \wedge \\ &(\exists \alpha \in I_\alpha,\ \|I_\alpha\| \geq \Delta\alpha \mid y = \mathcal{R}_\alpha(x),\ y \in \mathcal{S})\}. \end{aligned} \tag{1}$$

Where I_α stands for the angle interval and $\|I_\alpha\|$ for its size. Narrower angle intervals, i.e. more precise angle definition, lead to bigger viability regions and wider intervals to smaller regions. An example of the viability regions can be found in A.

The concept of *robustness* is defined on top of that of viability. A state in the robust region is a viable state that can always be mapped into the robust region by choosing the appropriate angle of attack. This angle should be viable, i.e. it must be selected from an interval of at least $\Delta\alpha$. For example, for the walking gait, this can be expressed as,

$$\begin{aligned} \rho^W(\Delta\alpha) = &\{x |\ x \in \rho^W(\Delta\alpha) \wedge \\ &\big(\exists \alpha \in I_\alpha,\ \|I_\alpha\| \geq \Delta\alpha \mid y = \mathcal{W}_\alpha(x),\ y \in \rho^W(\Delta\alpha)\big)\}. \end{aligned} \tag{2}$$

Where I_α stands for the angle interval and $\|I_\alpha\|$ for its size. This assumes that the controller can select an angle of attack for each step. In particular, this includes constant angle of attack policies and some of the self-stable regions identified in [9] belong to a robust region. However, this does not mean that the system remains in the self-stable region for each step, since that would imply that the angle of attack is selected precisely. Instead, robustness implies that if the system was in that region at time t, it can remain close to it, even if the angles are selected with finite resolution.

The gaits commonly used by humans are symmetric, meaning that the dynamical behavior of the left leg mirrors the one of the right leg. In our model this is possible when two conditions are satisfied: the velocity in the vertical direction at $\mathcal{S}$ is zero and there is an angle of attack α that can bring the system back to the same state.

In the subsequent section we will show that the discovery of robustness as a useful criterion to induce gait transitions allows for qualitative comparisons with experimental biomechanical data. In particular we present results in terms of *Froude number*, *hip excursion*, *gait duty factor*, and *vertical ground reaction forces*. The Froude number is the ratio between the weight and the centripetal force ${}^{w^2 l_o}/_{g}$, where g is the acceleration due to gravity, l_o is the natural length of the leg and w is the angular velocity of the body around the foot in contact with the ground. Hip excursion denotes the amplitude of vertical oscillations of the hip. The gait duty factor is the fraction of the total duration of a gait cycle in which a given foot is on the ground. The vertical ground reaction force is vertical component of the normal force exerted by the ground.

3 Results

We report the results obtained from the study of gait transitions in the SLIP model following the criterion of robustness detailed in Section 2.1. It turns out that the concept of robust gaits offer an alternative explanation for the onset of gait transitions in bipedal locomotion, comparable with arguments based on metabolic costs.

We begin our exposition with a detailed explanation of the conditions, in terms of decrease of robustness, that may trigger gait transitions. From there we move on to describe the mechanism underlying robust gait transitions. The results of those two sections are combined to present qualitative comparison with biomechanical observables, followed by a short description of robust hopping.

The definition of robust gait applies for symmetric and non-symmetric

gaits. Figure 1a shows the area of the robust regions in the section $\mathcal{S}$ for different energies and different interval lengths $\Delta\alpha$. With this model we identify three different gaits: running, walking and grounded running. Grounded running has the same phases as walking but in the transition from the single support to the double support the vertical velocity of the center of mass is positive while in walking the velocity is negative (Appendix A). Results show that the grounded running gait is less robust that walking and running. For a $\Delta\alpha$ bigger than 0.5°, the grounded running gait covers less than 15% of the initial conditions in the section $\mathcal{S}$.

Figure 1b shows the area of the viable transitions to the robust regions in the section $\mathcal{S}$ for different energies and different interval lengths $\Delta\alpha$. For example, the viable transition to robust running considers the initial conditions outside robust running that under walking or grounded running can be brought to robust running in one step. Given that this transitions are viable the angle of attack can be selected from an interval of length $\Delta\alpha$. A similar condition is applied to calculate the viable transition to robust walking or robust grounded running. For a $\Delta\alpha$ bigger than 0.75°, the viable transition to robust grounded running gait covers less than 10% of the initial conditions in the section $\mathcal{S}$. Figure 1c shows the total area of robust regions and viable transitions with and without grounded running. Results show that for a $\Delta\alpha$ bigger than 0.5° grounded running does not cover different initial conditions from walking and running.

Figure 1d shows the range of forward speed for robust running and walking at several energies and different interval lengths $\Delta\alpha$. Results show that the length of the interval affects the maximum Froude number in the walking gait. The bigger the $\Delta\alpha$, the lower the walking Froude number. In addition considering an interval length lower than 1°, robust walking exists only at low locomotion energies, while running increases robustness for higher energies. For an interval length bigger than 1° walking walking is not possible in all the low energy levels.

The results of the system with an interval length lower than 1° are consistent with the experimental results reported in [19], where it was shown that imposed fast walking required higher attention than running at similar speeds. Furthermore, normal switching between gaits did not required high attentional demand.

3.1 Conditions for transitions

We studied the transitions for a robustness criterion of $\Delta\alpha$ equal to 1° because this was the limit condition in which the results of attentional demand can be qualitatively explained by the model. In addition we focused in the walking

and running gait given that grounded running does not provide new possible states from the ones identified in robust walking and robust running (Fig. 1c). All the possible states of the system in the section $\mathcal{S}$ lie in a hemispherical region (see equations (15)-(21) of [15] and Appendix A). In Fig. 1e-g, we marked the apex of this hemisphere with a star symbol. The closer the system is to the star, the higher the forward speed of the gait. Symmetric gaits are marked with a solid line, all symmetric gaits have $v_y = 0$. The figure shows that symmetric robust walking moves away from the apex of the hemisphere as energy increases, i.e. it becomes slower. At 830 *joule* symmetric robust walking is constrained to the rightmost side of the viability region reducing the speed of this gait considerably. Furthermore, at this energy the region of symmetric walking breaks down into two unconnected segments. This is also evident in Fig. 1d where the maximum speed of symmetric robust walking shows a strong slowdown with a sudden change of slope. The latter is a consequence of the rupture of the symmetric gait region. This milestone in the evolution of the gait can be used as a natural trigger for a gait transition.

The evolution of the area of robust walking, and robust running, are shown in detail in Figure 1e-f. This figures show that, at low energy, robust walking covers a wide region of the viable states of the system, while at high energy robust running covers a wider area. Around 800 J both robust gaits have similar area. Based on robustness alone, this will imply a transition. However, symmetric robust walking intersects the apex of the hemisphere producing the fastest forward speed up to energies of 810 J, favoring walking in terms of energy efficiency. When the energy is increased further, the area of robust walking decreases and symmetric robust walking is constrained to low speeds. Due to these facts, at energies close to 840 J, the speed of symmetric robust walking and running match. For higher energies the gait transition is imminent, since the only robust gait remaining is symmetric running.

3.2 Mechanism of gait transitions

Assuming that during locomotion the fastest robust gait patterns are preferred over slower or non-robust ones, we see that for energies below 840 J walking is the gait of choice and for energies above that value running would be chosen. Therefore, we study viable transitions at 840 J and compare them with results from an experiment on human gait transition. We consider transitions only when all angles of attack used in the process can be chosen from an interval of length 1° or greater, i.e. we define admissible transitions using the concept of viability (sec. 2.1).

We consider two mechanisms to execute gait transitions between symmetric robust gaits (symmetric gaits are known to be self-stable and therefore

a good choice for stable locomotion, see [9]). The first mechanism, which can only be used from walking to running, consist in moving from the robust region of walking to the viability (non-robust) region of the same gait, and from there select an angle of attack to go to the robust region of running. This mechanism can be used in robust walking between 830 J and 840 J (see Figure 2a). The second mechanism consist in going from a robust region of a given gait (walking or running) directly to the robust region of a different gait. This mechanism is applicable for robust running between 830 J and 840 J while in robust walking is only applicable around 840 J.

These mechanisms can be further constrained by selecting desired properties of the final gait. One possibility is to execute a transition in such a way that the final gait has the same (or as close as possible) Froude number as the initial gait. Another possibility is to execute a transition that sets the hip excursion of the new gait to a desired value (see Figure 2b for a graphical description). These constraints are referred in this study as strategies and they are used for the comparison between our simulated results and experimental data presented in the next section.

3.3 Qualitative Prediction of Biomechanical Observables

As we mention before, the biomechanical observables used to compare our results with experimental data are: Froude number, hip excursion, gait duty factor and vertical ground reaction forces. In the Appendix B-C, we extended this comparison to include angle of attack sequences and change of phase. We compare all our simulations against the experimental data reported in Figure 2 of [20], we will refer to this data as "experimental data" or "the experiment".

Figure 2a shows the transition regions at two energy levels. We painted the robust regions of running and walking with a solid color, the shaded regions inside these are transitions regions where the system can change the gait. The diagonal shading corresponds to regions where the system can change between robust gaits (non-symmetric) in only one step. The horizontal shading delimits the region where the system can go to the non-robust transition region, as described in 3.2. The right panel shows examples of a transition from walking to running and another from running to walking using the two mechanisms mentioned in the previous section. For the first transition, the system starts at symmetric robust walking (1), in the first step it moves to the non-robust transition region (2*) and executes the transition to robust running (3*). With two further steps the system is able to

reach symmetric robust running (4-5). The transition in the other direction starts at symmetric robust running (5). Then the system moves to the robust transition region (6*) from which, in a single step, it changes to robust walking (7*). With two more steps the system reaches symmetric robust walking (8-9). In both transitions, the hip excursion was kept as constant as possible.

Figure 2b shows the Froude number and the hip excursion of all symmetric robust gaits at 840 J. As indicated in the figure, vertical transitions keep the hip excursion constant, while horizontal transitions produce gaits with the same Froude number.

Figure 3 shows time series of hip excursion and duty factor for a transition at constant hip excursion, together with a transition at constant Froude number. In both situations we obtain a Froude number that is about 60% smaller than the one found in human gait transitions, which is around of 0.5 [20]. Nevertheless the SLIP model provides the best Froude number estimation to the date, when compared to other simple models, e.g. the IP model.

Ground reaction forces prior to the transition from walking to running have three main characteristics [21]. Firstly, they present an asymmetric double bell-shaped profile. Secondly, the earlier peak becomes bigger than the later one and, thirdly the depression between the peaks becomes more accentuated in the last step of walking, exactly before the transition. In the case of the transition from running to walking, it was reported that the vertical ground reaction forces decrease during the steps prior to the transition.

In Figure 4 we have plotted the vertical ground reaction forces for three different simulated examples. The first row of panels shows transitions from walking to running, and the second row of panels shows transitions in the other direction. Panels (a) and (b) show transitions keeping the Froude number constant. Panels (c) and (d) show transitions at constant hip excursion. The last example, presented in the panels (e) and (f), shows transitions that match the change in amplitude that was observed in the experiment. All cases qualitatively match the characteristics of the ground reactions reported in [21]. The decrement in the force of the last running step is due to the support of the second foot. A reduction of the peak in more than one step appears only on the case where we matched the hip excursion of the experimental data.

In Table 1, we present a summary of the comparison between the simulated examples and the experimental data. Each column is discussed next. Due to the variety of transitions that can be generated with the model, the number of steps to execute them can be select in a wide range, at least from

Strategy	# Steps	v_x	Δr	F_y	$\Delta\alpha$	$\Delta\phi$
Const. Froude number	✓	✗	✗	✓	✓	✗
Const. hip excursion	✓	✗	✗	✓	✓	✗
Fitting experiment	✓	✗	✓	✓	✓	✗

Table 1: Comparison between three transition strategies and experimental data. The symbol ✓ indicates qualitative matching between simulation and experiment, while the symbol ✗ indicates the opposite. v_x: forward speed of the center of mass; Δr: relative change in hip excursion before and after transition; F_y: vertical ground reaction forces; $\Delta\alpha$: change of the angle of attack during transition; $\Delta\phi$: change in phase of the oscillations of the hip before and after transition.

3 to 8 steps. From Figure 2b we can see that the Froude number of all these transitions are lower than 0.5, this reflects the fact that the simulations have lower forward speeds (v_x) than the observed in humans. As pointed before, the many transitions that can be simulated, permit the matching of the relative change in hip excursion (Δr) measured in the experiment. In all simulated transitions the vertical ground reaction forces (F_y) are qualitatively well reproduced. The selection of the angle of attack are qualitative similar to what we found in the experimental case: the system moves progressively from one gait to the other changing the angle of attack at each step. However, the oscillation of the hip before and after the simulated transitions presents a change of phase ($\Delta\phi$) that not always coincide with what is observed in reality. Details for these two observables are presented in the the Appendix B-C.

3.4 Robust Hopping Gait

At 840 J we identify a transition region in robust walking where the system can go in one step to robust running. Among the states in this transition region, there a some that are mapped directly into the transition region of robust running. By selecting alternatively the right angles of attack, the system can sequentially walk and run, producing the hopping gait. Fig. 5 shows an example of this gait. By looking at the vertical ground reaction forces in the figure, we see the different phases that compose this gait; from single stance phase to double stance phase then to single stance phase and finally to flight phase.

4 Discussion

Herein we have modeled bipedal locomotion using the SLIP model. This model conserves the total mechanical energy and at first glance it may seem inapposite for the prediction of gait transitions, since work has to be done on the system to increase the speed of locomotion. Nevertheless, by looking at the behavior of the model at different energies, we can emulate the situation where work is done on the system.

We proposed robustness as a new measure of the easiness of locomotion. Robustness measures the level of attention that needs to be dedicated to take a step; the more robust a gait is, the less attention that is needed to take the next step.

According to our results, the selection of the gait can be based on two criteria: efficiency, which is the selection of the gait with the highest forward speed; and robustness, which defines how easy is to maintain the given gait. This second criterion is consistent with the experimental results of attentional demand in locomotion reported in [19]. Based on these criteria, walking is the best choice for energies below 840J, and running is more appropriate for higher energies. This resembles what is observed in human locomotion.

Using robustness as the leading criterion, we identify transition regions that allow the system to go from one gait to the other even in the case of imprecise angle selection. These transition regions are present for energies from 830 J to 840 J (Fig. 2a). At 840 J, symmetric robust running and walking share all the possible velocities, facilitating gait transitions. In the case of an increment of energy, to keep robustness and move forward faster, a walking system can execute a transition to robust running at 840 J. The transition can be reversed when the system decreases its energy. Note that the mechanisms of transition shown in Fig. 2a (right panel), have the following properties. One mechanism connects the robust region of both gaits, while the other one connects the non-robust viability region of walking with robust running. The latter mechanism is not reversible, meaning that the system cannot go from running back to this region in a single step. The transitions connecting robust regions are reversible and the system can oscillate between the two gaits robustly. Is in this situation where the hopping gait emerges. This locomotion pattern is frequently used by children when playing joyfully.

The existence of non-empty transition regions (Fig. 2b) implies that the system has multiple alternatives to change gaits. These alternatives will produce different changes of forward speed and hip excursion. We show three different scenarios: constant hip excursion, hip excursion similar to experimental data and constant Froude number.

When the transition matches the hip excursion of the experimental data, the Froude number varies from 0.16 in walking to 0.08 in running, while in the experiment it is almost constant (slowly varying treadmill speed, see [20] for details on the experiment). As explained before, in all simulated cases the absolute values of Froude number are lower than in the experiments. The hip excursion has an amplitude of 5.2 cm in walking and 8.3 cm which also similar to the one reported in [20] which is around 7 cm.

When the transition keeps the Froude number constant the hip excursion decreases from 5.7 cm in walking to 3.7 cm in running. This contradicts the behavior observed in our experimental data. The simulated Froude number for this transition is about 0.17.

The robustness criterion induces an underestimation of the forward speed at gait transitions. The highest Froude number achieved using the previous strategies is around one third of the one observed in humans (0.5). However, given the strong simplifications in the model the result is encouraging. To reduce the gap between simulated and experimental Froude number, the model can be extended to include the displacement of the point where the leg is in contact with the ground during the stance phase [22].

All transitions presented here produce similar results concerning the duty factor. Walking has a duty factor around 0.7 and running has a duty factor around 0.4, in accordance with the experiment. Furthermore, in all transitions from walking to running the model predicts a progressive change in the vertical component of the reaction forces, i.e. the relation between the first and the second peak of the force during the transition. This also applies to the transitions from running to walking. In particular, the ground reaction forces corresponding to transitions matching the hip excursion of the experimental data (Fig. 4) introduces a progressive reduction of the force peak in more than one step. All these results qualitatively reproduce the experimental results reported in [21].

5 Conclusion

The comparison between experimental data and simulations using the SLIP model shows that the model is not able to generate accurate quantitative predictions. Most strikingly, the forward speed in the simulations are considerable slower than that observed experimentally. This difficulty can be overcome by adding a more detailed description of the contact between leg and ground. Nevertheless, the SLIP model can be used as a conceptual model to explain the many aspects of bipedal locomotion such as the mechanics of running, walking, hopping and gait transitions.

Our findings indicate that robustness can play an important role in inducing gait transition, complementing the usual view focused solely in energy expenditure. The robustness criterion is analogous to the attentional demand during locomotion and may play an important role deciding the gait transition events. To our knowledge this is the first time such a criterion is included in a numerical model of locomotion.

Acknowledgements The research leading to these results has received funding from the European Community's Seventh Framework Programme FP7/2007-2013-Challenge 2-Cognitive Systems, Interaction, Robotics- under grant agreement No 248311-AMARSi.

Authors contribution **HMS** developed the computational and mathematical model, run the simulations and performed data analysis. **JPC** collaborated in development of the mathematical models, the data analysis and the interpretation of results. **YI** collected and contributed the experimental data. All authors contributed to the writing of this manuscript.

References

[1] P. Holmes, R. J. Full, D. Koditschek, and J. Guckenheimer. The dynamics of legged locomotion: Models, analyses, and challenges. SIAM Rev., 48(2):207–304, 2006.

[2] G. A. Cavagna, N. C. Heglund, and C. R. Taylor. Mechanical work in terrestrial locomotion: two basic mechanisms for minimizing energy expenditure. Am. J. Physiol.-Reg. I., 233(5):R243–R261, 1977.

[3] S. Mochon and T. A. McMahon. Ballistic walking. J. Biomech., 13(1):49–57, 1980.

[4] S. H. Collins. A three-dimensional passive-dynamic walking robot with two legs and knees. Int. J. Robot. Res., 20(7):607–615, July 2001.

[5] R.J. Full and D.E. Koditschek. Templates and anchors: neuromechanical hypotheses of legged locomotion on land. J. Exp. Biol., 202(23):3325–3332, 1999.

[6] Manoj Srinivasan and Andy Ruina. Computer optimization of a minimal biped model discovers walking and running. Nature, 439(7072):72–75, 2005.

[7] R. Blickhan. The spring-mass model for running and hopping. J. Biomech., 22(1112):1217 – 1227, 1989.

[8] B. Andrews, B. Miller, J. Schmitt, and J.E. Clark. Running over unknown rough terrain with a one-legged planar robot. Bioinspir Biomim, 6(2):026009, 2011.

[9] H. Geyer, A. Seyfarth, and R. Blickhan. Compliant leg behaviour explains basic dynamics of walking and running. P. Roy. Soc. B - Biol. Sci., 273(1603):2861–7, November 2006.

[10] Manoj Srinivasan. Fifteen observations on the structure of energy-minimizing gaits in many simple biped models. Journal of The Royal Society Interface, 8(54):74–98, 2011.

[11] M Ernst, H Geyer, and R Blickhan. Extension and customization of self-stability control in compliant legged systems. Bioinspiration & Biomimetics, 7(4):046002, 2012.

[12] Michael Ernst, Hartmut Geyer, and Reinhard Blickhan. Spring-legged locomotion on uneven ground: a control approach to keep the running speed constant. In International Conference on Climbing and Walking Robots (CLAWAR), pages 639–644. World Scientific, 2009.

[13] Andre Seyfarth and Hartmut Geyer. Natural control of spring-like running-optimized self-stabilization. In Proceedings of the Fifth International Conference on Climbing and Walking Robots (CLAWAR 2002), Professional Engineering Publishing Limited, London, pages 81–85, 2002.

[14] Katie Byl and Russ Tedrake. Metastable walking machines. The International Journal of Robotics Research, 28(8):1040–1064, 2009.

[15] Harold Roberto Martínez Salazar and Juan Pablo Carbajal. Exploiting the passive dynamics of a compliant leg to develop gait transitions. Phys. Rev. E, 83(6):066707, Jun 2011.

[16] R. M. Alexander. Optimization and gaits in the locomotion of vertebrates. Physiol. Rev., 69(4):1199–1227, October 1989.

[17] A. E. Minetti, L. P. Ardigo, and F. Saibene. The transition between walking and running in humans: metabolic and mechanical aspects at different gradients. Acta Physiol. Scand., 150(3):315–323, 1994.

[18] Stacey A Combes and Robert Dudley. Turbulence-driven instabilities limit insect flight performance. P. Natl. Acad. Sci.-Biol., 106(22):9105–8, June 2009.

[19] Bruce Abernethy, Alastair Hanna, and Annaliese Plooy. The attentional demands of preferred and non-preferred gait patterns. Gait Posture, 15(3):256 – 265, 2002.

[20] Yuri P Ivanenko, Francesca Sylos Labini, Germana Cappellini, Velio Macellari, Joseph McIntyre, and Francesco Lacquaniti. Gait transitions in simulated reduced gravity. J. Appl. Physiol., 110(3):781–8, March 2011.

[21] Li Li and Joseph Hamill. Characteristics of the vertical ground reaction force component prior to gait transition. RQES, 73(3):229–237, 2002.

[22] Peter G. Adamczyk, Steven H. Collins, and Arthur D. Kuo. The advantages of a rolling foot in human walking. J. Exp. Biol., 209(20):3953–3963, 2006.

[23] J. W. Eaton. GNU Octave Manual. Network Theory Limited, http://www.octave.org, 2002.

A Equations of motion

We define a running gait as a trajectory that switches from the single stance phase to the flight phase and back to the single stance phase. A walking gait is defined as a trajectory that switches from the singles stance phase to the double stance phase and back again to the single stance phase.

The state in the flight phase is represented in Cartesian coordinates of the position of the point mass and its velocity $\vec{X}_{ff} = (x, y, v_x, v_y)^T$,

$$\dot{\vec{X}}_{ff} = \begin{pmatrix} v_x \\ v_y \\ 0 \\ -g \end{pmatrix}, \tag{3}$$

where g is the acceleration due to gravity.

The state in the single stance phase is represented in polar coordinates $\vec{X}_s = \left(r, \theta, \dot{r}, \dot{\theta}\right)^T$, where r is the length of the spring and θ is the angle

spanned by the leg and the horizontal, growing in clockwise direction. Thus, the equations of motion are:

$$\dot{\vec{X}}_s = \begin{pmatrix} \dot{r} \\ \dot{\theta} \\ \frac{k}{m}(r_0 - r) + r\dot{\theta}^2 - g\sin\theta \\ -\frac{1}{r}\left(2\dot{r}\dot{\theta} + g\cos\theta\right) \end{pmatrix}. \tag{4}$$

It is important to note that $\theta(t_{TD}) = \alpha$, i.e. the angular state at the time of touchdown is equal to the angle of attack. The parameter r_0 defines the natural length of the spring.

In the double stance phase the state is also represented in polar coordinates $\vec{X}_d = \left(r, \theta, \dot{r}, \dot{\theta}\right)^T$, with the origin of coordinates in the new touchdown point. The motion is described by:

$$\dot{\vec{X}}_d = \begin{pmatrix} \dot{r} \\ \dot{\theta} \\ \frac{k}{m}[(r_0 - r) + \left(1 - \frac{r_0}{r_\male}\right)\ldots \\ \quad (x_\male\cos\theta - r)] + r\dot{\theta}^2\ldots \\ \quad - g\sin\theta \\ -\frac{1}{r}[\frac{k}{m}\left(1 - \frac{r_0}{r_\male}\right)x_\male\sin\theta\ldots \\ \quad + 2\dot{r}\dot{\theta} + g\cos\theta] \end{pmatrix} \tag{5}$$

$$r_\male = \sqrt{r^2 + x_\male^2 - 2rx_\male\cos\theta}, \tag{6}$$

where $x_\male$ is the horizontal distance between the two contact points and $r_\male$ is the length of the back leg.

The event functions are parameterized with the angle of attack and the natural length of the springs.

Switches from the flight phase to the single stance phase are defined by:

$$\mathcal{F}_{ff\to s}\left(\vec{X}_{ff}, \alpha, r_0\right) : \begin{cases} y - r_0\cos\alpha = 0 \\ v_y < 0 \end{cases}, \tag{7}$$

which means that the mass is falling and the leg can be placed at its natural length with angle of attack α. Therefore, the motion is now defined in the

single stance phase. The switch in the other directions is simply:

$$\mathcal{F}_{s\to ff}\left(\vec{X}_s, r_0\right) : r - r_0 = 0. \tag{8}$$

These are the only two event functions involved in the running gait. The map from one phase to the other is defined by:

$$x = -r\cos\theta \qquad y = r\sin\theta. \tag{9}$$

It is important to have in mind that the origin of the single stance phase is always at the touchdown point.

For the walking gait, we have to consider switches between single and double stance phases:

$$\mathcal{F}_{s\to d}\left(\vec{X}_s, \alpha, r_0\right) : \begin{cases} r\sin\theta - r_0\cos\alpha = 0 \\ \theta > \frac{\pi}{2} \end{cases}, \tag{10}$$

which is similar to (7) with the additional condition that the mass is tilted forward. Additionally, if we consider the sign of the vertical speed, we differentiate between walking gait with v_y ¡ 0 and Grounded Running gait with v_y ¿ 0.

The switch from the double stance phase to the single stance phase is defined by:

$$\mathcal{F}_{d\to s}\left(\vec{X}_d, r_0\right) : r_{\sigma} - r_0 = 0, \tag{11}$$

with r_{σ} as defined in (6). The map from the double stance phase to the single stance phase is the identity. In the other direction we have:

$$r_d = r_0 \quad \theta_d = \alpha, \tag{12}$$

$$x_{\sigma} = r_0\cos\alpha - r_s\cos\theta_s, \tag{13}$$

where the subscripts indicate the corresponding phase.

If the system falls to the ground ($y \leq 0$), attempts a forbidden transition (e.g. double stance phase to flight phase), or renders $v_x < 0$ (motion to the left,"backwards"), we consider that the system fails.

The state of the model is observed when the trajectory of the system intersects the section $\mathcal{S}$ defined in the single stance phase, i.e. only one leg touching the ground and oriented vertically (Figure 6). The results are visualized using the values of the length of the spring r and the radial component of the velocity which, in $\mathcal{S}$, equals the vertical speed v_y (vx is obtained from

these values and the equation of constant energy). It is important to note that all possible values of r, v_y , and v_x , for a given value of the total energy E, lie on an ellipsoid.

$$E = \frac{1}{2}k\left(r_0 - r\right)^2 + \frac{1}{2}m\left(v_x^2 + v_y^2\right) + mgr \tag{14}$$

This intermittent observation of the system renders the continuous evolution of the model into a mapping that transforms states in the section at a time t, to states in the section at $t + \Delta t$. The interval Δt is the time the system takes to reach a new vertical posture, only during periodic gaits it is equivalent to the period of the gait.

Using the maps we calculated the viability regions in the section $\mathcal{S}$. The viability regions are the initial conditions that can perform an step selecting an angle of attack from a continuous interval of length $\Delta\alpha$ the biggest interval size found with the system is 23°. Figures 7-8 show different viable regions as a function of the interval length.

B Angle of attack estimation from empirical data

In the experimental data of reference [20] the angle of the right limb is measure against the vertical. We use this information to estimate the angle of the leg at landing based in two facts. First, the angle of the leg changes more its velocity in the swing phase (the foot is not in contact with ground) than in the support phase (the foot is in contact with the ground), and second, as soon as the leg changes from the swing phase to the support phase there is a big change of the angular velocity due to the impact of the food against the ground when it lands.

The angle of attack identified using this conditions allow the comparison of the strategy in human locomotion and the proposed model. The model qualitatively develops a similar strategy. The difference of the angle of attack between the steady state gait (e.g. walking or running) from the experiment and the model is around five degrees. To facilitate the qualitative comparison of the angle of attack, we evaluate the change of the angle of attack against the angle of attack of walking. Using this measurement, we can avoid the difference of five degrees and focus in the strategy for gait transition.

Fig. 9 and Fig. 10 show that the strategy developed with the model has similar steps and matches the change of the angle of attack in the transition. Fig. 9 shows a more drastic change of the angles of attack compare with the

experiment result, however the data of the experiment is from one leg which allow the identification of the angle of attack every two steps. This can be emulated with the model selecting only the even or the odd steps. In any of these cases, the change of the angles of attack is going to look less drastic and qualitatively more similar to the ones from the experiment.

C Change of phase of hip excursion before and after transition

Strategy	$\mathcal{W} \to \mathcal{R}$	$\mathcal{R} \to \mathcal{W}$
Const. Froude number	36.3°	35.3°
Const. hip excursion	55.3°	51.5°
Fitting experiment	109.0°	110.9°
Experiment	−35.0°	86.8°

Table 2: Change of phases for three strategies and experimental data. None of the transitions shows a phase change in full accordance with the experimental data. The absolute value of the phase change for the transition from walking to running at constant Froude number is very close to the experimental value, however the direction of the change is opposite.

As shown in Figure 11 (left axis), during walking and running the hip follows and oscillatory trajectory over time. We compare the phase of these oscillations with respect to the moment of transition. The moment of transition was identified as follows:

1. Calculate the analytic signal of the hip trajectory by means of the Hilbert transform, e.g. `hilbert` function in GNU Octave's signal package [23].

2. Obtain the phase of the signal from the angle of the analytic signal.

3. Take the time derivative of the phase, this is an approximation of the frequency of the oscillations as a function of time.

4. Search for the highest peak in the frequency signal. This point separates the regions of walking from the regions of running.

Figure 11 shows the frequency signal superimposed to the experimental data. The transition point is indicated with a vertical arrow. Taking this point as the origin of time, we calculate the initial phase of walking and the initial

phase of running, by means of fitting a first order polynomial to the phase signal of each gait. This is shown in Figure 12 when applied to the experimental data. The change of phase is calculated as the difference of these initial phases normalized to the interval $(-\pi, \pi]$. The exact same analysis was applied to all the signals, simulated and experimental.

The changes of phase for the three transition strategies presented in the paper are summarized in Table 2. All the simulated examples are able to match the direction of the change of phase in the running to walking transition. However, none of the transitions shows a phase change in full accordance with the experimental data. The absolute value of the phase change for the transition from walking to running at constant Froude number is very close to the experimental value, however the direction of the change is opposite.

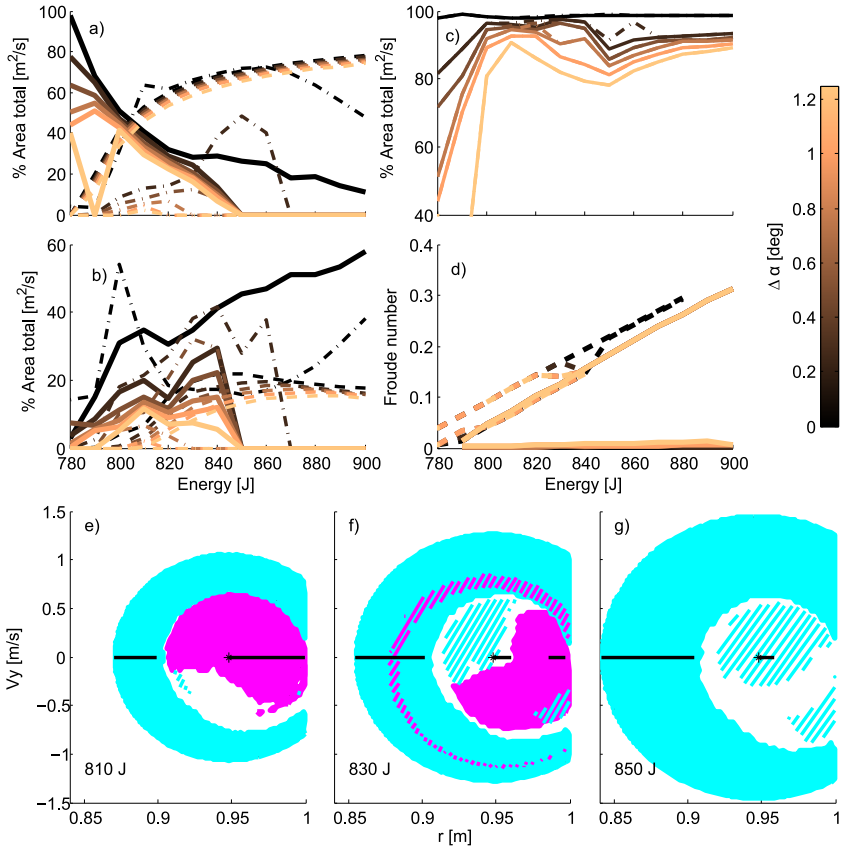

Figure 1: (Color online) Robust regions. For panels **(a)** - **(d)** the (copper) gray color scale represents the interval size used to calculate the robust region. **(a)** shows the robust region area in the section $\mathcal{S}$ for running (dashed line), walking (continuous line), and grounded running (dash-dotted line). **(b)** shows the area of viable transitions that brings the system to robust running (dashed line), robust walking (continuous line), and robust grounded running (dash-dotted line) in the section $\mathcal{S}$. **(c)** shows the total area in the section $\mathcal{S}$ cover by the robust gaits and the viable transitions. The dash-dotted line represents all the gaits, and the continuous line represents walking and running. **(d)** shows the maximum and minimum Froude number for a robust gait at the section $\mathcal{S}$ for different energies. Robust walking is depicted with the dashed line, and robust running is depicted with the continuous line. In panels **(e)** - **(g)** filled patches represents robust running ((blue) light gray) and robust walking ((magenta) dark gray) in the section $\mathcal{S}$. The dashed region represents viable transition to robust running using walking ((blue) light gray), and to robust walking using running ((magenta) dark gray).

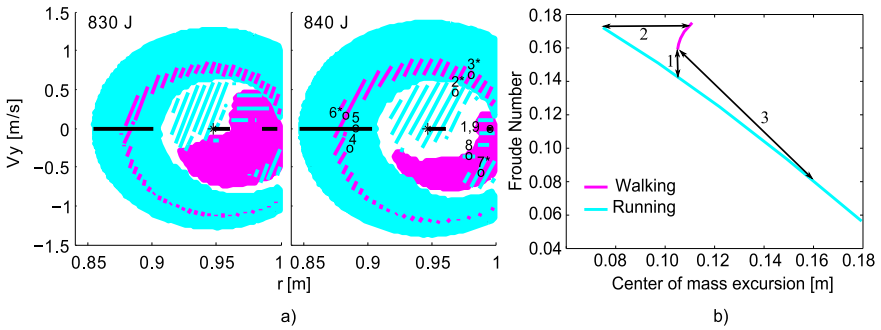

Figure 2: (Color online) Viable transitions. In all panels (blue) light gray color represents running and (magenta) dark gray color represents walking. **(a)** shows viable transitions at two energy levels. Filled patches corresponds to robust regions. Shaded regions inside these are viable transitions regions. Diagonal shading corresponds to regions where the system can change between robust gaits (non-symmetric) in only one step. The horizontal shading delimits the region where the system can go to the non-robust transition region. The right panel shows two transition using both mechanisms. See text for details. **(b)** shows the Froude number versus hip excursion for symmetric robust running and walking at 840 J. Arrows indicate: (1) constant hip excursion, (2) constant Froude number and (3) relative change of the amplitude of the hip excursion fitted to experimental data.

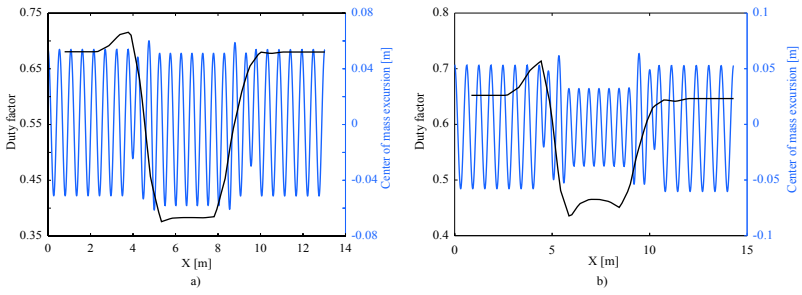

Figure 3: (Color online) Hip excursion and gait duty factor for transition at constant hip excursion **(a)**; and constant Froude number **(b)**. The (blue) light gray color represents the hip excursion and the black line represents the duty factor. The plots show several steps before and after each transition.

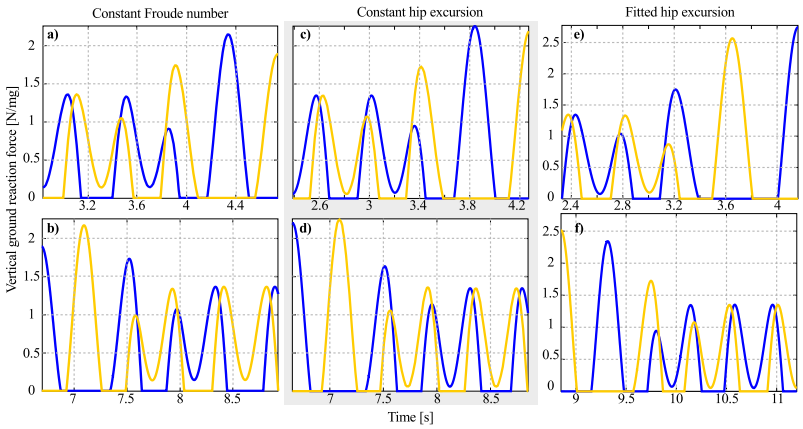

Figure 4: Vertical ground reaction forces during transitions. The six panels show a transition from symmetric robust walking to symmetric robust running with three different strategies, (a)-(b) constant Froude number, (c)-(d) constant hip excursion, (e)-(f) hip excursion similar to the experimental data. The forces present an asymmetric double bell-shaped profile. In the walking to running transition, (a)-(c) and (e), the earlier peak becomes bigger than the later one, exactly before the transition. The transitions in the other direction, running to walking (b)-(d) and (f) show vertical ground reaction forces that decrease considerably in the last running step due to the support of the second foot. The selection of a hip excursion similar to the experimental data introduces a progressive reduction of the force peak in more than one step (f). All forces are normalized with respect to the weight of the system.

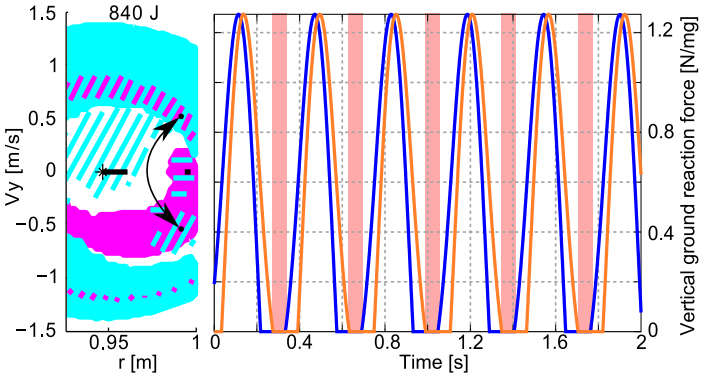

Figure 5: (Color online) Vertical ground reaction forces during hopping. Panel (a) shows the transition regions in section $\mathcal{S}$ for $E = 840$ J; the arrows show the states in the robust transition region that are used alternately. Panel (b) shows the ground reaction forces for each leg. The (pink) gray rectangles show the different flight phases. The forces from the legs are indicated with solid lines with different colors.

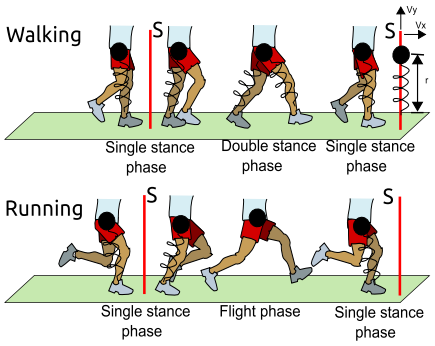

Figure 6: (Color online) Illustration of the evolution of the SLIP model for running and walking. The different phases are indicated as well as the section S where the system is observed.

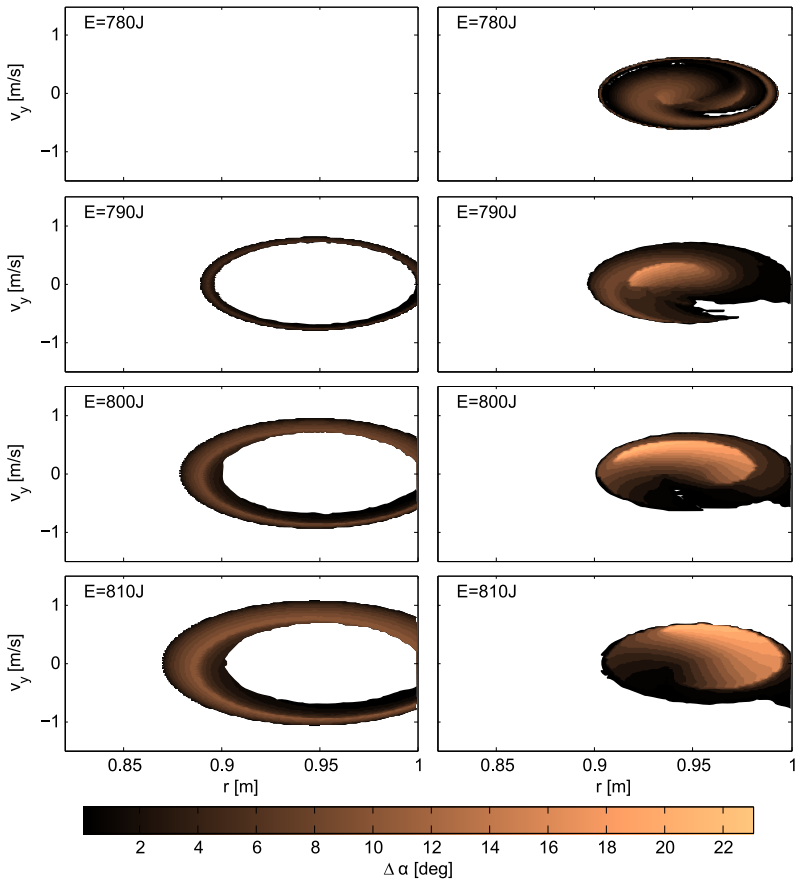

Figure 7: (Color online) Viability regions for running and walking. The (cooper) gray scale color represents the viability regions for energies between [780J-810J]. The first column shows the viability region for running and the second column for walking

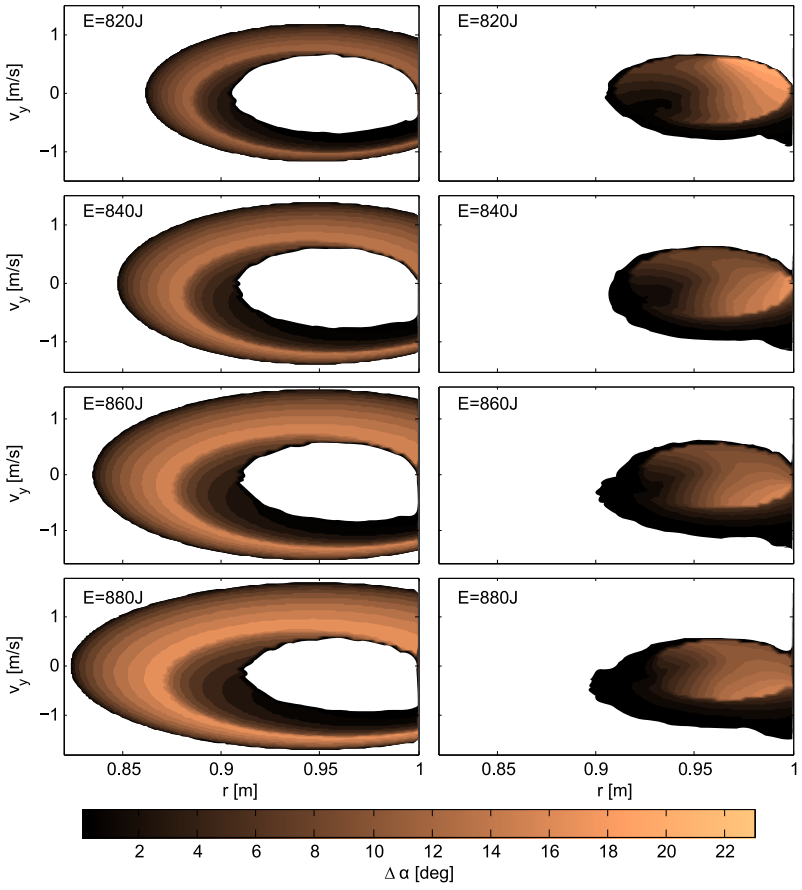

Figure 8: (Color online) Viability regions for walking and running. The (cooper) gray scale color represents the viability regions for energies between [820J-880J].The first column shows the viability region for running and the second column for walking

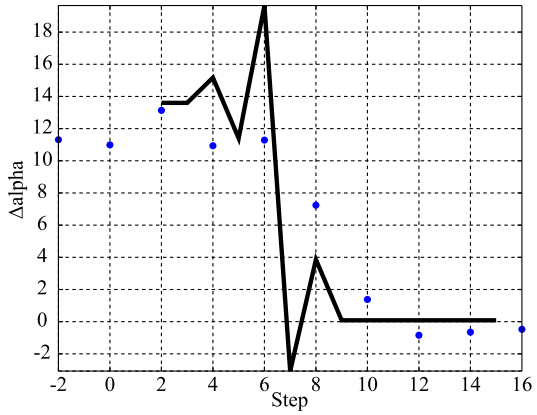

Figure 9: (Color online) Change of the angle of attack in the running to walking transition. The solid line represent the change of the angle of attack in the model and the doted line represent the change of the angle of attack in a human experiment. In both case there is a transition from running to walking.

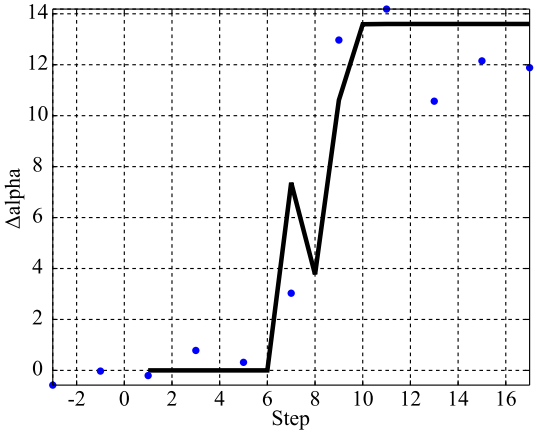

Figure 10: (Color online) Change of the angle of attack against in the walking to running transition. The solid line represent the change of the angle of attack in the model and the doted line represent the angle of attack in a human experiment. In both case there is a transition from walking to running.

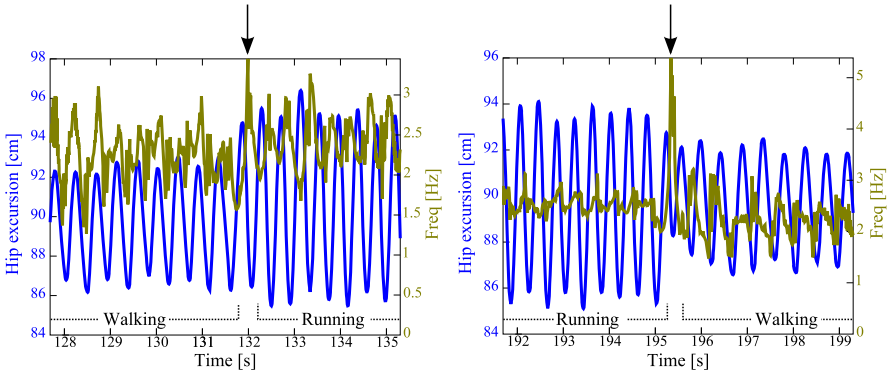

Figure 11: (Color online) Transition point determination. Plot of the experimental data (left axis) and the the derivative of the phase signal (right axis). this derivative gives a frequency signal that presents a peak during the transition that is used to determine the transition point (vertical arrow).

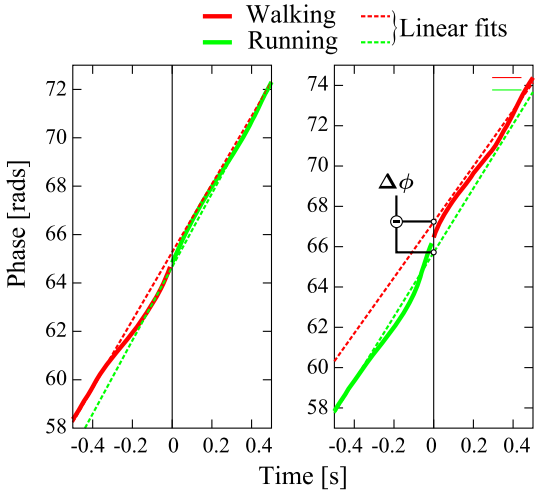

Figure 12: (Color online) Phase difference calculation. Taking the point of transition as the origin of time, the phase difference is calculate from the intercept of linear fits applied to the two parts of the phase signal. Solid lines show the phase signal for walking and running. Dashed lines show the linear fits.

Appendix D

Covariation of Body Parameters Compensates for Mass Disturbances in Human Locomotion

Reprinted from:

Martínez, H. R.(2013). *Covariation of Body Parameters Compensates for Mass Disturbances in Human Locomotion*, submited to the Journal of Experimental Biology.

Covariation of Body Parameters Compensates for Mass Disturbances in Human Locomotion

Harold Roberto Martínez Salazar [1a]

[a]Artificial Intelligence Laboratory, Department of Informatics, University of Zurich, Andreasstrasse 15, 8050 Zurich, Switzerland

[1]If you have queries relating to the content of the paper, please contact martinez@ifi.uzh.ch

Summary

In this paper, we introduce an experimental study with human subjects. We performed the experiment on a treadmill, and collected data for three loading conditions during walking and running. We adopted the Spring Loaded Inverted Pendulum (SLIP) model as a mathematical framework to realize the data analysis. This model has been used in the literature to explain the dynamics of a wide variety of gaits. In contrast with previous studies, we redefine the SLIP model in terms of three non-dimensional variables related to the stiffness, the time and the distance. This reformulation generalizes the equation of motion, and allows comparisons across subjects. Results show that there is a compensation for the change of mass that can be explained in terms of the dimensionless parameters of the model. A direct consequence of the mass compensation is that the control strategy of the gaits does not have to change. We strongly believe that this analysis can be extended to study other important aspects of human gaits.

1 Introduction

The study of bipedal locomotion has motivated the development of conceptual models to explain the most relevant principles ruling the dynamics of a gait Holmes et al. (2006). The spring-loaded inverted pendulum (SLIP)(Blickhan (1989)) is one of this models that has been used extensively to explain the running gait. Geyer et al. (2006) proposed the SLIP model as a unifying framework to describe walking as well by adding an extra massless spring representing the second leg.

This unified perspective explains the exchange of kinetic and potential energy of the center of mass (CoM) for walking and running in human bipedal locomotion. In running, the kinetic and potential energy of the CoM are in phase, while during walking the kinetic and potential energy of the CoM are out of phase, i.e. the maximum height of the CoM corresponds to the minimum of its speed Cavagna et al. (1977). In addition, the model correctly reproduces the vertical oscillations of the CoM observed experimentally (Geyer et al. (2006); Full and Koditschek (1999)). Furthermore, the SLIP model can show gait transitions at constant energy as it is reported in Martínez Salazar

and Carbajal (2011). Based on this findings, Martínez and Carbajal (2011) showed that these transitions enable the system to generate compound gaits like hopping which is a combination of running and walking. The explanatory capabilities of this model have been exploited in the area of robotics as well. In this field, the model has been successfully used for design and control of running machines(Andrews et al. (2011); Schmitt (2007); McMahon and Cheng (1990); Cham et al. (2004)).

The SLIP model consist of a point mass (the body) attached to a massless spring (the leg) (Fig. 1). The angle of attack (α) is the angle spanned by the landing leg and the horizontal at the time the foot collides with the ground. Given that the legs in the SLIP model are massless, their swinging motion is not described by the Newton's laws. For this reason, a control policy sets this angle at touchdown. In this research, we assume that the angle of attack at touchdown is kept constant.

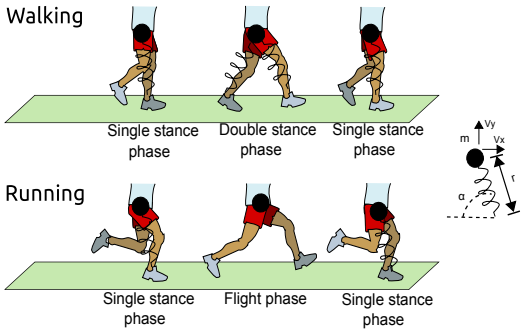

Figure 1: (Color online) Illustration of the evolution of the SLIP model for running and walking. The different phases are indicated. Due to the passive properties of these models, control is necessary only during the swing of the leg. The angle of attack (α) is the angle between the landing leg and the horizontal at the collision time with the ground

In this study, we analyze the effect of variations of mass in the human gait under constant locomotion speed. We account for subject differences in body mass and ground reaction force (GRF) with a non-dimensional analysis technique. First, we fitted the experimental data with the SLIP model. Second, we derived three dimensionless variables from the parameters of the SLIP model. And third, we compared the changes on the these variables as a function of the change in

mass. Our results show that changes in the mass are compensated within the subject leading to a similar dimensionless system.

This paper is organized as follows. In section 2, we describe the experiments, we define the models used for data analysis, and the algorithm used to find the correct model parameters to fit the experimental data. In section 3, we show the data collected in the experiments, the accuracy of the model fitting, and the changes in the non-dimensional parameters as a function of the mass variations. Later, in section 4, we discuss about the relations in the model with the change of mass and the implications for locomotion control. We conclude the paper in section 5 with our conclusion.

2 Materials and methods

In this section we introduce the experiments, the model that we used to analyze the data collected, and the procedure that we used to fit the model to the experimental data.

Experiment

We measured kinetic data using a split-belt force treadmill. The force plates underneath the frame measured GRFs and moments in three axes, at a sampling rate of 960 Hz. Four subjects (three male and one female subjects; Avg. body mass 65.34 kg SD 7.07 kg) signed informed consent forms approved by the University of Michigan Health Sciences Institutional Review Board, and participated in this study. All subjects were considered to be in good health, and had no known gait abnormalities.

For all subjects, we collected data during three treadmill walking and running trials. In the walking condition the speed was held constant at 1.5 $\mathrm{m/s}$ for all trials. In the first trail all subjects walked normally in the treadmill for 60 s. In the second trial all subjects walked with a weighted belt weighting 9.3 kg for 60 s. In the third trial all subjects walked with a weighted belt and a weighted vest with 20.5 kg for 60 s. In the running condition the speed was held constant at 2.5 $\mathrm{m/s}$

for all trials. In the running experiment we followed the same mass variations and locomotion time used in the walking experiment. Subjects were given rest periods of up to 3 minutes between trials in both conditions.

Model

As explained previously, we use the SLIP model to study the effect of increments of mass in bipedal locomotion. A complete description with full details can be obtained in Ref. Martínez Salazar and Carbajal (2011); herein we provide a succinct recapitulation. The model represents the different phases of a gait with three sub-models or phases. Each phase represents the motion of a point mass under the influence of: only gravity (flight phase), gravity and a linear spring (single stance phase), gravity and two linear springs (double stance phase). The point mass represents the body and the massless linear springs model the forces in the legs. We define a running gait as a trajectory that switches from the single stance phase to the flight phase and back to the single stance phase. A walking gait is defined as a trajectory that switches from the single stance phase to the double stance phase and back again to the single stance phase.

The equation of motion of the flight phase is described in Cartesian coordinates as a parabolic motion in which the system is affected only by the gravitational field.

$$\begin{pmatrix} \ddot{x} \\ \ddot{y} \end{pmatrix} = \begin{pmatrix} 0 \\ -g \end{pmatrix}, \tag{1}$$

where $\ddot{x}$ is the acceleration of the center of mass in the horizontal direction, $\ddot{y}$ is the acceleration of the center of mass in the vertical direction, and g is the acceleration due to gravity.

We can write also the equation of motion of the single stance phase in Cartesian coordinates.

$$\begin{pmatrix} \ddot{x} \\ \ddot{y} \end{pmatrix} = \begin{pmatrix} \frac{k}{m}(r_0 - r_1)\cos\theta \\ \frac{k}{m}(r_0 - r_1)\sin\theta - g \end{pmatrix}, \tag{2}$$

where m is the mass, k is the constant of elasticity of the spring, g is gravity, r_0 is the natural length

of the spring, r_1 is the length of the spring, and θ is the angle spanned by the leg and the horizontal, growing in clockwise direction.

The equation of motion of the double stance phase in Cartesian coordinates is

$$\begin{pmatrix} \ddot{x} \\ \ddot{y} \end{pmatrix} = \begin{pmatrix} \frac{k}{m}(r_0 - r_1)\cos\theta + \frac{k}{m}(r_0 - r_2)\cos\beta \\ \frac{k}{m}(r_0 - r_1)\sin\theta + \frac{k}{m}(r_0 - r_2)\sin\beta - g \end{pmatrix}, \tag{3}$$

where m is the mass, k is the constant of elasticity of the springs, g is gravity, r_0 is the natural length of the springs, r_1 is the length of the spring of the rear leg, θ is the angle spanned by the rear leg and the horizontal (growing in clockwise direction), r_2 is the length of the spring of the hind leg, β is the angle spanned by the hind leg and the horizontal (growing in clockwise direction)

We can define the non-dimensional distance $\hat{l}$ as $\hat{l} = l/r_0$, where l is a dimensional distance and r_0 is the natural length of the spring, and the dimensionless time $\hat{t}$ as $\hat{t} = t\sqrt{g/r_0}$, where t is time, g is gravity and r_0 is the natural length of the spring. Using this relations we can convert the velocities ($\dot{\hat{l}} = \dot{l}/\sqrt{gr_0}$), and accelerations ($\ddot{\hat{l}} = \ddot{l}/g$) to the non-dimensional space. With these definitions we can rewrite all the previous differential equations in the dimensionless space. In the case of the flight phase the equation of motion is:

$$\begin{pmatrix} \ddot{\hat{x}} \\ \ddot{\hat{y}} \end{pmatrix} = \begin{pmatrix} 0 \\ -1 \end{pmatrix}, \tag{4}$$

where $\ddot{\hat{y}}$ is the non-dimensional acceleration of the center of mass in the horizontal direction, and $\ddot{\hat{y}}$ is the non-dimensional acceleration of the center of mass in the vertical direction.

The equation of motion of the single support phase in the non-dimensional space is equal to:

$$\begin{pmatrix} \ddot{\hat{x}} \\ \ddot{\hat{y}} \end{pmatrix} = \begin{pmatrix} \hat{k}(1 - \hat{r_1})\cos\theta \\ \hat{k}(1 - \hat{r_1})\sin\theta - 1 \end{pmatrix} \tag{5}$$

$$\hat{k} = \frac{kr_0}{gm}, \tag{6}$$

where $\hat{k}$ is the non-dimensional stiffness of the spring, and $\hat{r_1}$ is the dimensionless length of the leg.

In a similar way we can rewrite the equation of motion of the double stance phase as:

$$\begin{pmatrix} \ddot{\hat{x}} \\ \ddot{\hat{y}} \end{pmatrix} = \begin{pmatrix} \hat{k}(1-\hat{r_1})\cos\theta + \hat{k}(1-\hat{r_2})\cos\beta \\ \hat{k}(1-\hat{r_1})\sin\theta + \hat{k}(1-\hat{r_2})\sin\beta - 1 \end{pmatrix} \tag{7}$$

$$\hat{k} = \frac{kr_0}{gm}, \tag{8}$$

where $\hat{k}$ is the non-dimensional stiffness of the springs, $\hat{r_1}$ is the dimensionless length of the rear leg, and $\hat{r_2}$ is the non-dimensional length of the hind leg. One important result from the reformulated system is that single stance phase and the double stance phase do not require another dimensionless number. therefore, we need only three parameters (non-dimensional stiffness $\hat{k} = \frac{kr_0}{gm}$, non-dimensional time $\hat{t} = t\sqrt{g/r_0}$, and non-dimensional length $\hat{l} = l/r_0$) to represent any gait based on the SLIP model. The Combination of these three parameters allow us to convert other important physical quantities to the non-dimensional space e.g. energy, force, velocities, etc.

Model Fits

The model implementation and data analysis were performed in MATLAB(2009, The MathWorks). We used the MATLAB *fminsearch* function to fit the SLIP model to the experimental GRF. We selected the squared error between the experimental GRF and the GRF generated by the model as a quality measure of the fitting. This measure considered the vertical and the horizontal GRF, as shown in Eq. 9

$$error = \sqrt{\sum_{i=0}^{n} [\Delta t(f_x(t_i) - \hat{f_x}(t_i))]^2 + [\Delta t(f_y(t) - \hat{f_y}(t_i))]^2}, \tag{9}$$

where $f_x(t_i)$ is the measurement of the total horizontal force at time t_i, $f_y(t_i)$ is the measurement of the total vertical force at time t_i, $\hat{f_x}(t_i)$ is the model approximation of the total horizontal force

at time t_i, $f_y\hat{(}t_i)$ is the model approximation of the total vertical force at time t_i, and Δt is the time between samples (e.g. $t_{i+1} - t_i$). The quality measure is calculated within a stride, i.e. the leading foot touches the ground at t_0, and again at t_n.

The function *fminsearch* needed a initial guess trajectory to select the appropriate SLIP model parameters. This guess was selected from all the possible symmetric gaits that can be generated from the SLIP model with parameters $k = 15$ kNm, $m = 80$ kg, $r_0 = 1$ m, and $g = 9.81$ m/s^2 between 780 J and 2000 J. The selection was performed based on two measures. One was the duty factor (the fraction of the total duration of a gait cycle in which a given foot is on the ground), and the other was the ratio between the peak vertical force and the peak horizontal force. The trajectory which produced the closest values compared to the experimental data was selected as initial guess for the fitting process. Herein, the mass obtained from the vertical force, and gravity are maintained constant.

Assuming that the parameters of the SLIP model does not change as a function of the mass then the dimensionless constant of elasticity $\hat{k} = \frac{kr_0}{gm}$ changes only by the selection of a new mass in the system. Based on this assumption changes on the non-dimensional elasticity $\Delta\hat{k}$ should follow Eq.10

$$\Delta\hat{k} = \frac{kr_0/gm_2 - kr_0/gm_1}{kr_0/gm_1}, \tag{10}$$

where m_2 is the mass of the system with additional weight, m_1 is the mass of the system without additional weight. Simplifying Eq. 10 we get Eq. 11.

$$\Delta\hat{k} = -\frac{\Delta m}{1 + \Delta m}, \tag{11}$$

where Δm is the change of mass ($\frac{m_2 - m_1}{m_1}$). Doing Taylor series expansion of Eq.11 around $\Delta m = 0$ (i.e. small increments of mass), we get that $\Delta\hat{k} \approx -\Delta m$. This means that the dimensionless elasticity is reduced in the same proportion that the mass is incremented.

3 Results

In this section, we introduce the results of the experiments and the fitting parameters of the SLIP model. Fig. 2 shows the GRF of all the subjects for the walking and running conditions. The second row of Fig. 2 shows the mean GRF in the non-dimensional space for the walking trials. In the non-dimensional space the GRF of each subject is similar. For each subject the three different trials seems to overlap showing the same profile of force in the vertical and horizontal direction. The results of subject three show a small difference between the trials, while the amplitude is similar the period of the locomotion is not. The bigger the mass the smaller the time between steps. The fourth row of Fig. 2 shows the mean GRF in the non-dimensional space for running trials. For all the subjects, the bigger the mass the shorter the flight phase. For this reason, the duty factor increases as a function of the weight. Furthermore, the dimensionless vertical GRF magnitude changes as a function of the mass. The bigger the mass the smaller the peak force. The table 1 shows the appropriate parameters of the model that best fit the experimental data. The column error in the table indicates the mismatch between the experiment and the model as a percentage of the area of the experimental GRF. The column α in table 1 shows the angle of attack that is selected each step by the model. The column $\sqrt{r_0/g}$ shows the constant that converts the non-dimensional time to seconds. The column $\frac{kr_0}{gm}$ depicts the dimensional stiffness of the system. All these quantities are generated from the fitting procedure. The column mass indicates the mass value estimated from the integration of the vertical force, and the column gait shows the locomotion pattern used in the experiment. The fitting procedure shows that the model can represent the experimental data with an error lower than 1%. The change in the mass for all the subjects through the experiments is around 33%, however the angle of attack (control strategy) changes less than 2.67% in walking and less than 4.58% in running.

Fig. 3 shows an example of the model fitting to the experimental data in subject two. The fitting procedure assumes a symmetric gait, for this reason the same angle of attack is used for both legs.

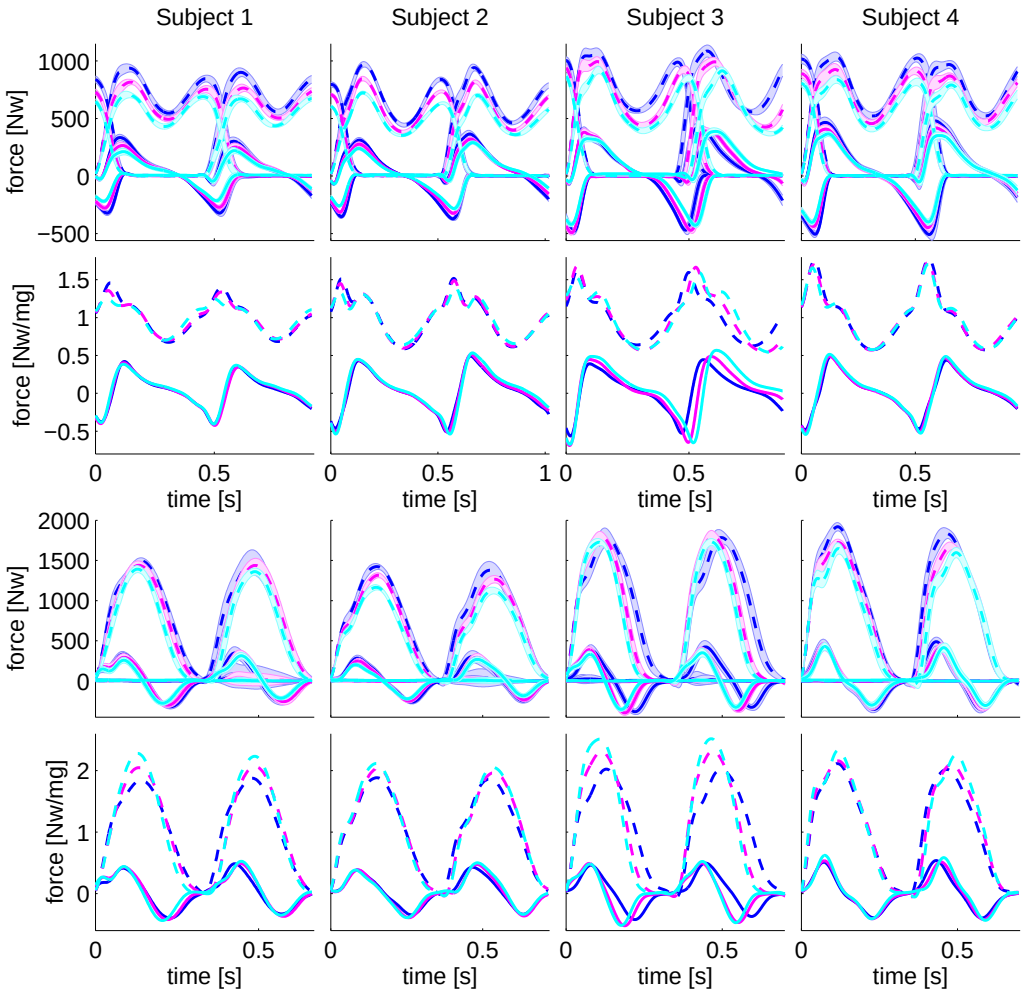

Figure 2: (Color online) GRF for all the subjects. Each column shows the data of each subject. The light gray (cyan) shows the data collected with out additional weight. The gray (magenta) shows the data collected with the weighted belt, and the dark gray shows the data collected with the weighted belt and the weighted vest. The dashed lines depict the vertical GRF and the continuous lines the horizontal GRF. From top to bottom, the first row shows the data collected in the walking experiment. The standard deviation of the measurements are depicted in the shadow area. The second row shows the combined vertical and horizontal GRF of each subject in the non-dimensional space for the walking experiment. The third row shows the data collected in the running experiment, and the fourth row shows the mean total vertical and horizontal GRF of each subject in the non-dimensional space for the running experiment.

Table 1: Results fitting the data with the SLIP model

Gait	Subject	Mass	kr_0/mg	$\sqrt{r_0/g}$	α	$max\ \Delta\alpha(\%)$	$error(\%)$
Walking	subject 1	62.62	17.46	0.22	64.37		0.42
		71.68	17.33	0.22	64.06	0.70	0.34
		82.87	17.21	0.23	63.92		0.33
	subject 2	56.64	18.26	0.26	63.51		0.51
		66.01	18.13	0.26	63.19	0.60	0.44
		77.00	17.88	0.26	63.13		0.41
	subject 3	70.05	15.70	0.24	60.60		0.72
		79.37	16.21	0.24	61.74	2.67	0.58
		90.63	15.51	0.22	62.22		0.46
	subject 4	72.03	17.00	0.25	62.84		0.48
		81.34	16.96	0.25	63.13	0.46	0.43
		92.73	16.90	0.25	63.09		0.39
Running	subject 1	62.36	15.28	0.43	62.90		0.59
		71.83	12.83	0.46	60.57	4.17	0.56
		82.85	11.99	0.48	60.38		0.57
	subject 2	56.27	15.41	0.43	65.24		0.66
		65.94	13.93	0.44	63.65	4.17	0.59
		77.26	13.05	0.45	62.63		0.63
	subject 3	70.24	17.30	0.42	63.11		0.57
		79.29	15.87	0.51	61.53	2.94	0.54
		90.59	15.50	0.53	63.34		0.60
	subject 4	72.22	14.81	0.44	62.54		0.82
		81.52	13.48	0.48	61.09	4.58	0.80
		92.71	12.45	0.47	59.80		0.90

The experimental data of subject two shows that this assumption is close to the reality even when the human locomotion can be as in this case clearly asymmetric. In addition, in the running gait, the vertical GRF sometimes has a notch, however, despite these source of error, the SLIP model can reproduce the experimental data with an average error of 0.45% for walking and 0.63% for running. We use the parameters from the fitting procedure to measure the similarity between the experimental trials. To analyze the results across all subjects, we compare the changes of the dimensionless SLIP parameters against the change of mass. The left panel of Fig. 4 shows the linear regression of the change of non-dimensional stiffness as a function of the change of mass. This regression is very close to an horizontal line which tell us that the number $\frac{kr_0}{gm}$ is maintained constant even when there are increments in the mass m. The coefficient of determination of this regression

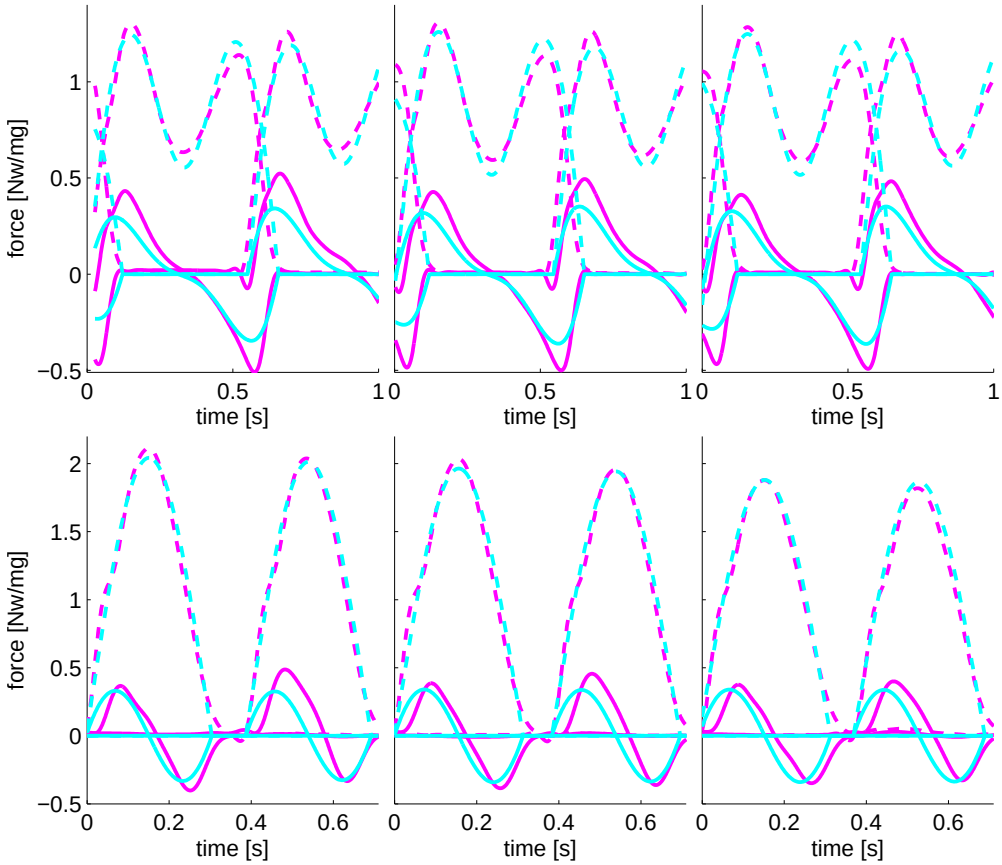

Figure 3: (Color online) Comparison between the experimental GRF and the GRF generated with the SLIP model. The data collected from subject two in the walking and running experiment is shown in gray (magenta). The light gray (cyan) shows the model approximation. The dashed lines depict the vertical GRF and the continuous lines depict horizontal GRF. From top to bottom, the first row shows the walking experiment, and the second row shows the running experiment. The most left panels show the data collected without extra weight, the panels in the center show the data collected with the weighted belt, and the most right panels show the data collected with the weighted belt and the weighted vest.

R^2 is equal to 0.26. This coefficient compares the error obtained from the regression against a horizontal line going through the mean of all Y values. A value of R^2 close to zero indicates that knowing X does not help you predict Y. This confirm this idea that the non-dimensional stiffness does not change. In general the stiffness compensate for the changes on the mass. The solid gray

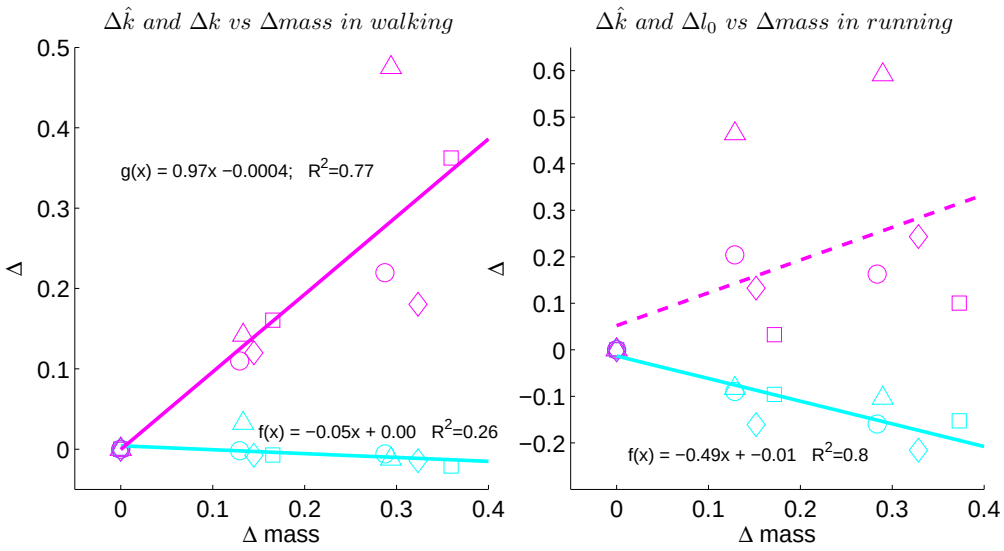

Figure 4: (Color online) Comparison between changes in the non-dimensional stiffness and changes in the mass. The markers represent the data of each subject for each experiment. The light gray (cyan) markers show the change of the non-dimensional stiffness. The light gray (cyan) line is the linear regression that fits the change of the non-dimensional stiffness as a function of the change of the mass. The left panel shows the data comparison for the walking experiment. In this panel, the gray (magenta) markers show the change of the stiffness, and the gray (magenta) line is the linear regression that fits the change of the stiffness as a function of the change of the mass. The right panel shows the data comparison for the running condition. In this panel, the gray (magenta) markers show the change of the natural length.

(magenta) line in the left panel of Fig. 4 shows the linear regression between the change of the constant of elasticity and the change of the mass. This relation has a slope of 0.97 which is very close to one. This means that the constant of elasticity grows almost in the same proportion as the mass. However, the compensation can also be produced by the joint action of the stiffness and natural length r_o. The last trial of subject three shows this behavior (left panel Fig. 4; marker (△) in gray (magenta)). Here, the SLIP model that fits the data of the trial with the biggest mass shows a particularly high stiffness, this increment in the stiffness is compensated by a reduction of the natural length of the leg. The natural length is used to define all the dimensionless parameters included the non-dimensional time. For this reason a decrement in the natural length of the leg will increase the stepping frequency. This explains why the subject three in the last trial reduces

the walking period.

The right panel of Fig. 4 shows that the non-dimensional stiffness decreases. The solid light gray (cyan) line shows the linear regression between the changes of dimensionless stiffness and the changes of mass. The regression has a slope of -0.49. We introduced in Eq. 11 the lienar relation between these parameters under the assumption of non-compensation. In that case, we expected a slope of -1. This implies, that there is a compensation for the changes in mass however this compensation is not as strong as in walking. Furthermore, the compensation is not carried out by the stiffness but by an increment in the natural length of the leg. The stiffness in the running trials do not increase, in the contrary it is slightly reduced when the subject has a bigger mass. The combination of these two effects, on one hand decrease the stepping frequency, and on the other hand increases the contact time of the foot with the ground. For this reason, the increment of mass in running increase the duty factor (Fig. 2).

4 Discussion

This model has proven its capability to represent several different features of human locomotion, for this reason is not surprising that it approximates the experimental data. The approximation errors are small, however in the running experiment the approximation error is bigger than that in the walking experiment (table 1). This can happen because the SLIP model assumes a spring with a linear constant of elasticity. However, experimental studies have shown that human legs have a nonlinear constant of elasticity Dumke et al. (2010); Blum et al. (2009). A change similar to Rummel and Seyfarth (2008) can be introduced into the SLIP model to cope with the nonlinearity of the leg stiffness, or similar to Iida et al. (2008) to consider the relation of biarticular muscles involve in locomotion. This may help to reduce the nonlinear effect making the model closer to the experimental data. The SLIP model assumes a contact point foot, which forbids the displacement of the contact point and reduces the transmission of the energy to forward locomotion. The introduction of a rolling foot Adamczyk et al. (2006); Whittington and Thelen (2009) can improve this aspect

approximating better the horizontal force.

The simplicity of the SLIP model allow us to rewrite it with three different non-dimensional parameters. The dimensionless analysis allows a more general study of the human locomotion based on the relations of a small set of variables that describe the dynamics. Under this representation we can study how a change of one of these variables can affect the locomotion. In this study, we focus our attention in how changes in mass affect the human gait at constant speed of locomotion. We identified for walking and running a compensation of the change of mass that tries to keep the non-dimensional stiffness constant (Fig. 4). In the case of walking, the mechanism is to increase the stiffness of the leg. With this strategy, the dimensionless stiffness is practically constant. The compensation in running uses the natural length of the leg instead of the stiffness. We speculate that, this mechanism can be better than increasing the stiffness because in running the knee bents more, and an increment in the stiffness might require more effort. The findings in physiology showed that there are neural strategies to control the length and tension of muscles. These control strategies have motivated the development of muscle servo models Houk and Rymer (2011) to show how these fundamental aspects are carefully varied by our nervous system.

We have also identified in one trial a compensation carried out by the relation between the stiffness and the natural length of the leg (left panel Fig. 4; marker ($\triangle$) in gray (magenta)). We speculate that this behavior can be plausible in a subject that prefers to walk in her toes. In this condition, probably when we increase drastically the mass there is a point in which the subject will use the whole foot as a support decreasing the natural length of the leg and increasing the constant of elasticity of the leg.

One consequence of keeping the same non-dimensional constant of elasticity in the SLIP model is that the strategy of control (constant angle of attack) does not have to change. This idea is supported by the results of the fitting process. In table 1 we can see that even when the change of the mass is around 33% the constant angle of attack changes less than 4%. This is true even for the running experiment, in which the compensation of the change of the mass is about 50%.

Non-dimensional analysis using the SLIP model allow us to compare the relevant variables that

describe the dynamics of human locomotion. Furthermore, we can analyze across several subjects. However, we have to remember that this is an abstraction and that the natural length r_0 is not the length of the leg but the natural length of the equivalent spring that represents the leg. The same happens with the angle of attack which is not the same as the angle between the human leg and the ground, but between the equivalent spring and the ground. We believe that similar analysis to the one presented in this study can be developed to understand the control strategy adopted in human locomotion in the presence of other disturbances.

5 Conclusion

We used the SLIP model to represent human gaits as it endows the analysis with a more general representation based on three dimensionless parameters: non-dimensional stiffness $\hat{k} = \frac{kr_0}{gm}$, non-dimensional time $\hat{t} = t\sqrt{g/r_0}$, and non-dimensional length $\hat{l} = l/r_0$. The Combination of these quantities allow us to convert other important physical quantities to the dimensionless space like energy or force. We studied how the change of mass affects the human gait while keeping the locomotion speed constant. We identified a compensation of the change of the mass that can be explained in terms of the dimensionless SLIP model parameters. A direct consequence of the mass compensation is that the control strategy of the gaits does not have to change. We strongly believe that this analysis can be extended to study other important aspects in the human gait.

Acknowledgements We want to thank Dr. Hugo Gravato Marques for his review of the manuscript. A very special thanks to Prof. Dr. Art Kuo for his support to our research facilitating his lab to run the experiment and his valuable comments. The research leading to these results has received funding from the European Community's Seventh Framework Programme FP7/2007-2013-Challenge 2-Cognitive Systems, Interaction, Robotics- under grant agreement No 248311-AMARSi.

References

Adamczyk, P. G., Collins, S. H. and Kuo, A. D. (2006). The advantages of a rolling foot in human walking. *J. Exp. Biol.* **209**, 3953–3963.

Andrews, B., Miller, B., Schmitt, J. and Clark, J. (2011). Running over unknown rough terrain with a one-legged planar robot. *Bioinspir Biomim* **6**, 026009.

Blickhan, R. (1989). The spring-mass model for running and hopping. *J. Biomech.* **22**, 1217 – 1227.

Blum, Y., Lipfert, S. W. and Seyfarth, A. (2009). Effective leg stiffness in running. *Journal of Biomechanics* **42**, 2400 – 2405.

Cavagna, G. A., Heglund, N. C. and Taylor, C. R. (1977). Mechanical work in terrestrial locomotion: two basic mechanisms for minimizing energy expenditure. *Am. J. Physiol.-Reg. I.* **233**, R243–R261.

Cham, J. G., Karpick, J. K. and Cutkosky, M. R. (2004). Stride period adaptation of a biomimetic running hexapod. *The International Journal of Robotics Research* **23**, 141–153.

Dumke, C. L., Pfaffenroth, C. M., McBride, J. M. and McCauley, G. O. (2010). Relationship between muscle strength, power and stiffness and running economy in trained male runners. *Int J Sports Physiol Perform* **5**, 249–61.

Full, R. and Koditschek, D. (1999). Templates and anchors: neuromechanical hypotheses of legged locomotion on land. *J. Exp. Biol.* **202**, 3325–3332.

Geyer, H., Seyfarth, A. and Blickhan, R. (2006). Compliant leg behaviour explains basic dynamics of walking and running. *P. Roy. Soc. B - Biol. Sci.* **273**, 2861–7.

Holmes, P., Full, R. J., Koditschek, D. and Guckenheimer, J. (2006). The dynamics of legged locomotion: Models, analyses, and challenges. *SIAM Rev.* **48**, 207–304.

Houk, J. C. and Rymer, W. Z. (2011). *Neural Control of Muscle Length and Tension*. John Wiley and Sons, Inc.

Iida, F., Rummel, J. and Seyfarth, A. (2008). Bipedal walking and running with spring-like biarticular muscles. *Journal of Biomechanics* **41**, 656–667.

Martínez, H. and Carbajal, J. (2011). From walking to running a natural transition in the slip model using the hopping gait. In *Robotics and Biomimetics (ROBIO), 2011 IEEE International Conference on*, pp. 2163 –2168.

Martínez Salazar, H. R. and Carbajal, J. P. (2011). Exploiting the passive dynamics of a compliant leg to develop gait transitions. *Phys. Rev. E* **83**, 066707.

McMahon, T. A. and Cheng, G. C. (1990). The mechanics of running: How does stiffness couple with speed? *J. Biomech.* **23, Supplement 1**, 65 – 78. ¡ce:title¿International Society of Biomechanics¡/ce:title¿.

Rummel, J. and Seyfarth, A. (2008). Stable running with segmented legs. *The International Journal of Robotics Research* **27**, 919–935. 10.1177/0278364908095136.

Schmitt, J. M. (2007). Incorporating energy variations into controlled sagittal plane locomotion dynamics. *ASME Conference Proceedings* **2007**, 1627–1635.

Whittington, B. R. and Thelen, D. G. (2009). A simple mass-spring model with roller feet can induce the ground reactions observed in human walking. *J Biomech Eng* **131**, 011013.

Appendix E

The SLIP Model Predicts an Anthropometric Leg for Walking and Running

Reprinted from:

Martínez, H. R.(2013). *The SLIP Model Predicts an Anthropometric Leg for Walking and Running*, submited to the Journal of Theoretical Biology.

The SLIP Model Predicts an Anthropometric Leg for Walking and Running

Harold Roberto Martínez Salazar[a,*]

[a]*Artificial Intelligence Laboratory, Department of Informatics*
University of Zurich, Andreasstrasse 15, 8050 Zurich, Switzerland

Abstract

The spring loaded inverted pendulum (SLIP) model is a conceptual model of bipedal locomotion. This model has been proposed as a unified framework to explain the dynamics of a wide variety of gaits. In this study, we extend the SLIP model to the rod-SLIP model in which we consider mass on the legs. Results show that under certain conditions the rod-SLIP model can reproduce the symmetric gaits identified in the SLIP model. These conditions resemble the length of a human leg and give mathematical support to the leg contraction control strategies in running. From the control perspective, the results show plausible mechanisms that biped creatures can probably use to carry out gait transitions and stable locomotion with energy efficiency, given that these mechanisms exploit the passive dynamics of the system.

Keywords: SLIP model, human leg, bipedal locomotion, gait transitions, human locomotion, biomechanics

1. Introduction

In the field of bipedal locomotion, researchers have proposed several mathematical models to elucidate the most important principles governing the gait dynamics. These models can be understood either as detail representations or conceptual models. The former uses mechanical elements such as springs, dampers and multi-segmented legs to represent different leg components or neuromuscular structures (Siegler, Seliktar, and Hyman (1982); Pandy (2003); Zajac, Neptune, and Kautz (2003); Valero-Cuevas, Hoffmann, Kurse, Kutch, and Theodorou (2009)). The mathematical complexity of these representations prevents their extensive use. In contrast, simpler mathematical models have been adopted as conceptual models of bipedal locomotion (Holmes, Full, Koditschek, and Guckenheimer (2006)).

The spring-loaded inverted pendulum (SLIP) (Blickhan (1989)) is one of these conceptual models introduced to explain the running gait. Further work by Geyer et al. (Geyer, Seyfarth, and Blickhan (2006)) proposed this model as a unifying framework to describe running and walking; since it suitably explains the ground reaction forces produced in these gaits. This mathematical framework also generates the vertical oscillations of the CoM observed experimentally in walking and running (Geyer et al. (2006); Full and Koditschek (1999)). This model has also proven to be useful to explain gait transitions at constant energy Martínez Salazar and Carbajal (2011) as well as compound gaits like hopping (combination of running and walking) Martínez and Carbajal (2011). Furthermore, the findings from this model have been used in the area of robotics for design and control of running machines (Andrews, Miller, Schmitt, and Clark (2011); Schmitt (2007); McMahon and Cheng (1990); Cham, Karpick, and Cutkosky (2004)).

The SLIP model consist of a point mass (the body) attached to massless springs (the legs). For this reason, the swinging motion of the legs is not described by the Newton's laws. To cope with this situation, a control strategy that selects the angle of the leg at touchdown is introduced. The strategy generally selects the same angle (angle of attack) at each step (Geyer et al. (2006)). McGeer (1990) considered mass on the legs, a coil spring at the hip which helps the swinging motion of the leg and round feet. With these modifications, the system performs passively the gaits without an external controller that defines the swinging motion. This study showed the stability properties of passive dynamic runner. Inspired in the previous results, Owaki, Osuka, and Ishiguro (2008, 2009) used a similar model but with point

*Principal corresponding author
Email address: martinez@ifi.uzh.ch (Harold Roberto Martínez Salazar)

feet. These studies showed that the relation between the leg spring constant and the hip coil spring constant defines different stable gait patterns such as walking and running. Furthermore, they explained the stabilization mechanism present in this system based on the analysis of a Poincaré map.

In this study, we extend the SLIP model and introduce the rod-SLIP model which has spring legs with mass. As a difference with the model proposed in McGeer (1990); Owaki et al. (2008) our model does not consider a spring at the hip. Furthermore, in our research we test the effect of the mass on the leg instead of the elasticity constant. Results show the conditions in which the rod-SLIP model can reproduce the symmetric gaits found in the SLIP model. In addition, we show that the properties of the leg can be estimated directly from the SLIP model. Furthermore, assuming a leg with human-like mass distribution, our model directly predicts a leg with human-like length for running and walking. The conditions that allow the system to produce stable gaits passively (without actuation) lead us to hypotheses on control strategies e.g. a mathematical foundation for the leg contraction strategy in running, and plausible mechanisms that biped creatures can apply to perform gait transitions and stable locomotion.

This paper is organized as follows. In section 2, we define the models used in this study, the simulation conditions, and the data analysis procedure. In section 3 we show the results from the models previously introduced and compare them. Later, in section 4, we discuss the implications of the results for gait transitions and locomotion control. We conclude the paper in section 5 with our conclusion.

2. Materials and methods

In this section, we introduce a succinct description of the SLIP model and three new different models used in this study. We also indicate the condition in which these models were simulated and how the data analysis was performed.

SLIP Model

The SLIP model represents the different phases of running or walking with three sub-models or phases. Each phase represents the motion of a point mass under the influence of: only gravity (flight phase), gravity and a linear spring (single stance phase), gravity and two linear springs (double stance phase). The massless linear springs model the forces from the legs and the point mass represents the body. We implemented the model following the framework described in Martínez Salazar and Carbajal (2011) therefore herein we provide a short summery of the model; a complete description with full details can be obtained from that reference. The running gait is a trajectory that switches from the single stance phase to the flight phase and back to the single stance phase. A walking gait is defined as a trajectory that switches from the single stance phase to the double stance phase and back again to the single stance phase.

The flight phase is represented with the differential equation Eq. 1 in Cartesian coordinates,

$$\ddot{y} = -g, \tag{1}$$

where g is the acceleration due to gravity.

The single stance phase is represented in polar coordinates, where r is the length of the spring and θ is the angle spanned by the leg and the horizontal, growing in clockwise direction. The equations of motion are:

$$\begin{pmatrix} \ddot{r} \\ \ddot{\theta} \end{pmatrix} = \begin{pmatrix} \frac{k}{m}(r_0 - r) + r\dot{\theta}^2 - g\sin\theta \\ -\frac{1}{r}\left(2\dot{r}\dot{\theta} + g\cos\theta\right) \end{pmatrix}, \tag{2}$$

the parameter r_0 defines the natural length of the spring.

In the double stance phase the state is also represented in polar coordinates with the origin of coordinates in the new touchdown point. The motion is described by:

$$\begin{pmatrix} \ddot{r} \\ \ddot{\theta} \end{pmatrix} = \begin{pmatrix} \frac{k}{m}[(r_0 - r) + \left(1 - \frac{r_0}{r_\sigma}\right)(x_\sigma \cos\theta - r)] + r\dot{\theta}^2 - g\sin\theta \\ -\frac{1}{r}[\frac{k}{m}\left(1 - \frac{r_0}{r_\sigma}\right)x_\sigma \sin\theta + 2\dot{r}\dot{\theta} + g\cos\theta] \end{pmatrix} \tag{3}$$

$$r_\sigma = \sqrt{r^2 + x_\sigma^2 - 2rx_\sigma \cos\theta}, \tag{4}$$

where x_σ is the horizontal distance between the two contact points and r_σ is the length of the back leg.

In the case of the single stance phase, the energy E of the system in the midstance (the support leg forms a right angle with the ground) lies on an ellipsoid described in Eq. 5

$$E = \frac{1}{2}k\,(r_0 - r)^2 + \frac{1}{2}m\left(v_x^2 + v_y^2\right) + mgr \tag{5}$$

where v_x is the velocity in the horizontal direction, v_y is the velocity in the vertical direction, r represents the compression of the spring, m is the total mass of the system, r_0 is the natural length of the spring, k is the constant of elasticity of the spring, and g is gravity. We selected 5185 initial conditions inside this ellipsoid for energies E in the range $[780, 900]$J at intervals of 10 J. From these initial conditions we identified and simulate all the symmetric gaits. The model was implemented in MATLAB(2009, The MathWorks) and simulations were run using the variable step integrator routine ode45.

Compound Pendulum Constraint to the SLIP model (CPC-SLIP model)

We looked for the main features of a leg to allow a legged system closely reproduce the SLIP model behavior. We assumed that a leg is a rigid planar pendulum and its mass is much lower than the point mass in the SLIP model. Under these assumptions, the dynamics of a legged system is basically described by the SLIP model, and the pendulum dynamics is negligible in terms of changes on the position of the center of mass. The Fig. 1 shows the legged system, in which the attachment point of the leg O follows a predefined SLIP trajectory. These trajectories are generated from the symmetric gaits of the SLIP model. Following these ideas, the dynamics of the system can be described as a pendulum that moves constrained to a predefined trajectory. The equation of motion of this system allow us to find the appropriate pendulum which can passively match the angle of attack for a symmetric gaits.

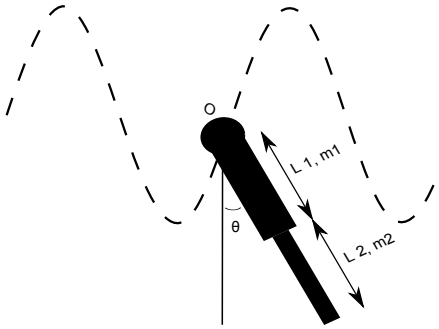

Figure 1: Pendulum coupled to the trajectory of a symmetric gait. The dashed line shows the trajectory of the symmetric gait from the SLIP model. The pendulum has two sections one with length l_1 and mass m_1, and another with length l_2 and mass m_2.

The center of mass cm of the pendulum is given by the Eq. 6

$$cm = l_1\frac{m_1}{2(m_1 + m_2)} + (2l_1 + l_2)\frac{m_2}{2(m_1 + m_2)} \tag{6}$$

where m_1 is the mass of the upper segment, m_2 is the mass of the lower segment, l_1 is the length of the upper segment, and l_2 is the length of the lower segment. The moment of inertia of the pendulum around its center of mass is given by the Eq. 7

$$I_{pndlm} = {l_1}^2\frac{m_1}{12} + {l_2}^2\frac{m_2}{12} + m_2 m_1\frac{(l_1 + l_2)^2}{4(m_1 + m_2)} \tag{7}$$

In human legs the thigh and the shank have a similar length, but the thigh has almost twice the mass as the shank. Assuming a condition similar to a human leg we can rewrite the cm and the inertia of the pendulum I_{pndlm} as Eq. 8 and Eq. 9.

$$cm = 5l/6, m_1 = 2m_2, l_1 = l_2 = l \tag{8}$$

$$I_{pndlm} = 11\frac{l^2 m_2}{12}, m_1 = 2m_2, l_1 = l_2 = l \tag{9}$$

The equations of motion of the system can be derived from the Lagrangian of the system. The position of the center of mass can be calculated from the restricted path that follows the point O and the angle of the pendulum with respect the vertical (θ). Eq. 10 shows this position of the center of mass $\vec{p}$,

$$\vec{p} = \begin{pmatrix} x(t) \\ y(t) \end{pmatrix} + 5\frac{l}{6}\begin{pmatrix} sin(\theta) \\ -cos(\theta) \end{pmatrix}, \tag{10}$$

where $x(t)$ and $y(t)$ represent the trajectory that follows the point O in the horizontal and vertical direction respectively. θ is the angle of the pendulum measured with respect the vertical axis, and l is the length of the upper or lower segment. The kinetic energy T is

$$T = 3m_2|\dot{\vec{p}}|/2 + I_{pndlm}\dot{\theta}/2, \tag{11}$$

where m_2 is the mas of the lower segment, $\dot{\vec{p}}$ is the velocity of the point O and $\dot{\theta}$ is the angular velocity of the pendulum. The potential energy V can be written as:

$$V = 3m_2 g(y(t) - \frac{5l}{6}cos(\theta)), \tag{12}$$

where g is gravity. The Lagrangian L for this system is

$$L = T - V, \tag{13}$$

where T is the kinetic energy, and V the potential energy. Given that there are no external forces acting on the system the equations of motion of the pendulum can be written in terms of the variable θ (Eq. 14)

$$\frac{\partial}{\partial\theta}L = \frac{d}{dt}\frac{\partial L}{\partial\dot{\theta}} \tag{14}$$

Solving Eq. 14 we obtain:

$$\ddot{\theta} = -\frac{5}{6l}(\ddot{x}cos(\theta) + (\ddot{y} + g)sin(\theta)) \tag{15}$$

where $\ddot{\theta}$ is the angular acceleration, $\ddot{x}$ and $\ddot{y}$ define the acceleration of the point O. We define η equal to $\frac{5}{6l}$ and we look for its appropriate value in the range [0.0075 1.5]. The trajectories from the SLIP model provided as well the initial conditions to integrate the Eq. 15. In this model, the dynamics of the leg is described only when is in contact with the ground. For this reason, we were able to identified the time when the leg detached from the ground. We used the velocity and position of the leg at the detached time as initial conditions for all the values of η. We used the $fminsearch$ function from MATLAB to identified the η values that were able to produce the appropriate angle of attack. The error minimized by $fminsearch$ was $error = (\alpha_{desired} - \alpha_{model})^2$ where $\alpha_{desired}$ is the angle of attack of the symmetric gait and α_{model} is the angle produced by the passive swing of the pendulum in the CPC-SLIP model.

The rod-SLIP a Model with Mass on the Legs

The CPC-SLIP model has been developed under the assumption that the point mass of the SLIP model is much bigger than the mass in the leg. We developed another mathematical model the rod-SLIP in which the spring has inside a pendulum. With this model, we investigated the relation between the mass of the leg and the point mass at the joint, which allows a SLIP model behavior. in this model we simplified the leg structure and assumed a planar rod pendulum. The rod-SLIP model has three different phases as well as the SLIP model. Figure 2 shows the single stance phase (a), double stance phase (b), and flight phase (c). The equation of motion of each phase were obtained using the Lagrangian of the system. For all the different phases, we defined a generalize coordinate system q which is used by the function $CoG_{b_i}(q)$ to compute the vector of the center of mass of the rigid body b_i. With the function

$\dot{CoG}_{b_i}(q) = \frac{\partial CoG_{b_i}(q)}{\partial q}\frac{dq}{dt}$, we computed the velocity of the center of mass of the rigid body b_i. The moment of inertia at the center of mass of each rigid body does not depend on the phase. The legs have a moment of inertia $I_{leg} = \frac{m_n ln^2}{12}$, and the inertia at the hip of the point mas is zero.

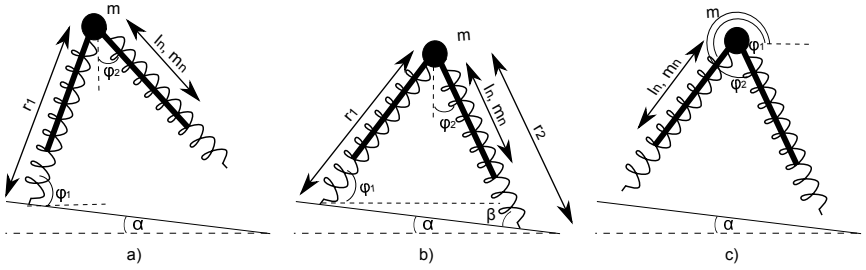

Figure 2: Phases of the rod-SLIP model. With three different phases the rod-SLIP model represents running and walking. (a) shows the single stance phase, which represents the system under the influence of gravity and a linear spring. (b) Shows the double stance phase, here the system is under the influence of gravity and two linear springs. (c) shows the flight phase, which represents the system under the influence of gravity. Given that inside each linear spring there is a rod pendulum the swinging motion of the leg in (a) and (c) is described by the newton's equations of motion.

In the single stance phase we defined $q = (\phi_1, r_1, \phi 2)^t$ where ϕ_1 is the angle of the leg in contact with the ground against the horizontal axis, r_1 is the distance between the contact point with the ground and the hip, and ϕ_2 is the angle of the leg without ground contact and the vertical axis. The Eq. 16 returns the position of the center of mass in the leg that is in contact with the ground. The Eq. 17 gives the position of the center of mass of the swinging leg. In this leg the length of the spring is equal to the rest length l_o. The Eq. 18 returns the position of the point mass that is in the hip and that represents the body mass.

$$CoG_{cntleg}(q) = \begin{bmatrix} r_1 - 0.5 ln cos(\phi_1) \\ r_1 - 0.5 ln sin(\phi_1) \end{bmatrix} \tag{16}$$

$$CoG_{leg}(q) = \begin{bmatrix} r_1 cos(\phi_1) + 0.5 ln sin(\phi_2) \\ r_1 sin(\phi_1) - 0.5 ln cos(\phi_2) \end{bmatrix} \tag{17}$$

$$CoG_{hip}(q) = \begin{bmatrix} r_1 cos(\phi_1) \\ r_1 sin(\phi_1) \end{bmatrix} \tag{18}$$

In the double stance phase we defined $q = (\phi_1, r_1)^t$ where ϕ_1 is the angle between the rear leg and the horizontal axis, r_1 is the distance between the contact point of the rear leg with the ground and the hip. In this phase, the position of the center of mass of all the rigid bodies can be calculated with Eq. 16, Eq. 17, and Eq. 18. Given that in this phase, the legs form a triangle with the ground we can take advantage of this constrain and write ϕ_2 in terms of ϕ_1 and r_1 the Eq. 19 shows the relation between the different edges of the triangle

$$r_2 = \sqrt{{r_1}^2 + base^2 - 2 base r_1 cos(\phi_1 + \alpha)} \tag{19}$$

where r_1 is the length of the rear leg, r_2 is the length of the front leg and *base* is the distance from one foot to the other. Using the sine law, we can write the relation of the angles in the triangle (Eq. 20). Eq. 21 shows the relation of ϕ_2, β and α (see Fig. 2b).

$$\beta = arcsin(r_1 sin(\phi_1 + \alpha)/r_2) \tag{20}$$

$$\phi_2 = pi/2 - \alpha - \beta \tag{21}$$

In the flight phase we defined $q = (x, y, \phi_1, \phi 2)$ where x is the position of the hip in the horizontal axis, y is the position of the hip in the vertical axis, ϕ_1 is the angle between the rear leg and the horizontal axis, and ϕ_2 is the angle

between the front leg and the horizontal axis. The Eq. 22 returns the position of the hip. The Eq. 23 gives the position of the center of mass of the rear swinging leg, and the Eq. 24 returns the position of the center of mass of the front swinging leg. In this phase leg the length of the both springs are equal to the rest length l_o.

$$CoG^f_{hip}(q) = \begin{bmatrix} x \\ y \end{bmatrix} \tag{22}$$

$$CoG^f_{leg_1}(q) = \begin{bmatrix} x + lncos(\phi_1)/2 \\ y + lnsin(\phi_1)/2 \end{bmatrix} \tag{23}$$

$$CoG^f_{leg_2}(q) = \begin{bmatrix} x + lncos(\phi_2)/2 \\ y + lnsin(\phi_2)/2 \end{bmatrix} \tag{24}$$

With the definition of these equations we can calculate the total kinetic energy $T_{phase}(q, \dot{q})$ as it is shown in Eq. 25

$$T_{phase}(q, \dot{q}) = \sum_{i=1}^{n} 0.5 m_i \dot{CoG}^T_{b_i} \dot{CoG}_{b_i} + I_{b_i} W^2_{b_i} \tag{25}$$

where m_i is the total mass of the rigid body b_i and n is the total number of rigid bodies in the system. The potential energy of the system V_{phase} is defined as

$$V_{phase}(q) = \sum_{i=1}^{n} -CoG_{b_i} F^g_i + 0.5 K_i (l_o - r_i(q))^2, \tag{26}$$

where F^g_i is the weight of the rigid body b_i, K_i is the constant of elasticity of the spring in the body i, l_o is the natural length of the spring of the body i and r_i is its compression. With the definition of the energies we can write the Lagrangian as in Eq. 27

$$\frac{d}{dt}\left(\frac{\partial T}{\partial \dot{q}}\right)^T - \left(\frac{\partial T}{\partial q}\right) + \left(\frac{\partial V}{\partial q}\right) = 0 \tag{27}$$

The Eq. 27 is equal to zero because there are not external forces acting on the system. We can rearrange this terms to get the general equation of motion with out external forces as in Eq. 28.

$$M(q)\ddot{q} + b(q, \dot{q}) + G(q) = 0, \tag{28}$$

where:

$$M(q) = \frac{\partial \left(\frac{\partial T}{\partial \dot{q}}\right)^T}{\partial \dot{q}} \tag{29}$$

$$b(q, \dot{q}) = \frac{\partial \left(\frac{\partial T}{\partial \dot{q}}\right)^T}{d\dot{q}} \frac{dq}{dt} - \left(\frac{\partial T}{\partial q}\right)^T \tag{30}$$

$$G(q) = \left(\frac{\partial V}{\partial q}\right) \tag{31}$$

The equation of motion of each phase were generated solving the previous equations using the Symbolic Math Toolbox from MATLAB. As a difference with the SLIP model the rod-SLIP model produces impacts when switches from single stance phase to double stance phase or from flight phase to single stance phase i.e. the leg hits the ground. We generated the model transition assuming total inelastic conditions. In the case of a switch from single stance phase to double stance phase, we use two equations to calculate the new $\dot{q}$ after the impact. One is the conservation of the linear momentum along the landing leg, and the other is the conservation of the linear momentum along the rear leg. in the switch from the flight phase to the single stance phase we use three equations. The conservation of the linear

momentum along the landing leg, and the conservation of the angular momentum on the landing foot and on the hip.

With the rod-SLIP model, we investigated the conditions in which a leg with mass allows a behavior similar to the SLIP model. We took advantage of a rod pendulum constraint to the SLIP model (RPC-SLIP model). With this model, we identified the appropriate length of the rod pendulum based on the equation of motion of a pendulum rod constraint to a given trajectory as it is presented in Eq. 32

$$\ddot{\theta} = -\zeta(\ddot{x}cos(\theta) + (\ddot{y} + g)sin(\theta)), \tag{32}$$

where $\ddot{\theta}$ is the angular acceleration, $\ddot{x}$ and $\ddot{y}$ define the acceleration of the trajectory, and ζ is equal to $\frac{3}{2ln}$. This equation is similar to the CPC-SLIP model of Eq. 15. from this Eq. 15, we can convert the values of η to estimate the length ln of the rod pendulum. This estimation of the geometry of the leg together with the initial conditions of the symmetric gait are fundamental to identify the conditions in which the rod-SLIP model can reproduce symmetric gaits like the SLIP model. To compensate the energy looses produced by the impacts of the leg with ground the system walks and runs in an incline plane with angle α. We used the function $fminsearch$ from MATLAB to tune the parameters of the model and allow the system perform at least 20 steps. The data shown in this paper uses the results of simulations that were able to perform at least 5 steps.

3. Results

In this section, we present the results from the simulated models introduced in the previous section. The total length of the compound pendulum (Fig. 1) used in the simulation is equal to $2l$. The left panel of Figure 3 shows the result from the CPC-SLIP model for walking. These results show that between 800J and 830J the compound pendulum can have a total length in the range of 0.2m and 0.64m. For energies lower than 800J the total length is bigger than 0.4m. For energies bigger than 830J the total length is lower than 0.5m.

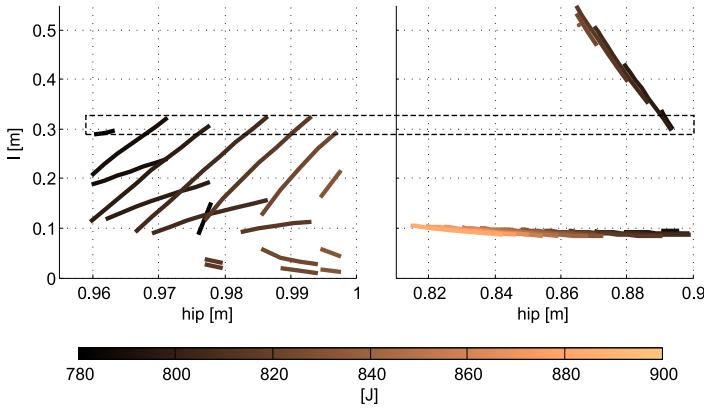

Figure 3: (Color online) Length of a compound pendulum segment in the CPC-SLIP model to match the SLIP model angle of attack. The left panel shows the valid segment length l for walking. The right panel shows the valid segment length for running. The total length of the pendulum is equal to $2l$ (Fig. 1). The compound pendulum reproduces symmetric gaits for the energies E in the range $[780, 900]$J. The horizontal axis hip refers to the vertical position of the hip when it is exactly above one foot. The region enclosed with the dashed rectangle show the length of the pendulum that can be used for walking and running

The right panel shows the result from the CPC-SLIP model for running. there are two sets of possible compound pendulums. Between 800J and 820J the total length is bigger than 0.6mand in the range $[800, 900]$J the total length is around 0.2m. In both conditions the length increases with the energy. These results show that the walking and running can be performed with a compound pendulum of 0.64m. However, for bigger energies running requires a lower total length.

Figure 4 shows the results from the simulations of the rod-SLIP model for walking. This model assumes a rod pendulum inside the linear spring. The total length of this pendulum is equal to l_n, and the panels of Fig. 4 depict the

appropriate l_n to produce similar gaits to the SLIP model as a function of the total mass of the pendulum m_n in kg. The solid lines represent the length of the pendulum under the RPC-SLIP model of Eq. 32, in which the total mass of the system is concentrated at the hip the dots represent the result from the rod-SLIP model.

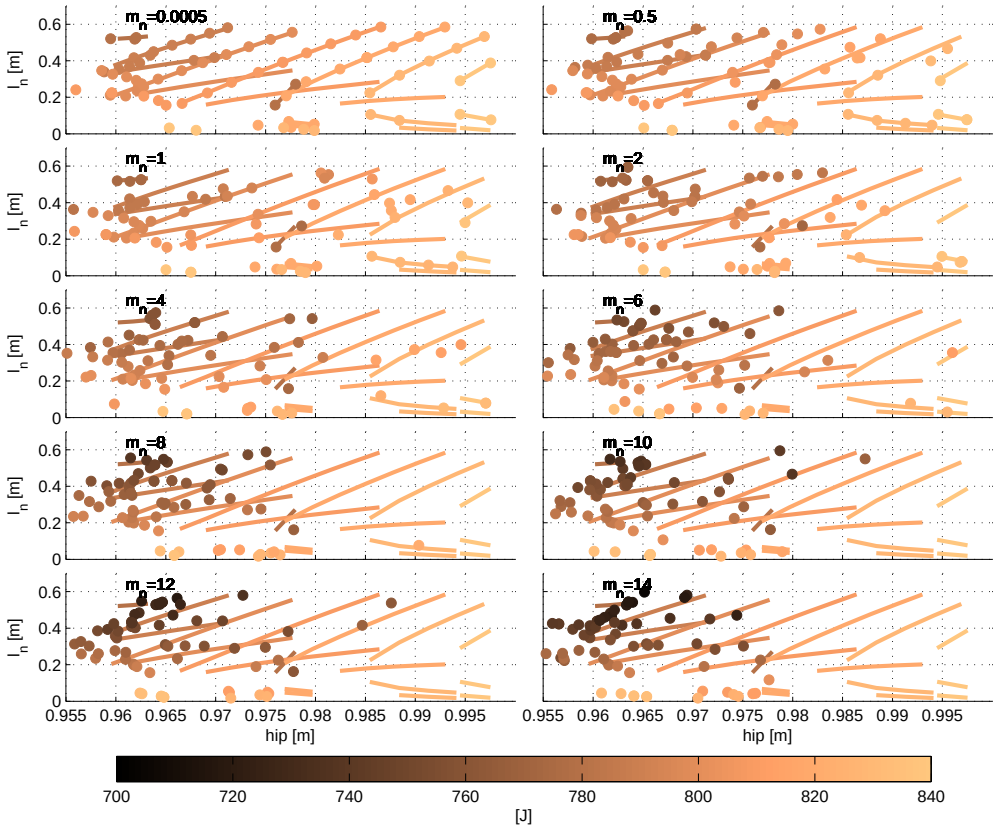

Figure 4: (Color online) Rod pendulum length to match the SLIP model walking gait. The panels show rod pendulums with different total mass m_n in kg. The solid lines show the expected length l_n of a rod pendulum that match the SLIP model walking in the case of a hip mass much bigger than the mass at the pendulum (RPC-SLIP model). The horizontal axis hip refers to the vertical position of the hip when it is exactly above one foot. In all the panels the total mass is equal to 80kg

The RPC-SLIP model predicts accurately the length of the pendulum until the mass at the legs is around 5% of the total mass. The more mass on the legs, the smaller vertical height of the hip. Furthermore when the mass on the legs is bigger than 20% of the total mass (m_n = 8kg), the bigger the total energy of the system, the smaller the total length of the pendulum.

Figure 5 shows the results from the simulations of the rod-SLIP model for running. The total length of this pendulum is equal to l_n. The panels of Fig. 5 depict the appropriate l_n to produce the symmetric running gait found in the SLIP model. Each panel shows the result for a different mass in the pendulum m_n in kg keeping the total mass of the system constant at 80kg. The solid lines represent the length of the pendulum under the RPC-SLIP model, in which the total mass of the system is concentrated at the hip. Simulation Results show that the RPC-SLIP model estimates accurately the length of the pendulum until the mass at the legs is around 5% of the total mass. For a mass bigger than the 10% of the total mass (m_n = 4kg) the total length of the pendulum is restricted to the lower bound of

0.2m.

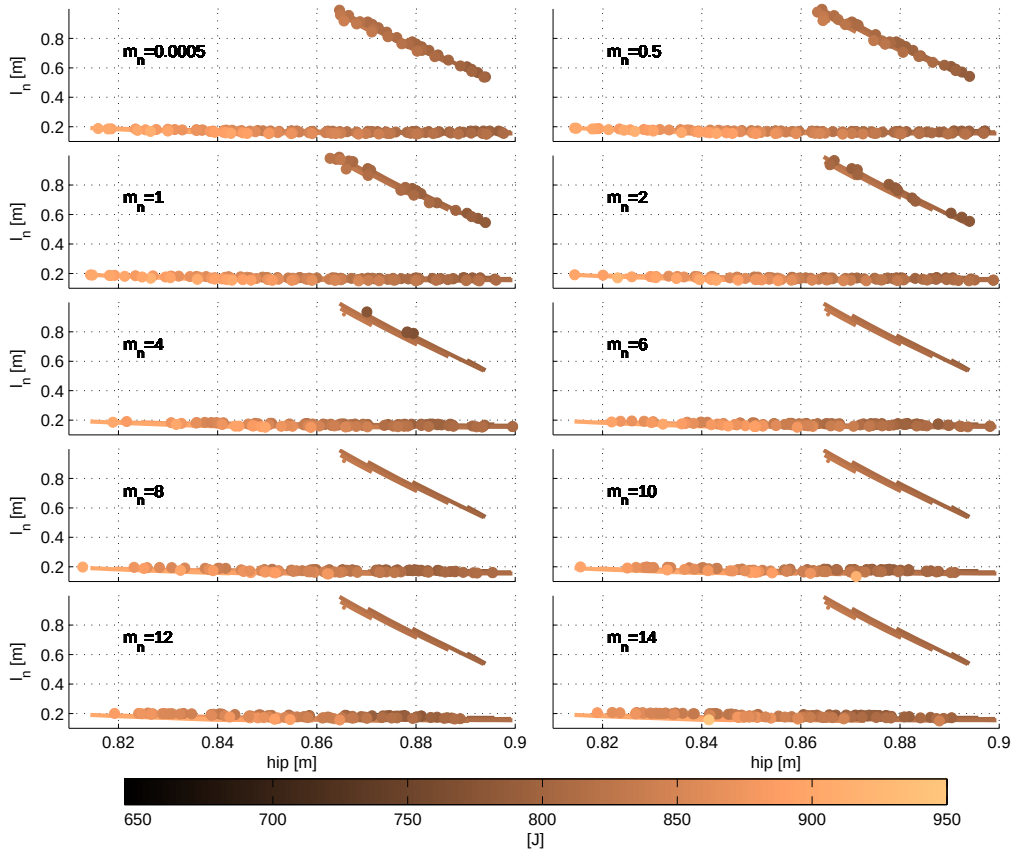

Figure 5: (Color online) Rod pendulum length to match the SLIP model running gait. The panels show rod pendulums with different total mass m_n in kg. The solid lines show the expected length l_n of a rod pendulum that match the SLIP model running in the case of a hip mass much bigger than the mass at the pendulum (RPC-SLIP model). The horizontal axis *hip* refers to the vertical position of the hip when it is exactly above one foot. In all the panels the total mass is equal to 80kg

4. Discussion

For this study, we selected a set of SLIP model parameters that approximate a human being. Under this condition, the model was used to generate the trajectories of the symmetric gaits. We introduced models based on these trajectories (CPC-SLIP model and RPC-SLIP model). With these new models, we identified that running and walking have a region in which the same kind of pendulum can be used to produce both gaits (Fig. 3). The size of this compound pendulum is 0.64m, which closely resembles the length of the thigh and shank which is in average around 0.75m Project, Army, Force, Navy, Panel, Committee, and States (1988).

The predictions of the model from CPC-SLIP model are validated with the simulation results from the rod-SLIP model. In the case of legs with less than 5% of the total mass (Fig. 4, and Fig. 5), the rod-SLIP model can reproduce similar gait patterns to the ones find in the SLIP model. However, a bigger mass affects the stability, and the system cannot perform the minimum of five steps required for the same conditions tested in the SLIP model. In humans the

thigh and shank of both legs have around 17% of the total mass Project et al. (1988). We believe that the instability in the rod-SLIP model can be decreased adding a non-linear stiffness and a rolling foot. Experimental studies have shown that human legs have a nonlinear constant of elasticity Dumke, Pfaffenroth, McBride, and McCauley (2010); Blum, Lipfert, and Seyfarth (2009), and simulation studies Rummel and Seyfarth (2008) have shown that this non-linearity can increases the stability of the system. The introduction of a rolling foot Adamczyk, Collins, and Kuo (2006); Whittington and Thelen (2009) allows the progression of the contact point between the leg and the ground. This progression transmits part of the total energy of the system to forward locomotion which allows a higher walking speed than in a point foot model. These aspects can be a key factor to increment the stability of the system even when the mass in the legs are around 17% of the total mass.

The results from the CPC-SLIP model show that in the case of symmetric walking there are several compound pendulums that can be used in the range of energies E $[780, 840]$J (Fig. 3). This suggest that the swing controller of the leg can be calculated based on the total energy of the system and the height of the hip. Given these parameters, the controller can tune the swinging of the leg to match a pendulum with the given total length. This strategy allows a robust walking for a broad range of energies without changing actually the dimension of the leg. This control strategy can also be applied to the running gait and gait transitions. The results show that different lengths of a compound pendulum like the one introduced in Fig 1 can be used to produce the same running pattern. At low energies the running gait can use a similar pendulum to the one needed in walking. For high energy levels the compound pendulum is smaller. From the perspective of a control strategy, a high energy running requires swinging controller that actuates the leg with a higher frequency emulating a reconfiguration of the leg (leg contraction). For lower energies the swinging control can select a lower frequency which emulates an extension of the leg. This can appropriately facilitate a gait transition from running to walking because in the walking gait the swinging strategy is the same.

The increment of mass in the legs restrict the pendulum that can be selected. In the case of walking (Fig. 4), the bigger is the energy the lower is the pendulum. This is different from the results in Fig. 3, in which most of the energies can use a variety of pendulums. We believe that the possibility of selecting as wide range of pendulums can also be seen as possible swinging frequencies. For this reason, if the human walking gait follows the CPC-SLIP model we would be able to identify different stepping frequencies for a given forward velocity. If this is the case, then the selection of this frequencies can be disturbed by adding more mass in the legs. We can measure the attention demand as the effort to compensate this disturbance similar to Abernethy, Hanna, and Plooy (2002). We expect that when adding more mass in the legs, the range of possible stepping frequencies is going to be reduced and the attention demand to produce the gait is going to increase.

5. Conclusion

In this study we used three different models to study the roll of the legs in locomotion. First, we used the SLIP model to generate all the possible symmetric gaits in the energy range $[780, 900]$J. The second model assumed a pendulum constraint to the trajectories generated by the SLIP. With this model, we found the appropriate pendulums that can reproduce the SLIP trajectories. Then, we proposed the rod-SLIP model, in which we consider mass in the legs. With this model we found in simulation the mass relation between the legs and the body that satisfy the estimation of the second model. We found that there is a pendulum that allows the system both gaits running and walking. Assuming a pendulum with human like mass distribution, we found that pendulum resembles the human leg length. The results from this study can also be interpreted from the control perspective which brings new ideas about plausible mechanisms that biped creatures could use to carry out gait transitions and stable locomotion. These mechanisms exploit the passive dynamics of the system, thus reducing the amount of energy to control the system.

Acknowledgements. We want to thank Naveen Kuppuswamy for his review of the manuscript. The research leading to these results has received funding from the European Community's Seventh Framework Programme FP7/2007-2013-Challenge 2-Cognitive Systems, Interaction, Robotics- under grant agreement No 248311-AMARSi.

References

S. Siegler, R. Seliktar, W. Hyman, Simulation of human gait with the aid of a simple mechanical model, J. Biomech. 15 (1982) 415 – 425.

M. G. Pandy, Simple and complex models for studying muscle function in walking, Philosophical Transactions of the Royal Society of London. Series B: Biological Sciences 358 (2003) 1501–1509.
F. E. Zajac, R. R. Neptune, S. A. Kautz, Biomechanics and muscle coordination of human walking: Part ii: Lessons from dynamical simulations and clinical implications, Gait & Posture 17 (2003) 1 – 17.
F. Valero-Cuevas, H. Hoffmann, M. Kurse, J. Kutch, E. Theodorou, Computational models for neuromuscular function, Biomedical Engineering, IEEE Reviews in 2 (2009) 110 –135.
P. Holmes, R. J. Full, D. Koditschek, J. Guckenheimer, The dynamics of legged locomotion: Models, analyses, and challenges, SIAM Rev. 48 (2006) 207–304.
R. Blickhan, The spring-mass model for running and hopping, J. Biomech. 22 (1989) 1217 – 1227.
H. Geyer, A. Seyfarth, R. Blickhan, Compliant leg behaviour explains basic dynamics of walking and running., P. Roy. Soc. B - Biol. Sci. 273 (2006) 2861–7.
R. Full, D. Koditschek, Templates and anchors: neuromechanical hypotheses of legged locomotion on land, J. Exp. Biol. 202 (1999) 3325–3332.
H. R. Martínez Salazar, J. P. Carbajal, Exploiting the passive dynamics of a compliant leg to develop gait transitions, Phys. Rev. E 83 (2011) 066707.
H. Martínez, J. Carbajal, From walking to running a natural transition in the slip model using the hopping gait, in: Robotics and Biomimetics (ROBIO), 2011 IEEE International Conference on, 2011, pp. 2163 –2168. doi:10.1109/ROBIO.2011.6181612.
B. Andrews, B. Miller, J. Schmitt, J. Clark, Running over unknown rough terrain with a one-legged planar robot., Bioinspir Biomim 6 (2011) 026009.
J. M. Schmitt, Incorporating energy variations into controlled sagittal plane locomotion dynamics, ASME Conference Proceedings 2007 (2007) 1627–1635.
T. A. McMahon, G. C. Cheng, The mechanics of running: How does stiffness couple with speed?, J. Biomech. 23, Supplement 1 (1990) 65 – 78. ¡ce:title¿International Society of Biomechanics¡/ce:title¿.
J. G. Cham, J. K. Karpick, M. R. Cutkosky, Stride period adaptation of a biomimetic running hexapod, The International Journal of Robotics Research 23 (2004) 141–153.
T. McGeer, Passive Bipedal Running, Proceedings of The Royal Society of London. Series B, Biological Sciences (1934-1990) 240 (1990) 107–134.
D. Owaki, K. Osuka, A. Ishiguro, On the embodiment that enables passive dynamic bipedal running, in: Robotics and Automation, 2008. ICRA 2008. IEEE International Conference on, 2008, pp. 341–346. doi:10.1109/ROBOT.2008.4543231.
D. Owaki, K. Osuka, A. Ishiguro, Understanding the common principle underlying passive dynamic walking and running, in: Intelligent Robots and Systems, 2009. IROS 2009. IEEE/RSJ International Conference on, 2009, pp. 3208–3213. doi:10.1109/IROS.2009.5354661.
A. R. Project, U. Army, U. A. Force, U. Navy, T.-S. A. R. Panel, T.-S. Committee, U. States, Anthropometry and Mass Distribution for Human Analogues: Military male aviators, v. 1, Anthropology Research Project, 1988. URL: http://books.google.ch/books?id=ZxRNXwAACAAJ.
C. L. Dumke, C. M. Pfaffenroth, J. M. McBride, G. O. McCauley, Relationship between muscle strength, power and stiffness and running economy in trained male runners, Int J Sports Physiol Perform 5 (2010) 249–61.
Y. Blum, S. W. Lipfert, A. Seyfarth, Effective leg stiffness in running, Journal of Biomechanics 42 (2009) 2400 – 2405.
J. Rummel, A. Seyfarth, Stable running with segmented legs, The International Journal of Robotics Research 27 (2008) 919–935. 10.1177/0278364908095136.
P. G. Adamczyk, S. H. Collins, A. D. Kuo, The advantages of a rolling foot in human walking, J. Exp. Biol. 209 (2006) 3953–3963.
B. R. Whittington, D. G. Thelen, A simple mass-spring model with roller feet can induce the ground reactions observed in human walking, J Biomech Eng 131 (2009) 011013.
B. Abernethy, A. Hanna, A. Plooy, The attentional demands of preferred and non-preferred gait patterns, Gait Posture 15 (2002) 256 – 265.

Appendix F

On the Influence of Sensor Morphology on Vergence

Reprinted from:

Martínez, H. R., Sumioka, H., Lungarella, M., Pfeifer, R.(2010). *On the Influence of Sensor Morphology on Vergence*, In From Animals to Animats 11 (pp. 146-155). Springer Berlin Heidelberg.

On the Influence of Sensor Morphology on Vergence

Harold Martinez, Hidenobu Sumioka, Max Lungarella, and Rolf Pfeifer

Artificial Intelligence Laboratory, Department of Informatics, University of Zurich, Andreasstrasse 15, 8050 Zurich, Switzerland
{martinez,sumioka,lunga,pfeifer}@ifi.uzh.ch
http://ailab.ifi.uzh.ch/

Abstract. In the field of developmental robotics, a lot of attention has been devoted to algorithms that allow agents to build up skills through sensorimotor interaction. Such interaction is largely affected by the agent's morphology, that is, its shape, limb articulation, as well as the position and density of sensors on its body surface. Despite its importance, the impact of morphology on behavior has not been systematically addressed. In this paper, we take inspiration from the human vision system, and demonstrate using a binocular active vision platform why sensor morphology in combination with other properties of the body, are essential conditions to achieve coordinated visual behavior (here, vergence). Specifically, to evaluate the effect of sensor morphology on behavior, we present an information-theoretic analysis quantifying the statistical regularities induced through sensorimotor interaction. Our results show that only for an adequate sensor morphology, vergence increases the amount of information structure in the sensorimotor loop.

Keywords: Embodied cognition, visual development, sensor morphology, information structure.

1 Introduction

In nature, living organisms are embodied and embedded in their ecological niches. Their neural structures have evolved to sample and process sensor inputs to create adaptive neural representations, and to select and control motor outputs to position their bodies or to impose changes on the environment [1]. Such sensorimotor activity involves a dynamic reciprocal coupling between organism and environment known as embodiment [2]. The implications of embodiment are far reaching and go beyond the mere interaction between a body and the environment in which it is embedded, to include also as the information-theoretic interrelations among the sensory system, the body, the environment, and the controller. Embodiment is understood as a fundamental aspect to develop cognitive capabilities because it enables a continuous flow of information between sensors, neural units, and effectors. The pattern of information flow defines complex sensorimotor networks, consisting of structured relations and dependencies among sensor, neural, and motor variables. This information structure, such as correlations, redundancies, and

S. Doncieux et al. (Eds.): SAB 2010, LNAI 6226, pp. 146–155, 2010.
© Springer-Verlag Berlin Heidelberg 2010

invariances in the sensorimotor loop makes learning, prediction, action selection, adaptability and developmental process possible [1],[3], [4].

Some algorithms employed to bootstrap the development of skills [5], [6], [7] are designed to restrict the action selection (repertoire) in order to increase predictability of the sensorimotor loop. In these cases, the objective function that drives the development of the agent is some quantitative measure of the agent's sensorimotor interaction (e.g. information gain, transfer entropy, the prediction error of the next sensor input, and the improvement in the prediction in the sensor input). Generally, in these mathematical frameworks, embodiment is simplified to the interaction with the environment.

In the application of the developmental algorithms there are some limitations, such as the number of sensor inputs, degrees of freedom (DOF), and convergence time among others. We claim that because of the embodiment, the sensor morphology and the robot body should be taken into account in order to exploit statistical dependencies and causal relations in the sensorimotor loop. Therefore appropriate sensor morphology could be the mechanism not only to decrease the convergence time, but also to sense information flow which increases the predictability, limiting the action space naturally.

In the first months of life, a child is able to develop sensorimotor competencies almost from scratch [8]. Behaviors such as tracking, saccadic movements and fixation start to develop at the beginning of a child's life and are mature after about three months [9], [10]. The development of behaviors like vergence could be explained as the result of the increment in predictability among actions and sensor inputs.

In this paper, we provide an information theoretical analysis that shows why the sensor morphology, and the sensorimotor coupling could bootstrap the development of vergence. The latter behavior increases the causality among actions and sensors, hence increasing the predictability of the future sensor stimulation, and enabling the agent to develop a model of the environment. In order to measure how much the agent can predict given specific sensor morphology we used transfer entropy as a measure of causality [11].

This paper is organized as follows. First, we describe the robot head platform used for our experiment, the sensor morphology, and the causality measure employed to quantify the results in the experiment. Then, we present the experiment and the related results. Before concluding the paper, we discuss our results and some of their implications for theories of infant development.

2 Materials and Methods

2.1 Robot

Our experimental testbed was the iCub robot head [12]. The iCub is an open humanoid platform, developed in the context of the RobotCub project, to promote studies in cognitive systems and embodied cognition. In contrast with other humanoid robots as QRIO, ASIMO, HOAP-2, the iCub robot head has 6 DOF

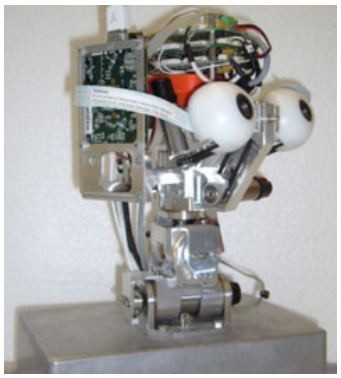

Fig. 1. iCub robot head

(Fig. 1) in order to emulate behaviors like vergence, smooth pursuit, and saccades, typical of the vision system. Both eyes can pan independently, and the common tilt movement is actuated by a belt system placed between the cameras. 3 DOF are used to control the neck of the head, while the other 3 DOF are used to control the cameras. Our experiments were conducted controlling just the latter 3 DOF. The neck of the robot was immobile during all the procedure. The image delivered by each camera has a resolution of 640x480 at 30 fps.

2.2 Sensor Morphology

The human vision system has to interpret a 3D world from 2D projections, and in this process the ocular movements play an important role. These motions are not an innate feature, but are developed through a prolonged interaction with the environment. Moreover, abilities such as stereopsis (depth perception from binocular vision that exploits parallax disparities) are a result of this development in the first months of life [13], [14].

The question is what mechanism drives this process, and what could be the contribution of the morphology of the eyes and the ocular muscles. In order to address this matter, we implemented a set of biologically plausible information processing mechanisms in the iCub head. Based on the results from Nothdurf (1990) [15], who showed how neurons respond to simple features such as intensity contrast, color, orientation, and motion, color was the main feature used in our experiments. These features define the pre-attentive visual cues [16]. In addition, the human vision is capable of binocular fusion; i.e. a single image is seen although each eye has a different image of the environment [17]. In our implementation we applied the average of both cameras to create the binocular single image. Another important aspect is foveation. Our eye has, in its center, a greater number of receptors than in the periphery. This was modeled with the log-polar transform, which changes the coordinate system from Cartesian (x,y) to the logarithm of the magnitude and the angle:

$$\rho(x, y) = M \cdot log(\sqrt{(x^2 + y^2)}) \; . \tag{1}$$

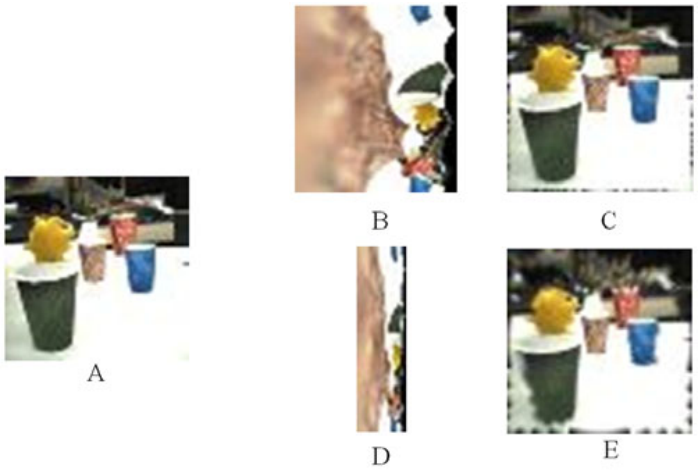

Fig. 2. Log-polar transform of 60x60 image. (A) Raw image. (B) Log-polar transform of A with M = 40. (C) Inverse log-polar transform from B. (D) Log-polar transform of A with M=12. (E) Inverse log-polar transform from D. Notice that the inverse transform is the reconstruction of the image with fewer pixels in peripheral area.

$$\varphi = arctan(\frac{y}{x}) \; . \tag{2}$$

Where x and y are the coordinates of the pixel in the picture, ρ is the logarithm of the magnitude and φ is the angle. The parameter M was used to increase or decrease the number of pixels used in the log-polar transform (Fig. 2). In our experiments, these aspects (color, foveation and image composition from the two cameras) were used to find out whether the vergence behavior increases information structure.

2.3 Information Metric

In order to present how the causality among the variables (actuators and sensors) relies on the morphology and specific behaviors, we used the transfer entropy [11]. This measure was selected to compare the results of the experiments, due to its capacity to find the nonlinear statistical dependencies which can be used to understand why a specific behavior could yield better causal relations among the data.

Originally, transfer entropy was introduced to identify the directed flow or transfer of information (also referred to as "causal dependency") between time series [11]. Given two time series X and Y, transfer entropy essentially quantifies the deviation from the generalized Markov property: $p(x_{t+1} \mid x_t) = p(x_{t+1} \mid x_t, y_t)$, where p denotes the transition probability. If this deviation is small, then Y does not have relevance on the transition probabilities of system X. Otherwise, if the deviation is large, then the assumption of a Markov process is not valid, The deviation of the assumption can be quantified by the transfer entropy, formulated as the Kullback-Leibler entropy:

150 H. Martinez et al.

$$T(Y \to X) = \sum_{X_{t+1}} \sum_{X_t} \sum_{Y_t} p(x_{t+1}, x_t, y_t) log(\frac{p(x_{t+1}|x_t, y_t)}{p(x_{t+1}|x_t)}) \ . \tag{3}$$

Where the sums are over all amplitude states, and the index $T(Y \to X)$ indicates the influence of Y on X. The transfer entropy is explicitly nonsymmetrical under the exchange of X and Y — a similar expression exists for $T(X \to Y)$ — and can thus be used to detect the directed exchange of information (e.g., information flow, or causal dependency) between two systems. As a special case of the conditional Kullback-Leibler entropy, transfer entropy is non-negative, any information flow between the two systems resulting in $T > 0$. In the absence of information flow, i.e., if the state of system Y has no influence on the transition probabilities of system X, or if X and Y are completely synchronized, $T(Y \to X) = 0$ bit.

2.4 Data Analysis

All numerical computations for data analysis were carried out in Matlab (Mathworks, Natick, MA), and were performed for data samples of 12,300 time steps. The resolution of the cameras was reduced to 60x60 pixels to facilitate the calculations. We used gray scale images to reduce computational costs for analyzing causal relations among sensor and motor variables. Given that the proposed sensor morphology is defined by the binocular single image and the foveation, we can still evaluate the effect of our proposed sensor for vergence. In order to calculate the transfer entropy between the images and the actions, we first generated a causality measure for each pixel, which was the sum of transfer entropy between each DOF and the pixel (Eq. 4). The causality of the image then was measured as the average causality of all the pixels (Eq. 5)

$$T_{p_j} = \sum_{E_i} T(E_i \to p_j) \tag{4}$$

$$T_I = \frac{\sum_{p_j} T_{p_j}}{|p|} \ , \tag{5}$$

where E_i is the i^{th} DOF time series, p_j is the j^{th} pixel time series, T_{p_j} is the causality induced by the 3DOF to the j^{th} pixel. T_I is the average causality in the frame averaging all the causality measured in each pixel. To calculate transfer entropy, time series were discretized to 8 states (3 bits) and joint probabilities and conditional probabilities were estimated using the naive histogram technique, that is, as normalized histograms. Temporal delays in [-25, 25] time steps across time series were introduced by shifting one time series relative to the other, thus allowing the evaluation of causal relationships across variable time offsets. Delayed causality was potentially introduced by the discrete nature of the updating of the control architecture and by the temporal persistence of sensor and motor states.

3 Experiment

In this experiment we compare different sensor morphologies and controllers in a fixed task. First, we tested different morphologies to find out which one could reduce the number of inputs to the system. Second, we tested different controllers to see how the sensor morphology restricts the space of coordinated behavior in terms of predictability.

In the setup we place the robot in front of four different cups (Fig. 3A). The objects were distributed in the field of view to force the robot to change the value of the 3 DOF of the cameras. The robot had to look at all of them in a predefined sequence. We used the color based tracker to change the attention of the robot to 4 different objects. In order to measure the influence of sensor morphology on vergence, we developed three different controllers: (1) the left camera performed random movements while the right one followed the sequence; (2) a controller that allowed parallel motions of the left and right camera; and (3) a controller that forced the vergence with both cameras to focus the object. We expect that the control quality (behavior) can affect the predictability, that is the possibility to explain the future based in the actual data and actions, hence validating that vergence is a behavior capable of increasing the causal relations among the pixels and the actions.

3.1 Setup

For the three controllers we tested four different sensor configurations: (1) the average of the left and right image. (2) The inverse log-polar of the average of the left and right image. (3) The log-polar of the average of the left and right image, and (4) a single image, the left camera (Fig. 3B). We used four different log-polar transformations (M = 8, 12, 20 and 40 which reduce the size of the image to 17%, 27%, 43%, and 83% respectively.) For each transformation we ran 8 different experiments for all different kinds of images.

3.2 Results

First, we compared different morphologies using a controller which performs an appropriate vergence. We evaluated in the experiment how the proposed sensor morphology can keep the predictability while it reduces the number of pixels. We compared the measures of transfer entropy of the left image against the average and the inverse average log-polar. As we can see in Figs. 4A-C the causality in all these sensor morphologies changes less than 5%, which means that the pixels in the center are dominant in the causal relation.

The tracker kept the zero disparity region in the center of the image. Therefore, in the log-polar transformation the receptors sample more the object than the periphery. We tested different number of receptors in the average log-polar morphology to see how the causality could be affected. In Figs. 4D-G we presented the results for four different examples. We found out that the reduction of receptors does not decrease the causality. Therefore this sensor morphology keeps the information structure with fewer pixels. This result could be used

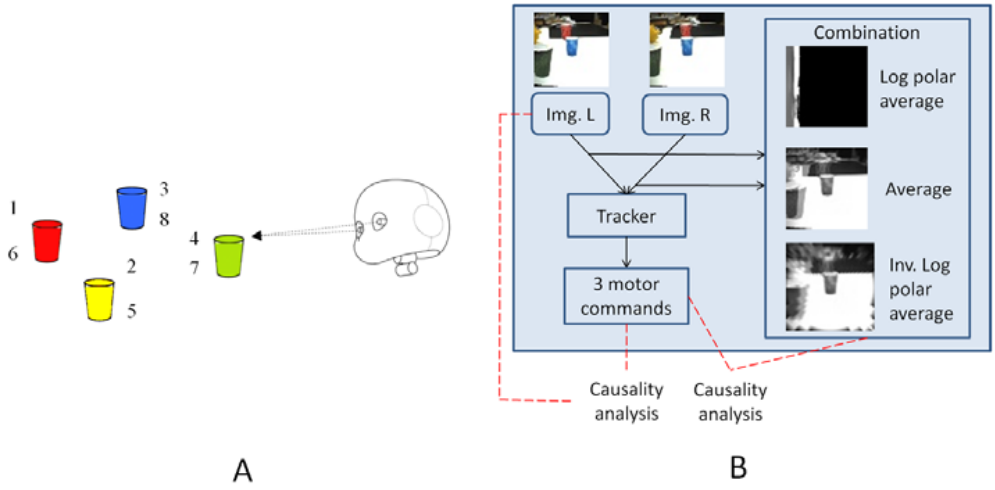

Fig. 3. Experimental setup. (A) The robot is looking at the different cups in the sequence given by the numbers, after 7 the robots starts again with 1. (B) Causal analysis among different sensor and control configurations.

in order to reduce the number of inputs in a developmental algorithm, taking advantage of the sensor morphology.

The different controllers represent different "qualities" of the vergence behavior. As shown in Figs. 4G-I the more accurate the control for vergence, the more causality appears in the sensorimotor loop. From this result we imply that that if the robot looks for predictability in terms of its sensorimotor coupling it has to do vergence.

4 Discussion

The log-polar transform and the average of the two images force the robot to develop vergence, because on the one hand, the log-polar transform allows to better sample the center of the image, and on the other hand, the average of both cameras blurred regions in the image that are not in the zero disparity region. Therefore vergence is aligning the zero disparity region in the center of the image, where the robot has more receptors. The more precise this behavior, the bigger the causal relation among pixels and actions.

The log-polar transform reduces the computational load, and additionally improves the learning, because these are the pixels with the higher causal relations even when the inputs are reduced to 17%. With a normal Cartesian pixel array the rest of the pixels in the learning process are just noise, due to the lack of structure, and in this sense the perception of the agent is decreased.

The causality can be interpreted as the predictability, which allows the agent to develop a model of the world [18]. If the agent is not able to perform vergence then the predictability decreases as it is presented in the experimental results. This means that the learning capability is limited by the predictive capacity of

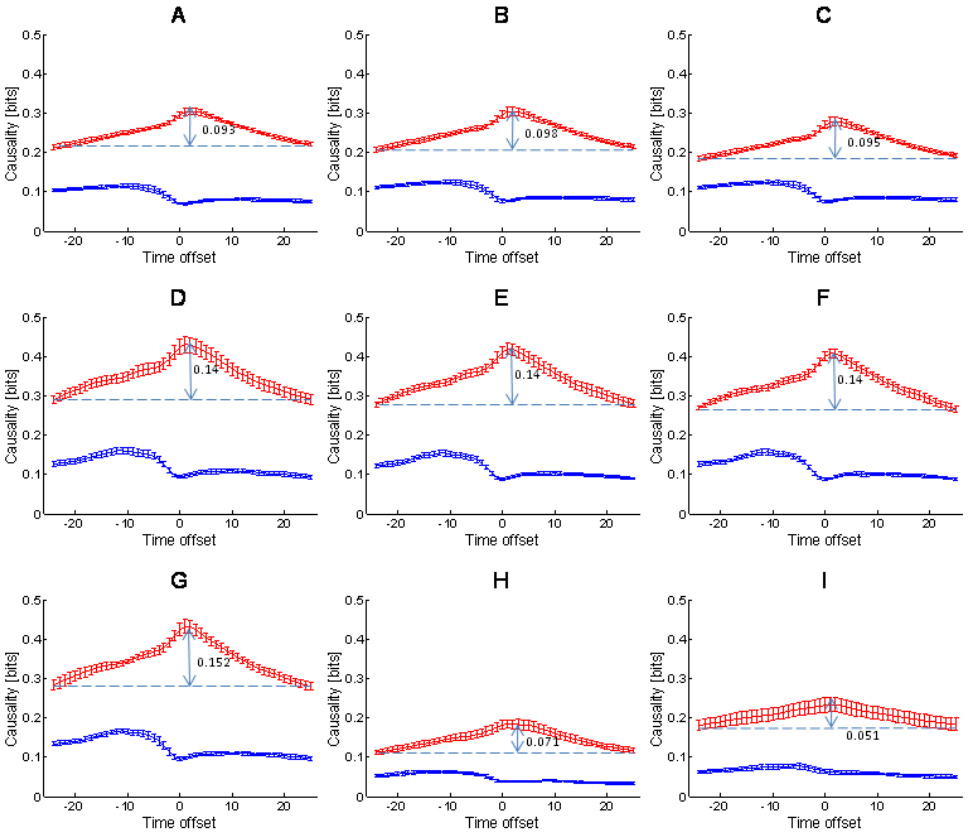

Fig. 4. Transfer entropy among pixels and motor signals. Plots A to I display the average causality as in Eq.(5), $T_{S\to M}$ (blue), $T_{M\to S}$ (red). In plots A to G the 3 DOF of the active vision system were controlled independently. (A) Left image. (B) Average image. (C) Average inverse log-polar image with M=8. (D) Average log-polar image with M=40. (E) Average log-polar image with M=20. (F) Average log-polar image with M=12. (G) Average log-polar image with M=8. (H) One camera tracked the object while the other mirrors its movement. The causality was calculated using the average log-polar transform with M=8. (I) The controller is equal to the one used in A, but with the addition of noise in the control signal sent to the left camera. The causality presented in (I) is using the average log-polar transform with M=8.

the sensorimotor loop. In other words, the robot is limited by the "quality" of its control. In this sense the sensor morphology and the combination of different sensor modalities shape the possible developmental behavior.

5 Conclusions

In this study, we implemented a set of biologically plausible information processing mechanisms based on the human vision system. We analyzed the transfer entropy as a function of the sensor morphology and the controller. Our experimental results demonstrate how an appropriate morphology reduces the amount of inputs and increases the predictability in the sensorimotor loop. The reduction of inputs to a system, and the increment of causal relations among motor actions and inputs are key aspects that increase the applicability of developmental algorithms in robots.

The vision system allows us to generate a belief of the environment beyond the simple 3D perception or spatial distribution. Thanks to the interaction with the world and the coupling with other sensor inputs, visual information allows prediction. Our capacity to use our attention towards what it is needed, like a reflex, and the capacity of prediction of our visual system, are two features that makes our vision system a fascinating tool to handle the world, and it is an incredibly complex system that is not easy to isolate or emulate in an artificial platform. In this experiment we show how from the coupling between the visual system and the proprioceptive system the vergence could emerge under the developmental mechanism of predictability. The possible extension of this result might be the development of an attention systems based not just on visual data but in the relations among different sensor systems. The development of the attention system then enables the agent to extract the information relevant for its own tasks providing the substrate for the emergence of behaviors such as eye hand coordination.

In the perspective of human infants our results show that the build up of behavior might be a result of better information structure. Actions like vergence allow us to predict better to understand better the environment, and the integration of several sensor modalities can therefore generate more complex final behaviors in order to achieve structure in several sensor systems.

Acknowledgments. This work was supported in part by the EU Project IST-2004-004370 ROBOTCUB and by the EU Project FP7-ICT-231864 EC-CEROBOT. We would also like to thank Alejandro Hernandez for his valuable comments.

References

1. Lungarella, M., Sporns, O.: Mapping information flow in sensorimotor networks. PLoS Comp. Bio. 2(10), e14 (2006)
2. Pfeifer, R., Lungarella, M., Iida, F.: Self-organization, embodiment, and biologically inspired robotics. Science 318, 1088–1093 (2007)

3. Koerding, K.P., Wolpert, D.M.: Bayesian decision theory in sensorimotor control. Trends Cogn. Sci. 10, 319–326 (2006)
4. Thelen, E., Smith, L.: A dynamic systems approach to the development of cognition and action. MIT Press/Bradford (1994)
5. Schmidhuber, J.: Driven by Compression Progress: A Simple Principle Explains Essential Aspects of Subjective Beauty, Novelty, Surprise, Interestingness, Attention, Curiosity, Creativity, Art, Science, Music, Jokes. In: Anticipatory Behavior in Adaptive Learning Systems, from Sensorimotor to Higher-level Cognitive Capabilities. LNCS (LNAI), pp. 48–76. Springer, Heidelberg (2009)
6. Oudeyer, P.-Y., Kaplan, F., Hafner, V.: Intrinsic Motivation Systems for Autonomous Mental Development. IEEE Trans. on Evol. Comp. 11(2), 265–286 (2007)
7. Barto, A., Singh, S., Chentanez, N.: Intrinsically motivated learning of hierarchical collections of skills. In: 3rd Int. Conf. Devel. Learn., pp. 112–119. IEEE Press, San Diego (2004)
8. Smith, P., Cowie, H., Blades, M.: Understanding children's development. Blackwell, Malden (1998)
9. Tondel, G., Candy, T.: Human infants' accommodation responses to dynamic stimuli. Investigative Ophthalmology & Visual Science 48(2), 949–956 (2007)
10. Aslin, R.N.: Development of binocular fixation in human infants. Journal of Exp. Child Psy. 23(1), 133–150 (1977)
11. Schreiber, T.: Measuring information transfer. Phys. Rev. Lett. 85, 461–464 (2000)
12. Beira, R., Lopes, M., Praça, M., Santos-Victor, J., Bernardino, A., Metta, G., Becchi, F., Saltarén, R.: Design of the Robot-Cub (iCub) Head. In: Conf. on Rob. and Auto., pp. 94–100. IEEE Press, Orlando (2006)
13. Birch, E., Petrig, B.: FPL and VEP Measures of Fusion, Stereopsis and Stereoacuity in Normal Infants. Vision Res. 36(9), 1321–1327 (1996)
14. Birch, E., Morale, S., Jeffrey, B., Oconnor, A., Fawcett, S.: Measurement of stereoacuity outcomes at ages 1 to 24 months: Randot stereocards. Journal of Ame. Asso. for Ped. Opht. and Stra. 9(1), 31–36 (2005)
15. Nothdurf, H.: Texture discrimination by cells in the cat lateral geniculate nucleus. Exp. Brain Res. 82, 48–66 (1990)
16. Itti, L., Koch, C.: Computational Modeling of Visual Attention. Nat. Rev. Neuro. 2(3), 194–203 (2001)
17. Wheatstone, C.: Contributions to the physiology of vision.-Part the First. On some remarkable, and hitherto unobserved, phenomena of binocular vision. Phil. Trans. of the Royal Soci. of London 128, 371–394 (1838)
18. Pearl, J.: Causality: Models, reasoning, and inference. Cambridge University Press, Cambridge (2000)

Appendix G

Curriculum Vitae

Wolfsmattstrasse 9
8953 Dietikon,
Switzerland.
+ 41 44 635 43 47
martinez@ifi.uzh.ch

Harold Roberto Martínez Salazar

My research interest is developmental robotics. I am interested in understanding the different aspects of embodied cognition and apply them in the design of robots. I have the knowledge and experience in structured programming, and object oriented programming. I have programmed microprocessors with assembler code in order to develop applications for control and digital processing. I have experience with artificial intelligent techniques such as reinforcement learning, neural networks, and inference fuzzy systems in control, identification and classification. I am also familiar with finite elements analysis to simulate both fluid dynamic and mechanical behavior.

Education

PhD studies April 2008 –June 2013
Artificial Intelligence Laboratory (AILAB)
Department of Informatics
University of Zurich, Switzerland

M. S. in Electrical Engineering May 2004
Fields: Artificial Intelligence, Control and Signal Processing.
Department of Electric Engineering
University of the Andes. Colombia

Bachelor in Electronic Engineering May 2003
Laureate Grade
Department of Electronic Engineering
University of the Andes, Colombia

Bachelor in Mechanical Engineering May 2002
Laureate Grade
Department of Mechanical Engineering
University of the Andes, Colombia

High School November 1996
Calasanz School, Colombia

Experience:

PhD candidate April 2008 –June 2013
Artificial Intelligence Laboratory (AILAB)
Department of Informatics
University of Zurich, Switzerland

- Development of application modules for the iCub robot in C++.
- Rapid prototyping using Solidworks CAD software and 3D printing technologies.
- Student supervision (for bachelor semester projects).
- Teaching assistance (creating and grading exercises and exams of undergraduates

and master students).
- Management of the European research project Amarsi (writing deliverables, presenting the results in to the European commission, coordination of the researchers involved in the project, answering comments from reviewers of the project, etc).
- Research practice (writing reviews, research papers, attending conferences, etc).

Maintenance Engineer June 2006 – March 2008
Smurfit Kappa Cartón de Colombia.
- Management of the instrumentation service center (keeping an inventory of the tools of each technician and the service center, ordering repair kits, assigning the available resource, etc).
- Development of the maintenance procedures.
- Support the different departments of the company in the maintenance routine.
- Train the technicians in new technologies to diagnostic and test control valves.
- Keep track of the radioactive sensors available in the factory.

Assessor of Information Systems July 2004 – June 2006
Foundation País Libre, Colombia
- Development of the information system SAED (Java application).
- Development of indicators to measure the assistance process.
- Periodic report about kidnapping and extortion based on geo-referenced data.
- Application of algorithms from artificial intelligence to understand the evolution of kidnapping and extortion.

Software Developer January 2004 – May 2004
GATTACA S.A, Colombia
- Development of an open-source music player in C++ using wxWindows

Teaching Activities:

Teaching Assistance 2008-2012
AI classes for bachelor and master students
AI Lab, University of Zurich, Switzerland
- Design and grading exercises and exams.
- Preparation of the lecture.
- Students supervision.

Lecturer in Object-Oriented Programming and Algorithms January 2006 – May 2006
Department of Systems Engineering
University of the Andes.
- Teaching the paradigm of object- oriented programming.
- Design practical exercises in Java
- Grading exercises and exams

Lecturer in Signal Processing May 2004 – June 2004
Department of Mechatronics Engineering.
Military University Nueva Granada.
- Teaching Signal Processing.
- Design practical exercises in Matlab
- Grading exercises and exams.

Lecturer in Technical Drawing January 2004 – May 2004
Department of Mechanical Engineering.
University of the Andes

- Teaching technical drawing with and without computational aid.
- Development of practical exercises with Solidedge.
- Grading exercises and exams.

Teaching assistant January 2002- December 2003
Department of Electric Engineering
University of the Andes. Colombia

- Development of practical exercises in for the laboratory of Control Systems and Digital Systems.
- Grading exercises.
- Students supervision.

Tutor 1998-2002
Faculty of Engineering
University of the Andes, Colombia

- Student supervision in Dynamics, Mechanical of Fluids, Thermodynamics, Digital Systems, and Circuits Analysis and Systems.
- Grading exercises.

Key Technologies:

Programming: C/C++, Java, VHDL.
Software: Eclipse, Solidedge, Solidworks, Ansys, Fluent, Matlab.

Languages:

Spanish: native language.
English: excellent both written and oral.
German: basic both written and oral.

Conference Papers:

Martinez, H., Sumioka, H., Lungarella, M., and Pfeifer, R. (2010). "On the Influence of Sensor Morphology on Vergence". *Proc. of the 11th Int. Conf. on Simulated Adaptive Behavior.*

Martinez, H., Lungarella, M., and Pfeifer, R. (2010). "On the Influence of Sensor Morphology on Vergence". *Proc. of the 9th IEEE Int. Conf. on Development and Learning.*

Damian, D., Martinez, H., Dermitzakis, K., Hernandez, A. and Pfeifer, R. (2010). "Artificial Ridged Skin for Slippage Speed Detection in Prosthetic Hand Applications". *IEEE/RSJ Int. Conf. on Intelligent Robots and Systems.*

Martinez, H., Sumioka, H. (2011). "Sensory System as a Tool to Highlight Information Structure in the Sensorimotor Loop". *International Conference on Morphological Computation ICMC.*

Martinez, H., Carbajal, Juan P. (2011). “From Walking to Running a Natural Transition in the SLIP Model Using the Hopping Gait”. *IEEE International Conference on Robotics and Biomimetics (ROBIO).*

Martinez, H., Carbajal, Juan P. (2012). “Can we design controllers for bipedal robots based on simple models (templates) of their dynamics?”. *International Conference on Dynamic Walking*.

Journal Papers:

Martinez, H., Carbajal J. (2011). “Exploiting the Passive Dynamics of a Compliant Leg to Develop Gait Transitions”. *Phys. Rev. E, vol. 83, no. 6, p. 066707, 2011.*

Damian, D., Hernandez, A., Martinez H., and Pfeifer R. (2012). “Slip Speed Sensory Feedback for Prosthetic Applications”. *IEEE Transactions on Biomedical Engineering.*